

JAERI 1275  
NEANDC(J)-78/U  
INDC(JAP) -65/L

Benchmark Tests of JENDL-1

---

February 1982

---

日本原子力研究所  
Japan Atomic Energy Research Institute

日本原子力研究所研究成果編集委員会

委員長 森 茂（理事）

委 員

朝岡 卓見（原子炉工学部）	田中 茂也（物理部）
安達 公道（安全工学部）	田中 正俊（核融合研究部）
石塚 信（動力試験炉部）	田村 早苗（大型トカマク開発部）
伊藤 彰彦（環境安全研究部）	仲本秀四郎（技術情報部）
上野 鑑（原子炉化学部）	長崎 隆吉（特別研究員）
岡本 次郎（高崎研究所）	沼宮内彌雄（保健物理部）
神原 忠則（材料試験炉部）	橋谷 博（原子炉化学部）
栗山 将（大阪研究所）	浜口 由和（物理部）
桜井 裕（研究炉管理部）	原 昌雄（動力炉開発・安全性研究管理部）
佐藤 一男（安全解析部）	更田豊治郎（企画室）
佐野川好母（高温工学部）	三井 光（高崎研究所）
四方 英治（製造部）	

Japan Atomic Energy Research Institute

Board of Editors

Shigeru Mori (Chief Editor)

Hiromichi Adachi	Takumi Asaoka	Toyojiro Fuketa
Yoshikazu Hamaguchi	Masao Hara	Hiroshi Hashitani
Makoto Ishizuka	Akihiko Ito	Masanori Kanbara
Isamu Kuriyama	Hiroshi Mitsui	Ryukichi Nagasaki
Hideshiro Nakamoto	Takao Numakunai	Jiro Okamoto
Hiroshi Sakurai	Konomo Sanokawa	Kazuo Sato
Eiji Shikata	Sanae Tamura	Masatoshi Tanaka
Shigeya Tanaka	Kaoru Ueno	

JAERI レポートは、日本原子力研究所が研究成果編集委員会の審査を経て不定期に公刊している研究報告書です。

入手の問合せは、日本原子力研究所技術情報部情報資料課（〒319-11茨城県那珂郡東海村）あて、お申しこしください。なお、このほかに財団法人原子力弘済会資料センター（〒319-11 茨城県那珂郡東海村日本原子力研究所内）で複写による実費頒布をおこなっております。

JAERI reports are reviewed by the Board of Editors and issued irregularly.

Inquiries about availability of the reports should be addressed to Information Section, Division of Technical Information, Japan Atomic Energy Research Institute, Tokai-mura, Naka-gun, Ibaraki-ken 319-11, Japan.

©Japan Atomic Energy Research Institute, 1982

編集兼発行 日本原子力研究所  
印 刷 いばらき印刷株

## Benchmark Tests of JENDL-1

Yasuyuki Kikuchi, Akira Hasegawa, Hideki Takano, Takanobu Kamei\*,  
Takeshi Hojuyama\*\*, Makoto Sasaki\*\*, Yuji Seki\*\*,  
Atsushi Zukeran\*\*\* and Iwao Otake\*\*\*\*

Working Group on JENDL Integral Tests

Japanese Nuclear Data Committee

Japan Atomic Energy Research Institute

Tokai-mura, Naka-gun, Ibaraki-ken

Received September 25, 1981

### Abstract

Various benchmark tests were made on JENDL-1. At the first stage, various core center characteristics were tested for many critical assemblies with one-dimensional model. At the second stage, applicability of JENDL-1 was further tested to more sophisticated problems for MOZART and ZPPR-3 assemblies with two-dimensional model.

It was proved that JENDL-1 predicted various quantities of fast reactors satisfactorily as a whole. However, the following problems were pointed out:

- 1) There exists discrepancy of 0.9% in the  $k_{\text{eff}}$ -values between the Pu- and U-cores.
- 2) The fission rate ratio of  $^{239}\text{Pu}$  to  $^{235}\text{U}$  is underestimated by 3%.
- 3) The Doppler reactivity coefficients are overestimated by about 10%.
- 4) The control rod worths are underestimated by 4%.
- 5) The fission rates of  $^{235}\text{U}$  and  $^{239}\text{Pu}$  are underestimated considerably in the outer core and radial blanket regions.
- 6) The negative sodium void reactivities are overestimated, when the sodium is removed from the outer core.

As a whole, most of problems of JENDL-1 seem to be related with the neutron leakage and the neutron spectrum.

It was found through the further study that most of these problems came from too small diffusion coefficients and too large elastic removal cross sections above 100 keV, which might be probably caused by overestimation of the total and elastic scattering cross sections for structural materials in the unresolved resonance region up to several MeV.

**Keywords:** Benchmark Tests, JENDL-1,  $k_{\text{eff}}$ , Reaction Rate Ratio, Reactivity Worth, Doppler Coefficient, Reaction Rate Distribution, Sodium Void Reactivity, Control Rod Worth, Structural Materials.

---

\* Nippon Atomic Industry Group Co., Ltd.

\*\* Mitsubishi Atomic Power Industries, Inc.

\*\*\* Energy Research Laboratory, Hitachi Ltd.

\*\*\*\* Power Reactor and Nuclear Fuel Development Corporation.

# JENDL-1 のベンチマークテスト

日本原子力研究所 シグマ研究専門委員会  
JENDL 積分評価ワーキンググループ

菊池康之・長谷川明・高野秀機・亀井孝信<sup>\*</sup>・宝珠山健<sup>\*\*</sup>  
佐々木誠<sup>\*\*</sup>・関 雄次<sup>\*\*</sup>・瑞慶覧篤<sup>\*\*\*</sup>・大竹 嶽<sup>\*\*\*\*</sup>

1981年9月25日受理

## 要 旨

JENDL-1について種々のベンチマークテストを行った。第1段階として、1次元モデルで多数の臨界集合体の炉心中心特性をテストした。第2段階としては、2次元モデルにより MOZART, ZPPR-3 炉心の詳細な特性をテストした。

JENDL-1は高速炉の種々の特性を、全体としては満足に予測する事が判明した。しかし以下の問題点も指摘された：

- 1)  $k_{\text{eff}}$  値が Pu 炉心と U 炉心で 0.9 %異なる。
- 2)  $^{239}\text{Pu}$  対  $^{235}\text{U}$  の核分裂率比が 3 %過小評価される。
- 3) ドップラー係数は約 10 %過大評価される。
- 4) 制御棒価値は 4 %過小評価される。
- 5)  $^{235}\text{U}$ ,  $^{239}\text{Pu}$  の核分裂率は外部炉心と径方向ブランケット内でかなり過小評価される。
- 6) 外部炉心における Na ボイド係数が負側に過大評価される。

これらの問題の大部分は中性子漏洩とスペクトルに関係しているように思われる。

さらに検討を続けた結果、これらの問題点の多くは、100 keV 以上のエネルギー領域における拡散係数の過小、弹性除去断面積の过大による事が判明した。さらにその原因是、数 MeV までの非分離共鳴領域における、構造材の全断面積、弹性散乱断面積の过大評価にあると思われる。

---

\* 日本原子力事業(株) NAIG 総合研究所

\*\* 三菱原子力工業(株)

\*\*\* 日立製作所(株) エネルギー研究所

\*\*\*\* 動力炉核燃料開発事業団

## Contents

<b>1.</b>	<b>Introduction . . . . .</b>	<b>1</b>
<b>2.</b>	<b>Benchmark Tests with One-dimensional Model . . . . .</b>	<b>2</b>
<b>2.1</b>	<b>Method . . . . .</b>	<b>2</b>
<b>2.2</b>	<b>Assemblies . . . . .</b>	<b>2</b>
<b>2.3</b>	<b>Effective Multiplication Factor . . . . .</b>	<b>3</b>
<b>2.4</b>	<b>Central Reaction Rate Ratio . . . . .</b>	<b>5</b>
<b>2.5</b>	<b>Central Reactivity Worth . . . . .</b>	<b>11</b>
<b>2.5.1</b>	<b>Absolute Value . . . . .</b>	<b>11</b>
<b>2.5.2</b>	<b>Normalized Worth . . . . .</b>	<b>13</b>
<b>2.6</b>	<b>Doppler Coefficient . . . . .</b>	<b>20</b>
<b>2.7</b>	<b>Analysis of Snell Experiments . . . . .</b>	<b>21</b>
<b>3.</b>	<b>Benchmark Tests with two-dimensional Model . . . . .</b>	<b>23</b>
<b>3.1</b>	<b>MOZART . . . . .</b>	<b>23</b>
<b>3.1.1</b>	<b>Reaction Rate Distribution in MZB . . . . .</b>	<b>23</b>
<b>3.1.2</b>	<b>Sodium Void Reactivity in MZB . . . . .</b>	<b>27</b>
<b>3.1.3</b>	<b>Control Rod Worth in MZC . . . . .</b>	<b>30</b>
<b>3.2</b>	<b>ZPPR-3 . . . . .</b>	<b>32</b>
<b>3.2.1</b>	<b>Worth of Multiple Control Rods in Phase 1B Core . . . . .</b>	<b>32</b>
<b>3.2.2</b>	<b>Fission Rate Distribution of <math>^{235}\text{U}</math> in Phase 2 Core . . . . .</b>	<b>34</b>
<b>4.</b>	<b>Summary and Discussion . . . . .</b>	<b>37</b>
<b>4.1</b>	<b>Problems Encountered through Benchmark Tests . . . . .</b>	<b>37</b>
<b>4.2</b>	<b>Intercomparison of Macroscopic Cross Sections . . . . .</b>	<b>37</b>
<b>4.3</b>	<b>Discussion . . . . .</b>	<b>38</b>
<b>4.4</b>	<b>Feedback on Nuclear Data Evaluation . . . . .</b>	<b>38</b>
<b>Acknowledgment . . . . .</b>		<b>39</b>
<b>References . . . . .</b>		<b>39</b>
<b>Appendices . . . . .</b>		<b>41</b>
<b>A1.</b>	<b>Production of Reactor Constants . . . . .</b>	<b>41</b>
<b>A2.</b>	<b>Benchmark Specification . . . . .</b>	<b>44</b>
<b>A2.1</b>	<b>Twenty-seven Assemblies with One-dimensional Model . . . . .</b>	<b>44</b>
<b>A2.1.1</b>	<b>Eighteen Assemblies Selected by Hardie et al. . . . .</b>	<b>44</b>
<b>A2.1.2</b>	<b>MZA and MZB . . . . .</b>	<b>44</b>
<b>A2.1.3</b>	<b>FCA Assemblies . . . . .</b>	<b>44</b>
<b>A2.2</b>	<b>Doppler Analysis . . . . .</b>	<b>51</b>
<b>A3.</b>	<b>Effects of Structural Material Cross Sections . . . . .</b>	<b>54</b>
<b>A3.1</b>	<b>Analysis with One-dimensional Model . . . . .</b>	<b>60</b>
<b>A3.1.1</b>	<b>Effective Multiplication Factor . . . . .</b>	<b>60</b>
<b>A3.1.2</b>	<b>Central Reaction Rate Ratio . . . . .</b>	<b>60</b>
<b>A3.1.3</b>	<b>Central Reactivity Worth . . . . .</b>	<b>60</b>
<b>A3.1.4</b>	<b>Doppler Coefficient . . . . .</b>	<b>64</b>
<b>A3.1.5</b>	<b>Snell Experiments . . . . .</b>	<b>65</b>
<b>A3.2</b>	<b>Analysis of MZB with Two-dimensional Model . . . . .</b>	<b>65</b>
<b>A3.3</b>	<b>Analysis of Large Fast Breeder Reactor . . . . .</b>	<b>72</b>
<b>A4.</b>	<b>Intercomparison of Group Constants among JENDL-1, JFS-2 and ENDF/B-IV . . . . .</b>	<b>74</b>

## 目 次

1. 序 論 .....	1
2. 一次元モデルによるベンチマークテスト .....	2
2.1 方法 .....	2
2.2 臨界集合体 .....	2
2.3 実効増倍率 .....	3
2.4 中心反応率比 .....	5
2.5 中心反応度価値 .....	11
2.5.1 絶対値 .....	11
2.5.2 規格化された値 .....	13
2.6 ドップラー係数 .....	20
2.7 スネル実験解析 .....	21
3. 二次元モデルによるベンチマークテスト .....	23
3.1 MOZART .....	23
3.1.1 MZB における反応率分布 .....	23
3.1.2 MZB における Na ボイド反応度 .....	27
3.1.3 MZC における制御棒価値 .....	30
3.2 ZPPR-3 .....	32
3.2.1 フェーズ 1 B 炉心における多数本制御棒価値 .....	32
3.2.2 フェーズ 2 炉心における $^{235}\text{U}$ 核分裂率分布 .....	34
4. 総括と議論 .....	37
4.1 ベンチマークテストからの知見 .....	37
4.2 巨視断面積の相互比較 .....	37
4.3 議 論 .....	38
4.4 核データ評価への提言 .....	38
謝 辞 .....	39
参照文献 .....	39
付 錄 .....	41
A 1 炉定数作成 .....	41
A 2 ベンチマークテスト仕様 .....	44
A 2.1 一次元モデルによる 27 炉心 .....	44
A 2.1.1 Hardie 等の選択による 18 集合体 .....	44
A 2.1.2 MZA と MZB .....	44
A 2.1.3 FCA 炉心 .....	44
A 2.2 ドップラー解析 .....	51
A 3 構造材断面積の効果 .....	54
A 3.1 一次元モデルによる解析 .....	60
A 3.1.1 実効増倍率 .....	60
A 3.1.2 中心反応率比 .....	60
A 3.1.3 中心反応度価値 .....	60
A 3.1.4 ドップラー係数 .....	64
A 3.1.5 スネル実験 .....	65
A 3.2 二次元モデルによる MZB 解析 .....	65
A 3.3 大型高速増殖炉の解析 .....	72
A 4 JENDL-1, JFS-2, ENDF/B-IV 炉定数相互比較 .....	74

## 1. Introduction

Japanese Evaluated Nuclear Data Library (JENDL) has been developed as the national standard neutron nuclear data library by Nuclear Data Center in JAERI in cooperation with Japanese Nuclear Data Committee (JNDC). Its first version (JENDL-1) mainly aimed to provide data for fast reactor calculations and its evaluation was made entirely on the basis of differential nuclear data. JENDL-1 contains the data from  $10^{-5}$  eV to 15 MeV for the following nuclides:

H,  $^6$ Li,  $^{10}$ B,  $^{12}$ C,  $^{23}$ Na,  $^{27}$ Al, Si, Cr,  $^{50}$ Cr,  $^{52}$ Cr,  $^{53}$ Cr,  $^{54}$ Cr,  $^{55}$ Mn, Fe,  $^{54}$ Fe,  $^{56}$ Fe,  $^{57}$ Fe,  $^{58}$ Fe, Ni,  $^{58}$ Ni,  $^{60}$ Ni,  $^{61}$ Ni,  $^{62}$ Ni,  $^{64}$ Ni, Cu,  $^{63}$ Cu,  $^{65}$ Cu,  $^{90}$ Sr,  $^{93}$ Zr, Mo,  $^{92}$ Mo,  $^{94}$ Mo,  $^{95}$ Mo,  $^{96}$ Mo,  $^{97}$ Mo,  $^{98}$ Mo,  $^{100}$ Mo,  $^{99}$ Tc,  $^{101}$ Ru,  $^{102}$ Ru,  $^{104}$ Ru,  $^{106}$ Ru,  $^{103}$ Rh,  $^{105}$ Pd,  $^{107}$ Pd,  $^{109}$ Ag,  $^{129}$ I,  $^{131}$ Xe,  $^{133}$ Cs,  $^{135}$ Cs,  $^{137}$ Cs,  $^{144}$ Ce,  $^{143}$ Nd,  $^{144}$ Nd,  $^{145}$ Nd,  $^{147}$ Pm,  $^{147}$ Sm,  $^{149}$ Sm,  $^{151}$ Sm,  $^{153}$ Eu,  $^{155}$ Eu,  $^{181}$ Ta,  $^{232}$ Th,  $^{233}$ Pa,  $^{234}$ U,  $^{235}$ U,  $^{238}$ U,  $^{239}$ Np,  $^{239}$ Pu,  $^{240}$ Pu,  $^{241}$ Pu and  $^{241}$ Am.

Its compilation started in 1973, and completed in 1975 for 28 fission product nuclides<sup>1,2)</sup> and in 1976 for the other nuclides<sup>3)</sup>.

Since then various benchmark tests have been made by the working group\* on JENDL integral tests of JNDC in order to prove its applicability to fast reactor calculations. Satisfactory results were obtained<sup>4)</sup> and JENDL-1 has been used for both analyses and design works of fast reactors. On the other hand, various problems were pointed out through these tests and experiences, particularly on the cross sections of structural materials, and they were further investigated by the same working group. This report describes details of the benchmark tests, discusses the problems encountered and suggests the way to improve the microscopic nuclear data of JENDL-1\*\*.

The first stage of the tests was done in 1976 on the core center characteristics for selected 27 assemblies. The calculation was based on one-dimensional diffusion and first-order perturbation approximations by using the reactor constants of JAERI-Fast set<sup>7)</sup> type with 70 groups. The results of these tests are described in Chapter 2. As the second stage, applicability was tested to more sophisticated problems in MOZART and ZPPR-3 cores with two-dimensional model. The details of the tests are written in Chapter 3. Various problems encountered through the tests are discussed in Chapter 4.

The methods to produce the reactor constants are described in Appendix 1. Benchmark specifications are given in Appendix 2. In Appendix 3, the effects of cross sections of Fe, Cr and Ni are discussed by replacing them with those of ENDF/B-IV. The group constants of JENDL-1 are compared graphically with those of JAERI-Fast set Version 2 (JFS-2) and ENDF/B-IV in Appendix 4.

---

\* Group Members: Y. Kikuchi (leader), A. Hasegawa, T. Nakagawa, T. Narita, H. Takano, K. Tsuchihashi, H. Yoshida (JAERI), S. Iijima, T. Kamei (NAIG), Y. Seki, T. Hojuyama, M. Sasaki (MAPI), H. Matsunobu (SAEI), A. Zukeran, S. Itoh (Hitachi), M. Yamamoto (FBEC), I. Otake (PNC)

\*\* Benchmark tests were also made<sup>5,6)</sup> for the fission product nuclides, but they are not included in this report.

## 2. Benchmark Tests with One-dimensional Model

### 2.1 Method

We calculated the following items of core center characteristics with 1-D model: Effective multiplication factor ( $k_{\text{eff}}$ ), central reaction rate ratios, central reactivity worths and Doppler reactivity coefficients. The fission rate ratios in equilibrium neutron spectrum in natural uranium are also calculated and compared with the experimental data\*.

The group constants of 70 group structure were produced with PROF-GROUCH-G-II code system<sup>8)</sup>. The self-shielding factors were obtained with TIMS-1<sup>9)</sup> by solving the neutron slowing down equation numerically. Details of the procedure are given in Appendix 1. Data of ENDF/B-IV were used for  $^9\text{Be}$ ,  $^{11}\text{B}$ ,  $^{16}\text{O}$  and  $^{242}\text{Pu}$  which are not contained in JENDL-1.

The effective multiplication factor, and the real and adjoint fluxes were calculated with a one-dimensional diffusion code EXPANDA-70D<sup>10)</sup>. The reaction rate ratios and central reactivity worths were calculated with the XPRTC code<sup>10)</sup> by using the real and adjoint fluxes obtained with EXPANDA-70D. The calculated results were compared with the measured data in the form of the calculation-to-experiment ratio (C/E), and were statistically arranged with the BENCH code<sup>11)</sup> as average values and standard deviations.

The Doppler reactivity coefficients were calculated with the first-order perturbation approximation by the use of the EXPANDA-70D code<sup>10)</sup>.

For comparison, the same items were calculated with the JAERI-Fast set, Version 2 (JFS-2) and with the group constants produced from ENDF/B-IV.

### 2.2 Assemblies

Hardie *et al.*<sup>12)</sup> selected 18 assemblies for tests of ENDF/B-IV; twelve Pu-cores and six U-cores with various fertile to fissile ratios (0.05 ~ 8.6) and core volumes (12 ~ 4000 litre). We adopted all of them\*\*, and added MOZART cores<sup>13)</sup> (MZA and MZB) and some FCA cores. Their main characteristics are shown in Table 2.1. The detailed specifications are given in Appendix 2. Corrections such as one to two dimensional, heterogeneity and transport are taken from Ref. (12) for the 18 assemblies selected by Hardie *et al.*, from Ref. (13) for the MOZART cores and from our preliminary calculation<sup>14)</sup> for the FCA cores. They are also given in Appendix 2.

As to the Doppler coefficients, we adopted small sample Doppler coefficient measurements at FCA-V-1, V-2, VI-1, VI-2, ZPPR-2 and ZPR-3-47, and whole core Doppler measurements at SEFOR. Precise specifications and necessary corrections are given in Appendix 2.

---

\* This type of experiment is called Snell experiment.

\*\* ZPR-3-54 was not considered in the statistical analyses of the results, because the leakage correction could not be adequately treated in the present model.

**Table 2.1** Characteristics of critical assemblies

Assembly Name	Fissile Fuel	Fertile to Fissile Ratio	Core Volume (l)	Remarks
VERA-11A	Pu	0.05	12	Pu + C, No U in core
VERA-1B	U	0.07	30	94% EU + C
ZPR-3-6F	U	1.1	50	
ZPR-3-54	Pu	1.6	190	Similar to ZPR-3-53 except an Fe reactor
ZPR-3-53	Pu	1.6	220	U reflector
FCA-V-2	Pu (+U)	2.3	200	Pu/EU = 1/3
FCA-V-1	U (+Pu)	2.6	142	Pu/EU = 1/4
SNEAK-7A	Pu	3.0*	110	
FCA-VI-2	Pu (+U)	3.2*	422	Pu core + EU driver
ZPR-3-12	U	3.8	100	Soft spectrum due to added C
MZA	Pu	3.9	570	
FCA-I-6	U	4.0	24	20% EU core with C reflector
FCA-I-1	U	4.0	30	20% EU core with Nat U blanket
FCA-3-2S	U	4.0	245	Soft spectrum due to added C
FCA-VI-1	Pu	4.4	423	Test region + DU blanket
ZPR-3-50	Pu	4.5	340	(ZPR-3-48) with additional C
ZPR-3-48	Pu	4.5	410	Soft spectrum due to added C, L/D = 1
ZPR-3-49	Pu	4.5	450	(ZPR-3-48) without Na
ZPR-3-56B	Pu	4.6	610	Ni reflector
ZPR-6-6A	U	5.0	4000	L/D = 0.8
ZPPR-2	Pu	5.1*	2400	Equal volume 2 zone core, L/D = 0.5
MZB	Pu	5.2	1800	
ZEBRA-2	U	6.2	430	
ZPR-6-7	Pu	6.5	3100	L/D = 0.9
SNEAK-7B	Pu	7.0	310	
ZPR-3-11	U	7.5	140	
ZEBRA-3	Pu	8.6	60	Hard spectrum (80% above 100 keV)

\* Averaged value of inner and outer cores with volume weights.

### 2.3 Effective Multiplication Factor

The C/E values of effective multiplication factor are given in **Table 2.2** and **Fig. 2.1**. The ZPR-3-54 assembly is omitted in the statistical analyses. The following are observed:

- 1) JENDL-1 predicts the  $k_{\text{eff}}$ -values very well on an average.
- 2) Discrepancy of 0.9% is observed between the Pu-fueled and U-fueled cores with JENDL-1. This can be partly explained by the fact that the different  $\nu_p$  values of  $^{252}\text{Cf}$  spontaneous fission were assumed as the standard in the JENDL-1 evaluation of  $\nu_p$  values for  $^{235}\text{U}$  and  $^{239}\text{Pu}$ :  $\nu_p(^{252}\text{Cf}) = 3.782$  was assumed for  $^{235}\text{U}$  and  $\nu_p(^{252}\text{Cf}) = 3.756$  for  $^{239}\text{Pu}$ .
- 3) Compared with JFS-2, the C/E values of JENDL-1 have a tendency to decrease slightly with increasing the fertile to fissile ratio.
- 4) Obvious differences are observed between the results of ZPR-3-53 and ZPR-3-54, which have the same core but different reflectors, i.e., natural uranium for ZPR-3-53 and iron for ZPR-3-54. The  $k_{\text{eff}}$ -value of ZPR-3-54 calculated with JENDL-1 is 2% higher than that of ZPR-3-53, while the  $k_{\text{eff}}$ -values of ZPR-3-54 are 4% lower with JFS-2 and ENDF/B-IV. This may suggest that iron cross sections of JENDL-1 give less leakage.
- 5) ENDF/B-IV underestimates the  $k_{\text{eff}}$ -values by 1% as a whole. Particularly the underestimate is significant for assemblies whose fertile to fissile ratio lies between 2.5 and 7.2 as seen in **Fig. 2.1**.

- 6) As to ENDF/B-IV, the present results are about 1% lower than those calculated by Hardie *et al.*<sup>12)</sup>. The reason of this disagreement is not clear, because we used the same models and corrections. This disagreement seems to be too large to be caused by the different methods of group constants production. Recently LeSage and McKnight<sup>15)</sup> discussed on the C/E discrepancies for several key integral parameters measured in ZPR assemblies including ZPR-3-48, ZPR-6-7, ZPPR-2 and ZPR-6-6A. The  $k_{\text{eff}}$ -values for these assemblies calculated by LeSage and McKnight with ENDF/B-IV agree with the presently calculated values with ENDF/B-IV and are lower than those calculated by Hardie *et al.*

**Table 2.2** Effective multiplication factors. Values in parenthesis are averaged over 17 assemblies selected by Hardie *et al.*)

Fuel	Assembly	Experimental	Calculated (C/E)			
			JENDL-1	JFS-2	ENDF/B-IV	ENDF/B-IV* (Hardie <i>et al.</i> )
Pu	VERA-11A	1.0000	0.9860	0.9924	0.9840	0.9945
	ZPR-3-54**	1.0000	1.0217	0.9544	0.9335	0.9620
	ZPR-3-53	1.0000	0.9994	0.9965	0.9772	0.9955
	FCA V-2	1.0000	1.0108	1.0091	0.9973	—
	SNEAK-7A	1.0000	0.9955	1.0051	0.9907	1.0022
	FCA VI-2	1.0000	1.0071	1.0045	0.9904	—
	MZA	1.0108	1.0027	1.0012	0.9831	—
	FCA VI-1	1.0000	0.9945	1.0004	0.9844	—
	ZPR-3-50	1.0000	0.9974	0.9985	0.9811	0.9948
	ZPR-3-48	1.0000	1.0005	1.0031	0.9885	1.0015
	ZPR-3-49	1.0000	1.0001	1.0042	0.9918	1.0021
	ZPR-3-56B	1.0000	0.9957	0.9967	0.9768	0.9882
	ZPPR-2	1.0000	1.0072	1.0087	0.9878	0.9976
	MZB	1.0040	0.9985	1.0013	0.9796	—
	ZPR-6-7	1.0000	0.9983	1.0033	0.9810	0.9917
	SNEAK-7B	1.0000	0.9898	1.0044	0.9892	0.9967
	ZEBRA-3	1.0000	0.9816	0.9980	0.9918	1.0004
Average of C/E		0.9978 (0.9955)	1.0017 (1.0010)	0.9859 (0.9854)	—	(0.9968)
Standard deviation of C/E		0.0074	0.0044	0.0057	—	(0.0043)
U	VERA-1B	1.0000	1.0077	1.0036	0.9942	1.0021
	ZPR-3-6F	1.0000	1.0195	1.0166	1.0083	1.0112
	FCA V-1	1.0000	1.0061	1.0059	0.9942	—
	ZPR-3-12	1.0000	1.0061	1.0070	0.9987	1.0055
	FCA I-6	1.0000	1.0093	0.9987	0.9965	—
	FCA I-1	1.0000	1.0120	1.0177	1.0129	—
	FCA III-2S	1.0000	1.0026	0.9881	0.9825	—
	ZPR-6-6A	1.0000	1.0139	1.0019	0.9895	0.9967
	ZEBRA-2	1.0000	0.9902	0.9852	0.9781	0.9965
	ZPR-3-11	1.0000	0.9999	1.0080	1.0050	1.0107
Average of C/E		1.0067 (1.0062)	1.0033 (1.0037)	0.9960 (0.9956)	—	(1.0038)
Standard deviation of C/E		0.0077	0.0100	0.0104	—	(0.0059)
All	Average of C/E	1.0012 (1.0008)	1.0023 (1.0020)	0.9898 (0.9890)	—	(0.9993)
	Standard deviation of C/E	0.0087	0.0071	0.0093	—	(0.0060)

\* Taken from Ref. (12).

\*\* Omitted in statistical analyses.

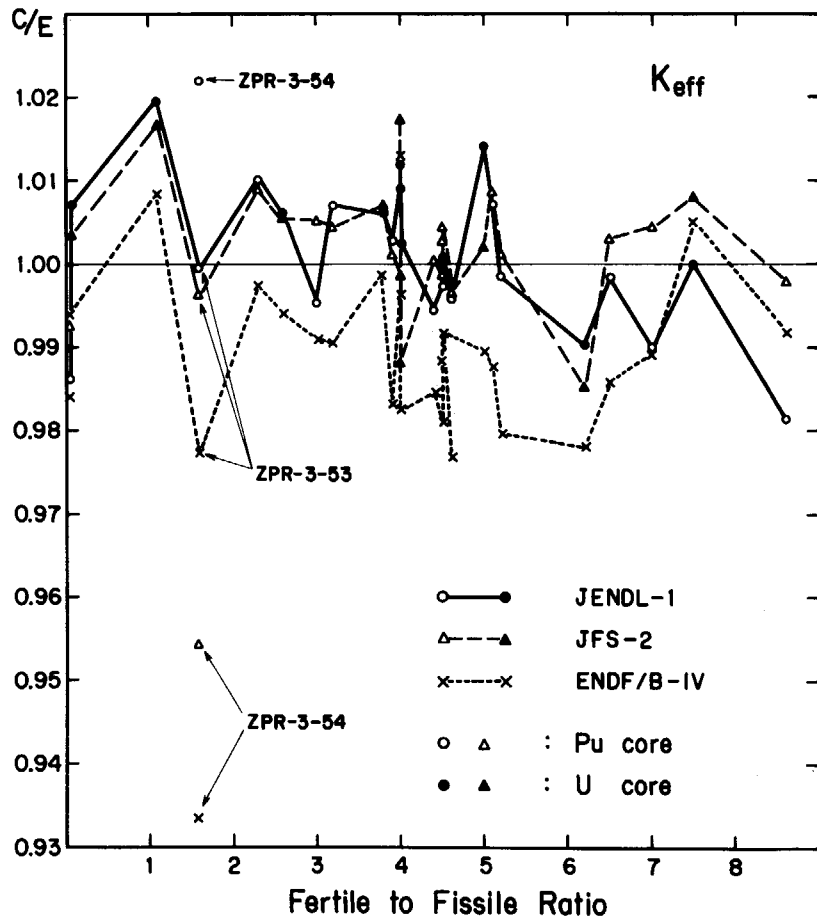


Fig. 2.1 C/E values of  $k_{\text{eff}}$  vs. fertile to fissile ratio.

## 2.4 Central Reaction Rate Ratio

The C/E values of central reaction rate ratios are given in **Tables 2.3 ~ 2.7** and their dependence on the fertile to fissile ratio is shown in **Fig. 2.2**. The results for FCA-I-6, as well as those for ZPR-3-54, are omitted in the statistical analyses because of experimental uncertainties.

### a) $^{238}\text{U}$ fission to $^{235}\text{U}$ fission

JENDL-1 predicts the ratios very well in the Pu-fueled cores but underestimates them by 5% in the U-fueled cores. The discrepancy between the Pu- and U- cores is smaller in the results obtained with JFS-2 and ENDF/B-IV. It can be seen from **Fig. 2.2**, however, that the C/E values for some assemblies much deviate from unity with any library set. Experimental conditions should be checked more carefully for such cases, because the fission rate of a fertile material such as  $^{238}\text{U}$  or  $^{240}\text{Pu}$  is very sensitive to the detector position in the fuel cell. Strong correlation is observed between the C/E values of  $^{238}\text{U}$  fission to  $^{235}\text{U}$  fission and those of  $^{240}\text{Pu}$  fission to  $^{235}\text{U}$  fission, as is seen from **Fig. 2.2**. This might also suggest some systematic errors in the fission rate ratio measurements for the fertile materials.

### b) $^{239}\text{Pu}$ fission to $^{235}\text{U}$ fission

JENDL-1 underestimates the ratios by about 3%. JFS-2 and ENDF/B-IV also underestimate them by about 2%. Fluctuation of the C/E values through the cores is small, as is seen from **Fig. 2.2**. Therefore the underestimate of this fission rate ratio is essential and further investigation should be required. The discrepancy of  $k_{\text{eff}}$  between the U- and Pu- cores may be partly attributed to the underestimate of this fission rate ratio.

**Table 2.3** Ratio of  $^{238}\text{U}$  fission rate to  $^{235}\text{U}$  fission rate at core center. Values in parenthesis are averaged over 17 assemblies selected by Hardie *et al.*

Fuel	Assembly	Experimental	Calculated (C/E)			
			JENDL-1	JFS-2	ENDF/B-IV	ENDF/B-IV* (Hardie <i>et al.</i> )
Pu	VERA-11A	0.077	1.129	1.094	1.086	1.090
	ZPR-3-54**	0.0254	1.129	1.199	1.197	1.176
	ZPR-3-53	0.0254	1.146	1.152	1.147	1.125
	FCA V-2	0.0396	1.053	1.091	1.106	—
	SNEAK-7A	0.0448	0.915	0.924	0.934	0.911
	FCA VI-2	0.0219	1.012	1.034	1.047	—
	MZA	0.0337	0.943	0.956	0.968	—
	FCA VI-1	—	—	—	—	—
	ZPR-3-50	0.0251	1.120	1.138	1.147	1.132
	ZPR-3-48	0.0326	0.997	1.019	1.027	1.026
	ZPR-3-49	0.0345	1.038	1.048	1.059	1.055
	ZPR-3-56B	0.0308	0.934	0.947	0.963	0.940
	ZPPR-2	0.0201	1.042	1.051	1.069	1.053
	MZB	0.0226	0.970	0.979	0.996	—
	ZPR-6-7	0.0230	0.911	0.916	0.933	0.914
U	SNEAK-7B	0.0330	0.963	0.981	1.000	0.965
	ZEBRA-3	0.0461	0.943	0.985	0.988	1.001
	Average of C/E	1.008 (1.014)	1.021 (1.023)	1.031 (1.032)	—	(1.019)
	Standard deviation of C/E	0.076	0.072	0.068	—	(0.076)
	VERA-1B	0.066	1.117	1.150	1.187	1.180
	ZPR-3-6F	0.078	0.901	0.955	0.987	1.000
	FCA V-1	0.0423	0.980	1.022	1.039	—
	ZPR-3-12	0.047	0.975	1.030	1.053	1.060
	FCA I-6**	0.054	1.017	1.099	1.125	—
	FCA I-1	0.057	0.934	0.997	1.022	—
All	FCA III-2S	0.039	0.838	0.874	0.883	—
	ZPR-6-6A	0.0245	0.903	0.926	0.938	0.926
	ZEBRA-2	0.0320	0.975	1.032	1.046	1.048
	ZPR-3-11	0.038	0.965	1.028	1.042	1.064
	Average of C/E	0.954 (0.973)	1.002 (1.020)	1.022 (1.042)	—	(1.046)
All	Standard deviation of C/E	0.073	0.074	0.080	—	(0.076)
	Average of C/E	0.988 (1.000)	1.014 (1.022)	1.028 (1.036)	—	(1.029)
	Standard deviation of C/E	0.079	0.073	0.073	—	(0.077)

\* Taken from Ref. (12).

\*\* Omitted in statistical analyses.

**Table 2.4** Ratio of  $^{239}\text{Pu}$  fission rate to  $^{235}\text{U}$  fission rate at core center.  
Values in parenthesis are averaged over 16 assemblies selected  
by Hardie *et al.*

Fuel	Assembly	Experimental	Calculated (C/E)		
			JENDL-1	JFS-2	ENDF/B-IV
Pu	VERA-11A	1.07	1.066	1.073	1.067
	ZPR-3-54**	0.928	0.930	0.945	0.931
	ZPR-3-53	0.928	0.932	0.938	0.922
	FCA V-2	1.104	0.950	0.962	0.967
	SNEAK-7A	1.016	0.946	0.953	0.957
	FCA VI-2	0.956	0.950	0.961	0.964
	MZA	1.013	0.960	0.969	0.974
	FCA VI-1	—	—	—	—
	ZPR-3-50	0.903	0.974	0.982	0.978
	ZPR-3-48	0.976	0.973	0.983	0.984
	ZPR-3-49	0.986	0.984	0.996	1.002
	ZPR-3-56B	1.028	0.927	0.936	0.942
	ZPPR-2	0.937	0.962	0.971	0.974
	MZB	0.949	0.963	0.971	0.976
	ZPR-6-7	0.953	0.946	0.954	0.957
U	SNEAK-7B	1.012	0.963	0.975	0.986
	ZEBRA-3	1.190	0.963	0.980	0.982
	Average of C/E	0.964 (0.967)	0.974 (0.976)	0.975 (0.977)	(0.982)
	Standard deviation of C/E	0.031	0.031	0.031	(0.036)
	VERA-1B	1.070	1.057	1.059	1.062
	ZPR-3-6F	1.22	1.003	1.014	1.017
	FCA V-1	1.161	0.912	0.925	0.930
	ZPR-3-12	1.12	0.971	0.987	0.993
	FCA I-6**	1.08	1.108	1.129	1.130
	FCA I-1	1.27	0.941	0.957	0.959
All	FCA III-2S	1.02	0.950	0.961	0.967
	ZPR-6-6A	—	—	—	—
	ZEBRA-2	0.987	0.984	0.999	1.007
	ZPR-3-11	1.19	0.960	0.976	0.980
	Average of C/E	0.972 (0.995)	0.985 (1.007)	0.990 (1.012)	(1.014)
	Standard deviation of C/E	0.041	0.038	0.039	(0.026)
	Average of C/E	0.967 (0.976)	0.977 (0.986)	0.980 (0.988)	(0.992)
	Standard deviation of C/E	0.035	0.034	0.034	(0.037)

\* Taken from Ref. (12).

\*\* Omitted in statistical analyses.

c)  $^{240}\text{Pu}$  fission to  $^{235}\text{U}$  fission

The fission rate ratio of  $^{240}\text{Pu}$  to  $^{235}\text{U}$  is well predicted with JENDL-1 on an average. It should be noted, however, that fluctuation of the C/E values is very large as shown in Fig. 2.2. The strong correlation with the results of fission rate ratio of  $^{238}\text{U}$  to  $^{235}\text{U}$  suggests some systematic errors in the measurements as mentioned above. Hence the experimental conditions should be reexamined.

d)  $^{238}\text{U}$  capture to  $^{235}\text{U}$  fission

The ratios of  $^{238}\text{U}$  capture to  $^{235}\text{U}$  fission are predicted fairly well with any set. However there exist discrepancies of 2 ~ 4% between the Pu- and U- cores.

e)  $^{238}\text{U}$  capture to  $^{239}\text{Pu}$  fission

The ratios are also predicted fairly well. The average C/E values are a little higher than those of the  $^{238}\text{U}$  capture to  $^{235}\text{U}$  fission rate ratio. This is consistent with the underestimate in the  $^{239}\text{Pu}/^{235}\text{U}$  fission rate ratio. The discrepancies between the Pu- and U- cores become larger than those of the ratio of  $^{238}\text{U}$  capture to  $^{235}\text{U}$  fission.

**Table 2.5** Ratio of  $^{240}\text{Pu}$  fission rate to  $^{235}\text{U}$  fission rate at core center.

Values in parenthesis are averaged over 11 assemblies selected by Hardie *et al.*

Fuel	Assembly	Experimental	Calculated (C/E)			
			JENDL-1	JFS-2	ENDF/B-IV	ENDF/B-IV* (Hardie <i>et al.</i> )
Pu	VERA-11A	0.475	1.029	1.032	1.041	1.035
	ZPR-3-54**	0.174	1.134	1.186	1.219	1.196
	ZPR-3-53	0.174	1.146	1.146	1.177	1.147
	MZA	0.260	0.934	0.996	0.995	—
	ZPR-3-50	0.159	1.262	1.306	1.332	1.311
	ZPR-3-48	0.243	0.988	1.048	1.051	1.040
	ZPR-3-56B	0.282	0.793	0.849	0.847	0.824
	ZPPR-2	0.170	1.037	1.110	1.102	1.081
	MZB	0.192	0.959	1.027	1.020	—
	ZEBRA-3	0.373	0.930	1.012	0.999	1.023
Average of C/E		1.009 (1.026)	1.058 (1.072)	1.063 (1.078)	—	(1.066)
Standard deviation of C/E		0.127	0.117	0.127	—	(0.136)
U	VERA-1B	0.399	1.139	1.147	1.202	1.186
	ZPR-3-6F	0.53	0.923	0.962	1.000	1.005
	ZEBRA-2	0.237	1.012	1.095	1.094	1.092
	ZPR-3-11	0.34	0.959	1.040	1.034	1.065
	Average of C/E	—	1.008	1.061	1.083	1.087
	Standard deviation of C/E	—	0.082	0.069	0.077	0.065
All	Average of C/E	—	1.009 (1.020)	1.059 (1.068)	1.069 (1.080)	(1.074)
	Standard deviation of C/E	—	0.115	0.105	0.114	(0.117)

\* Taken from Ref. (12).

\*\* Omitted in statistical analyses.

**Table 2.6** Ratio of  $^{238}\text{U}$  capture rate to  $^{235}\text{U}$  fission rate at core center.  
Values in parenthesis are averaged over 10 assemblies selected  
by Hardie *et al.*

Fuel	Assembly	Experimental	Calculated (C/E)			
			JENDL-1	JFS-2	ENDF/B-IV	ENDF/B-IV* (Hardie <i>et al.</i> )
Pu	SNEAK-7A	0.1376	0.963	0.963	0.986	0.979
	MZA	0.1314	1.019	1.016	1.040	—
	ZPR-3-48	0.138	0.953	0.953	0.974	0.963
	MZB	0.1351	1.020	1.017	1.047	—
	ZPR-6-7	0.136	1.016	1.015	1.046	1.044
	SNEAK-7B	0.131	1.011	1.006	1.033	1.025
	Average of C/E	0.997 (0.986)	0.995 (0.984)	1.021 (1.010)	—	(1.003)
Standard deviation of C/E			0.028	0.027	0.029	—
U	VERA-1B	0.131	0.967	0.962	0.976	0.927
	ZPR-3-6F	0.104	0.975	0.987	0.953	0.919
	ZPR-3-12	0.123	0.984	0.975	0.982	0.954
	ZPR-6-6A	0.139	1.005	0.999	1.029	1.017
	ZEBRA-2	0.136	0.972	0.965	0.988	0.968
	ZPR-3-11	0.112	0.993	0.996	0.978	0.949
	Average of C/E	0.983	0.981	0.984	—	0.956
Standard deviation of C/E			0.013	0.014	0.023	0.032
All	Average of C/E	0.990 (0.984)	0.988 (0.982)	1.003 (0.995)	—	(0.975)
	Standard deviation of C/E	0.023	0.023	0.032	—	(0.040)

\* Taken from Ref. (12).

**Table 2.7** Ratio of  $^{238}\text{U}$  capture rate to  $^{239}\text{Pu}$  fission rate at core center.  
Values in parenthesis are averaged over 9 assemblies selected  
by Hardie *et al.*

Fuel	Assembly	Experimental	Calculated (C/E)			
			JENDL-1	JFS-2	ENDF/B-IV	ENDF/B-IV* (Hardie <i>et al.</i> )
Pu	SNEAK-7A	0.135	1.021	1.014	1.034	1.026
	MZA	0.1297	1.061	1.048	1.068	—
	ZPR-3-48	0.141	0.983	0.972	0.993	0.970
	MZB	0.1424	1.060	1.047	1.074	—
	ZPR-6-7	0.143	1.072	1.063	1.091	1.086
	SNEAK-7B	0.129	1.054	1.035	1.051	1.046
	Average of C/E	1.042 (1.033)	1.030 (1.021)	1.052 (1.042)	—	(1.032)
Standard deviation of C/E			0.031	0.030	0.032	(0.042)
U	VERA-1B	0.122	0.918	0.912	0.920	0.873
	ZPR-3-6F	0.085	0.975	0.976	0.940	0.901
	ZPR-3-12	0.110	1.012	0.986	0.987	0.958
	ZEBRA-2	0.138	0.986	0.965	0.980	0.961
	ZPR-3-11	0.094	1.035	1.022	1.000	0.962
	Average of C/E	0.985	0.972	0.965	—	0.931
	Standard deviation of C/E	0.040	0.036	0.030	—	0.037
All	Average of C/E	1.016 (1.006)	1.004 (0.994)	1.012 (1.000)	—	(0.976)
	Standard deviation of C/E	0.045	0.044	0.053	—	(0.064)

\* Taken from Ref. (12).

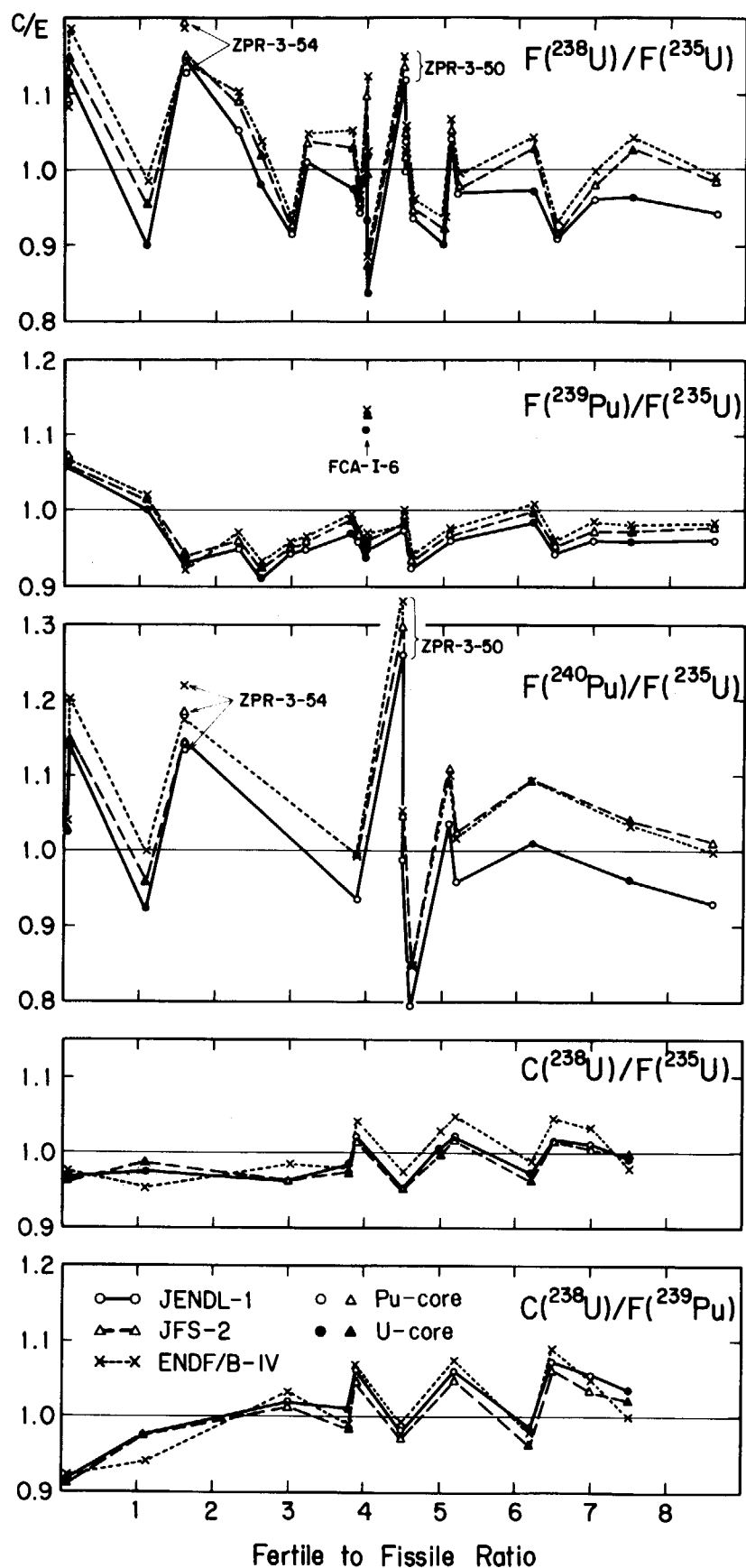


Fig. 2.2 C/E values of central reaction rate ratios vs. fertile to fissile ratio.

## 2.5 Central Reactivity Worth

### 2.5.1 Absolute Value

The central reactivity worths were calculated for  $^{239}\text{Pu}$  and  $^{235}\text{U}$  with the first-order perturbation approximation by changing the number density in the central small region. The calculated results are given in unit of  $\% \Delta k/k$  and the conversion coefficients to inhour were taken from Ref. (12). Therefore the calculations were restricted to 17 assemblies\* given in Ref. (12). The correction factors from 1-D to 2-D calculation were also taken from Ref. (12), which were calculated with ENDF/B-III.

The calculated results for  $^{239}\text{Pu}$  are given in **Table 2.8**. The average C/E value in the Pu-cores is about 15% larger than that in the U-cores with all the three sets. The same tendency was observed for  $^{235}\text{U}$  as shown in **Table 2.9**. The discrepancies between the Pu- and U- cores are larger than the standard deviation for Pu- or U- core. Hence these discrepancies seem to be systematic errors, some of which might be caused by the errors in the conversion coefficients between inhour and  $\% \Delta k/k$ . Furthermore very strong correlation is observed in the  $^{239}\text{Pu}$  and  $^{235}\text{U}$ - sample worths in each core as seen in **Fig. 2.3**.

In order to avoid this scaling problem, both the calculated and measured reactivity worths were normalized to those of  $^{239}\text{Pu}$ . The discrepancies between the Pu- and U- cores disappear with this normalization as seen in **Fig. 2.3**. It is also expected that the correction factor from 1-D to 2-D calculation could be cancelled considerably with the normalization.

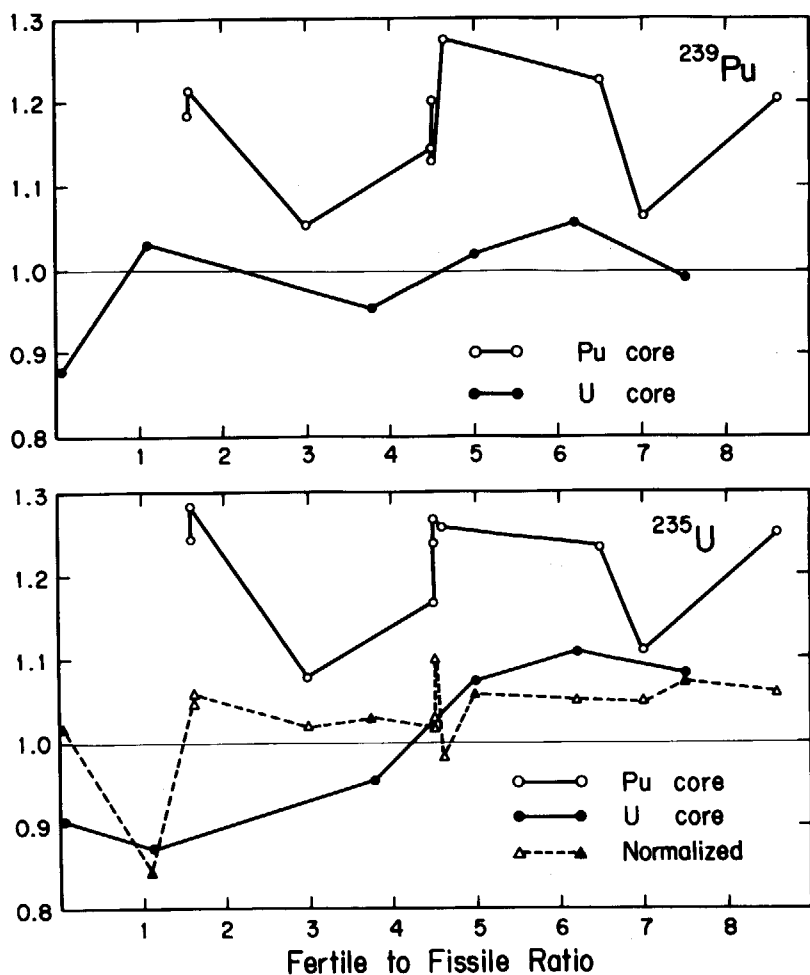


Fig. 2.3 C/E values of central reactivity worths of  $^{239}\text{Pu}$  and  $^{235}\text{U}$  vs. fertile to fissile ratio.

\* ZPPR-2 was omitted, because 1-D cylinder model was adopted.

**Table 2.8** Central reactivity worths of  $^{239}\text{Pu}$ 

Fuel	Assembly	Experimental* Inhour/kg	Factor* 1D → 2D	Inhour* %Δk/k	Calculated (C/E)		
					JENDL-1	JFS-2	ENDF/B-IV* (Hardie <i>et al.</i> )
Pu	VERA-11A	—	—	925.5	—	—	—
	ZPR-3-54**	738	1.048	968.8	1.184**	1.439**	1.475**
	ZPR-3-53	681	1.043	950.3	1.216	1.203	1.247
	SNEAK-7A	1023	0.917	911.8	1.056	1.037	1.051
	ZPR-3-50	564	1.049	930.1	1.145	1.140	1.158
	ZPR-3-48	445	0.994	932.5	1.202	1.177	1.178
	ZPR-3-49	415	1.049	934.4	1.131	1.104	1.102
	ZPR-3-56B	372	1.064	975.6	1.275	1.277	1.290
	ZPPR-2	120	1.000	963.4	—	—	1.133**
	ZPR-6-7	158	1.004	972.5	1.228	1.214	1.222
	SNEAK-7B	584	0.965	843.7	1.065	1.053	1.052
	ZEBRA-3	1144	0.985	837.9	1.204	1.181	1.160
	Average of C/E				1.169	1.154	1.162
	Standard deviation of C/E				0.071	0.074	0.079
U	VERA-1B	674	0.974	376.9	0.879	0.876	0.920
	ZPR-3-6F	452	1.002	407.2	1.029	0.983	0.984
	ZPR-3-12	436	0.995	427.6	0.954	0.958	0.945
	ZPR-6-6A	57	1.003	431.9	1.020	1.046	1.043
	ZEBRA-2	195	0.987	442.3	1.057	1.086	1.089
	ZPR-3-11	411	0.988	462.6	0.991	0.992	1.011
	Average of C/E				0.988	0.990	0.999
	Standard deviation of C/E				0.058	0.066	0.057
All	Average of C/E				1.097	1.088	1.097
All	Standard deviation of C/E				0.110	0.107	0.107

\* Taken from Ref. (12).

\*\* Omitted in statistical analyses.

**Table 2.9** Central reactivity worths of  $^{235}\text{U}$ 

Fuel	Assembly	Experimental* Inhour/kg	Factor* 1D → 2D	Inhour* %Δk/k	Calculated (C/E)		
					JENDL-1	JFS-2	ENDF/B-IV* (Hardie <i>et al.</i> )
Pu	VERA-11A	—	—	—	—	—	—
	ZPR-3-54**	567	1.047	1.246**	1.396**	1.552**	1.552**
	ZPR-3-53	520	1.045	1.287	1.173	1.338	1.338
	SNEAK-7A	757	0.918	1.077	1.026	1.055	1.055
	ZPR-3-50	464	1.049	1.168	1.101	1.169	1.169
	ZPR-3-48	334	0.994	1.239	1.174	1.189	1.189
	ZPR-3-49	282	1.049	1.267	1.197	1.205	1.205
	ZPR-3-56B	295	1.063	1.254	1.217	1.239	1.239
	ZPPR-2	90	1.001	—	—	1.249**	1.249**
	ZPR-6-7	133	1.004	1.233	1.180	1.204	1.204
	SNEAK-7B	435	0.965	1.110	1.063	1.068	1.068
	ZEBRA-3	721	0.986	1.250	1.199	1.173	1.173
	Average of C/E				1.209	1.148	1.182
	Standard deviation of C/E				0.070	0.064	0.080
U	VERA-1B	391	0.974	0.903	0.886	0.914	0.914
	ZPR-3-6F	320	1.002	0.847	0.800	0.813	0.813
	ZPR-3-12	285	0.996	0.953	0.937	0.952	0.952
	ZPR-6-6A	42	1.003	1.072	1.064	1.081	1.081
	ZEBRA-2	140	0.987	1.107	1.100	1.110	1.110
	ZPR-3-11	246	0.989	1.068	1.047	1.062	1.062
	Average of C/E				0.992	0.972	0.989
	Standard deviation of C/E				0.096	0.107	0.105
All	Average of C/E				1.122	1.078	1.105
All	Standard deviation of C/E				0.134	1.120	0.131

\* Taken from Ref. (12).

\*\* Omitted in statistical analyses.

### 2.5.2 Normalized Worth

The reactivity worths normalized to those of  $^{239}\text{Pu}$  are given in **Tables 2.10 ~ 2.18**. The fertile to fission ratio dependences are shown in **Figs. 2.4** and **2.5**. The calculated worths are obtained as the ratio of the perturbation cross sections, and the experimental data are given as the ratio of the worths in unit of inhour/mol. ZPR-3-6F were omitted in the statistical analyses, because extremely inconsistent values appeared between the worths of  $^{235}\text{U}$  and  $^{238}\text{U}$ . We also omitted VERA-11A and VERA-1B, which have very small core volume and often give very extreme C/E values.

#### a) Uranium-235

JENDL-1 overestimates the worths by 5% on an average. Little discrepancy is observed between the Pu- and U-cores. The other sets also overestimate the worths. This overestimate of the  $^{235}\text{U}$  worths normalized to the  $^{239}\text{Pu}$  worth is consistent with the underestimate of the fission rate ratio of  $^{239}\text{Pu}$  to  $^{235}\text{U}$  mentioned in section 2.4.

#### b) Uranium-238

JENDL-1 overestimates the worths of  $^{238}\text{U}$  by 4% on an average, while the other sets underestimate them. The discrepancy of 9% is observed with JENDL-1 between the Pu- and U-cores. The worth in ZPR-3-54 is higher than that in ZPR-3-53 with JENDL-1, while the opposite tendency is observed with the other sets. This is consistent with the observation in  $k_{\text{eff}}$ , as discussed in section 2.3; the iron cross sections of JENDL-1 allow less leakage and enhance the high energy spectrum.

#### c) Boron-10

JENDL-1 underestimates the worths of  $^{10}\text{B}$  by 8%. The other sets also underestimate them. Particularly the underestimate reaches 15% with ENDF/B-IV. The C/E values with JFS-2 are very similar to those with JENDL-1 in the Pu-cores and to those with ENDF/B-IV in the U-cores as seen in **Fig. 2.4**.

#### d) Sodium and Aluminium

The reactivity worths are very small for the light scattering materials such as carbon, oxygen, sodium and aluminium. The sign of the reactivity often changes according to the core composition as seen in **Tables 2.13** and **2.14**. Therefore it is not a good way to compare the worths of such nuclides as the C/E ratio. Hence the C/E values of sodium and aluminium worths should be read only as references.

#### e) Chromium, Iron and Nickel

It is rather difficult to well predict the reactivity worths of the structural material such as chromium, iron and nickel, since the relatively large component due to elastic and inelastic scattering depends strongly on the real and adjoint fluxes which are determined mainly by the cross sections of fissile and fertile materials.

JENDL-1 excellently predicts the worths of chromium, while the other sets overestimate them by more than 30%. As to the worths of iron the prediction with JFS-2 seems to be best, while JENDL-1 underestimates them by 10% and ENDF/B-IV overestimates them by 10%. The worths of nickel are overestimated by about 10% with any set.

**Table 2.10** Central reactivity worths of  $^{235}\text{U}$  normalized to those of  $^{239}\text{Pu}$ 

Fuel	Assembly	Experimental*	Calculated (C/E)			
			JENDL-1	JFS-2	ENDF/B-IV	ENDF/B-IV** (Hardie <i>et al.</i> )
Pu	VERA-11A***	0.551	1.116	1.091	1.097	—
	ZPR-3-54***	0.755	1.052	0.972	1.071	1.052
	ZPR-3-53	0.751	1.058	0.974	1.084	1.073
	SNEAK-7A	0.726	1.021	0.986	1.011	1.004
	ZPR-3-50	0.809	1.020	0.967	1.023	1.009
	ZPR-3-48	0.738	1.030	0.997	1.025	1.009
	ZPR-3-49	0.675	1.108	1.072	1.092	1.093
	ZPR-3-56B	0.779	0.985	0.956	0.975	0.960
	ZPPR-2	0.737	1.126	1.091	1.119	1.102
	ZPR-6-7	0.827	1.005	0.973	0.999	0.985
	SNEAK-7B	0.726	1.050	1.020	1.027	1.015
	ZEBRA-3	0.620	1.036	1.014	1.020	1.011
Average of C/E			1.044	1.005	1.037	1.026
Standard deviation of C/E			0.042	0.043	0.043	0.045
U	VERA-1B***	0.571	1.023	1.008	0.993	0.993
	ZPR-3-6F***	0.678	0.844	0.836	0.830	0.826
	ZPR-3-12	0.622	1.030	1.009	1.011	1.007
	ZPR-6-6A	0.719	1.058	1.025	1.042	1.036
	ZEBRA-2	0.703	1.050	1.018	1.028	1.019
	ZPR-3-11	0.589	1.075	1.054	1.058	1.050
Average of C/E			1.053	1.027	1.035	1.028
Standard deviation of C/E			0.016	0.017	0.018	0.016
All	Average of C/E	1.046	1.011	1.037	1.027	
All	Standard deviation of C/E	0.037	0.039	0.038	0.039	

\* Ratio of reactivity worths in unit of inhour/mol.

\*\* Deduced from the absolute values given in Ref. (12).

\*\*\* Omitted in statistical analyses.

**Table 2.11** Central reactivity worths of  $^{238}\text{U}$  normalized to those of  $^{239}\text{Pu}$ 

Fuel	Assembly	Experimental*	Calculated (C/E)			
			JENDL-1	JFS-2	ENDF/B-IV	ENDF/B-IV** (Hardie <i>et al.</i> )
Pu	VERA-11A***	0.0070	4.064	3.170	2.795	—
	ZPR-3-54***	-0.1106	0.910	0.755	0.714	0.691
	ZPR-3-53	-0.1098	0.882	0.885	0.842	0.817
	SNEAK-7A	-0.0385	1.140	1.100	1.075	1.129
	ZPR-3-50	-0.0743	0.914	0.876	0.844	0.813
	ZPR-3-48	-0.0528	0.970	0.907	0.882	0.874
	ZPR-3-49	-0.0448	1.059	1.001	0.979	0.937
	ZPR-3-56B	-0.0493	1.099	1.020	0.983	0.947
	ZPPR-2	—	—	—	—	—
	ZPR-6-7	-0.0686	0.913	0.864	0.833	0.829
	SNEAK-7B	-0.0413	1.142	1.097	1.074	1.063
	ZEBRA-3	-0.0313	1.006	0.979	0.957	0.872
Average of C/E			1.014	0.970	0.941	0.920
Standard deviation of C/E			0.095	0.087	0.090	0.105
U	VERA-1B***	0.0194	1.758	1.384	1.482	1.174
	ZPR-3-6F***	0.0060	2.126	2.114	2.543	2.651
	ZPR-3-12	-0.0265	1.137	1.029	1.011	0.944
	ZPR-6-6A	-0.0614	1.170	1.045	1.087	1.072
	ZEBRA-2	-0.0545	1.028	0.922	0.952	0.912
	ZPR-3-11	-0.0316	1.076	1.038	1.021	0.943
Average of C/E			1.103	1.009	1.018	0.968
Standard deviation of C/E			0.055	0.050	0.048	0.062
All	Average of C/E	1.041	0.982	0.965	0.935	
All	Standard deviation of C/E	0.094	0.080	0.087	0.097	

\* Ratio of reactivity worths in unit of inhour/mol.

\*\* Deduced from the absolute values given in Ref. (12).

\*\*\* Omitted in statistical analyses.

**Table 2.12** Central reactivity worths of  $^{10}\text{B}$  normalized to those of  $^{239}\text{Pu}$ 

Fuel	Assembly	Experimental*	Calculated (C/E)			
			JENDL-1	JFS-2	ENDF/B-IV	ENDF/B-IV** (Hardie <i>et al.</i> )
Pu	ZPR-3-54***	-2.405	0.683	0.664	0.588	0.574
	ZPR-3-53	-2.398	0.672	0.718	0.637	0.602
	SNEAK-7A	-0.788	0.986	1.010	0.931	0.916
	ZPR-3-50	-1.298	0.850	0.882	0.788	0.742
	ZPR-3-48	-0.839	0.902	0.904	0.829	0.807
	ZPR-3-49	-0.710	0.947	0.953	0.885	0.852
	ZPR-3-56B	-0.788	0.881	0.872	0.797	0.797
	ZPR-2	-0.791	0.993	0.987	0.895	0.879
	ZPR-6-7	-0.779	1.006	1.006	0.910	0.895
	SNEAK-7B	-0.541	1.013	1.010	0.949	0.943
	ZEBRA-3	-0.330	0.911	0.885	0.876	0.869
Average of C/E		0.916	0.923	0.850	0.830	
Standard deviation of C/E		0.097	0.087	0.087	0.095	
U	VERA-1B***	-0.612	1.123	1.082	1.065	1.021
	ZPR-3-6F***	-0.333	1.076	0.996	0.966	0.947
	ZPR-6-6A	-0.963	0.973	0.905	0.900	0.861
	ZEBRA-2	-0.966	0.808	0.751	0.747	0.705
	ZPR-3-11	-0.345	1.011	0.954	0.935	0.915
	Average of C/E	0.931	0.870	0.861	0.827	
Standard deviation of C/E		0.088	0.086	0.082	0.089	
All	Average of C/E	0.919	0.910	0.852	0.829	
All	Standard deviation of C/E	0.095	0.089	0.086	0.094	

\* Ratio of reactivity worths in unit of inhour/mol.

\*\* Deduced from the absolute values given in Ref. (12).

\*\*\* Omitted in statistical analyses.

**Table 2.13** Central reactivity worths of Sodium normalized to those of  $^{239}\text{Pu}$ 

Fuel	Assembly	Experimental*	Calculated (C/E)			
			JENDL-1	JFS-2	ENDF/B-IV	ENDF/B-IV** (Hardie <i>et al.</i> )
Pu	ZPR-3-53	0.00818	1.858	1.420	0.553	0.385
	ZPR-3-50	0.01928	0.609	0.430	0.065	-
	ZPR-3-48	-0.00137	1.510	1.641	2.248	1.743
	ZPR-3-49	0.00323	1.678	0.740	-1.402	0.945
	ZPR-3-56B	-0.00231	1.732	1.739	2.027	1.477
	ZPPR-2	-0.00414	0.931	0.981	1.111	0.951
	ZPR-6-7	-0.00412	0.909	0.972	1.099	0.923
	ZEBRA-3	-0.00881	1.119	0.952	1.080	1.003
	Average of C/E	1.293	1.109	0.848	1.061	
	Standard deviation of C/E	0.431	0.423	1.078	0.404	
U	VERA-1B***	0.00336	4.336	4.139	4.091	0.368
	ZPR-3-6F***	0.01239	0.425	0.449	0.372	0.313
	ZPR-6-6A	0.00027	0.341	-1.749	-0.805	-
	ZEBRA-2	0.00144	3.103	2.777	3.534	-0.330
	ZPR-3-11	-0.00335	1.539	1.329	1.593	1.680
	Average of C/E	1.661	0.786	1.441	0.675	
	Standard deviation of C/E	1.131	1.887	1.774	1.005	
All	Average of C/E	1.393	1.021	1.009	0.975	
All	Standard deviation of C/E	0.715	1.060	1.332	0.614	

\* Ratio of reactivity worths in unit of inhour/mol.

\*\* Deduced from the absolute values given in Ref. (12).

\*\*\* Omitted in statistical analyses.

**Table 2.14** Central reactivity worths of Aluminium normalized to those of  $^{239}\text{Pu}$ 

Fuel	Assembly	Experimental*	Calculated (C/E)		
			JENDL-1	JFS-2	ENDF/B-IV
Pu	ZPR-3-48	-0.00399	1.272	1.125	1.272
	ZPPR-2	-0.00566	1.094	1.013	1.095
	ZPR-6-7	-0.00479	1.268	1.184	1.278
	ZEBRA-3	-0.0107	0.995	0.840	0.899
	Average of C/E		1.157	1.041	1.136
	Standard deviation of C/E		0.118	0.131	0.155
U	VERA-1B**	0.00904	1.244	1.068	1.076
	ZPR-3-6F**	0.00089	0.791	0.938	0.477
	ZPR-3-12	-0.00159	1.439	1.322	1.719
	ZEBRA-2	-0.00278	1.484	1.326	1.408
	ZPR-3-11	-0.00478	1.373	1.172	1.352
	Average of C/E		1.432	1.273	1.493
All	Standard deviation of C/E		0.046	0.072	0.161
	Average of C/E		1.275	1.140	1.289
	Standard deviation of C/E		0.165	0.159	0.237

\* Ratio of reactivity worths in unit of inhour/mol.

\*\* Omitted in statistical analyses.

**Table 2.15** Central reactivity worths of Chromium normalized to those of  $^{239}\text{Pu}$ 

Fuel	Assembly	Experimental*	Calculated (C/E)		
			JENDL-1	JFS-2	ENDF/B-IV
Pu	ZPR-3-53	-0.00323	0.896	1.384	1.519
	ZPR-3-50	-0.00505	1.208	1.558	1.627
	ZPR-3-48	-0.00602	1.033	1.328	1.391
	ZPR-3-49	-0.00625	1.099	1.375	1.431
	ZPR-3-56B	-0.00745	0.852	1.065	1.106
	ZPPR-2	-0.00615	1.027	1.273	1.310
	ZPR-6-7	-0.00623	1.002	1.250	1.284
	Average of C/E		1.017	1.319	1.381
	Standard deviation of C/E		0.111	0.140	0.157
	ZPR-3-6F***	-0.00213	0.552	1.246	1.448
U	ZEBRA-2	-0.00617	1.022	1.392	1.424
	ZPR-3-11	-0.00813	0.989	1.217	1.285
	Average of C/E		0.989	1.305	1.355
	Standard deviation of C/E		0.016	0.088	0.070
All	Average of C/E		1.014	1.316	1.375
	Standard deviation of C/E		0.098	0.129	0.143

\* Ratio of reactivity worths on unit of inhour/mol.

\*\* Deduced from the absolute values given in Ref. (12).

\*\*\* Omitted in statistical analyses.

**Table 2.16** Central reactivity worths of Iron normalized to those of  $^{239}\text{Pu}$ 

Fuel	Assembly	Experimental*	Calculated (C/E)			
			JENDL-1	JFS-2	ENDF/B-IV	
Pu	ZPR-3-53	-0.00154	1.129	1.161	1.610	1.814
	SNEAK-7A	-0.00781	0.693	0.778	0.850	0.821
	ZPR-3-50	-0.00547	1.027	1.124	1.219	1.148
	ZPR-3-48	-0.00646	0.924	1.017	1.092	1.061
	ZPR-3-49	-0.00802	0.854	0.922	0.977	0.922
	ZPR-3-56B	-0.00772	0.766	0.818	0.866	0.805
	ZPPR-2	-0.00614	0.904	0.962	1.012	1.028
	ZPR-6-7	-0.00630	0.869	0.930	0.977	0.988
	SNEAK-7B	-0.00851	0.920	1.021	1.062	1.025
	Average of C/E	0.898	0.970	1.074	1.068	
U	Standard deviation of C/E		0.122	0.120	0.217	0.284
	ZPR-3-6F***	-0.00349	0.772	1.009	1.200	0.988
	ZPR-3-12	-0.00584	0.919	1.160	1.243	1.160
	ZEBRA-2	-0.00617	0.942	1.162	1.188	1.176
	ZPR-3-11	-0.00813	1.049	1.176	1.264	1.247
	Average of C/E	0.970	1.166	1.232	1.194	
	Standard deviation of C/E	0.057	7.273	0.032	0.038	
	Average of C/E	0.916	1.019	1.113	1.100	
	Standard deviation of C/E	0.113	0.134	0.201	0.252	

\* Ratio of reactivity worths on unit of inhour/mol.

\*\* Deduced from the absolute values given in Ref. (12).

\*\*\* Omitted in statistical analyses.

**Table 2.17** Central reactivity worths of Nickel normalized to those of  $^{239}\text{Pu}$ 

Fuel	Assembly	Experimental*	Calculated (C/E)			
			JENDL-1	JFS-2	ENDF/B-IV	
Pu	ZPR-3-53	-0.00739	1.318	1.073	1.137	1.103
	ZPR-3-50	-0.00940	1.179	1.174	1.207	1.153
	ZPR-3-48	-0.01006	1.125	1.161	1.185	1.181
	ZPR-3-49	-0.01283	0.997	1.025	1.034	1.074
	ZPR-3-56B	-0.01109	1.013	1.038	1.047	1.008
	ZPPR-2	-0.00974	1.016	1.063	1.065	1.090
	ZPR-6-7	-0.01003	0.975	1.026	1.026	1.051
	Average of C/E	1.089	1.080	1.100	1.094	
	Standard deviation of C/E	0.116	0.058	0.070	0.054	
	ZPR-3-6F***	-0.00655	1.651	1.524	1.615	1.679
U	ZPR-3-12	-0.01070	1.153	1.283	1.217	1.146
	ZEBRA-2	-0.01255	0.879	1.004	0.925	0.872
	ZPR-3-11	-0.01148	1.190	1.311	1.351	1.308
	Average of C/E	1.074	1.199	1.164	1.109	
	Standard deviation of C/E	0.139	0.139	0.178	0.180	
	Average of C/E	1.084	1.116	1.119	1.099	
	Standard deviation of C/E	0.123	0.105	0.117	0.109	

\* Ratio of reactivity worths on unit of inhour/mol.

\*\* Deduced from the absolute values given in Ref. (12).

\*\*\* Omitted in statistical analyses.

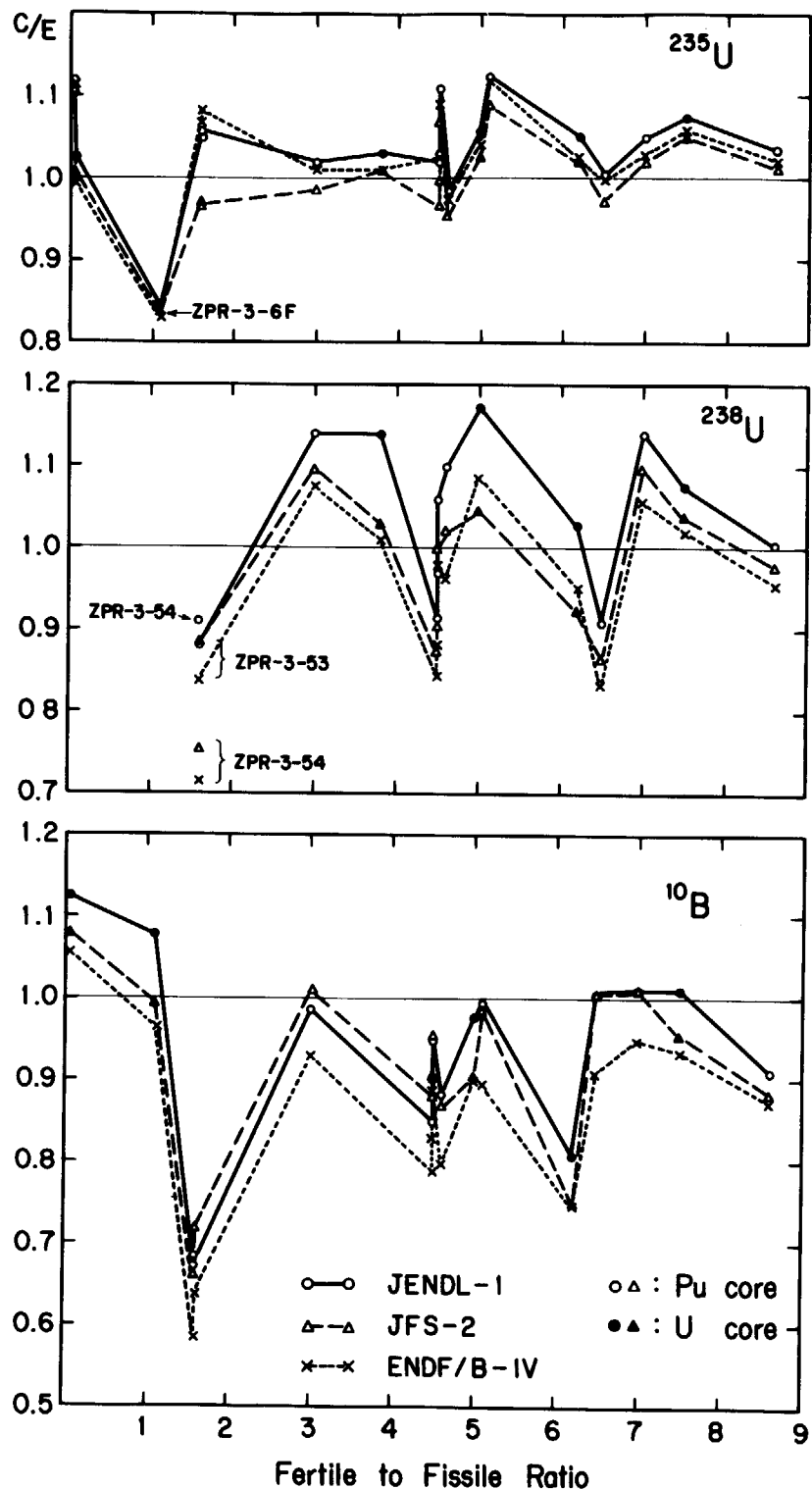
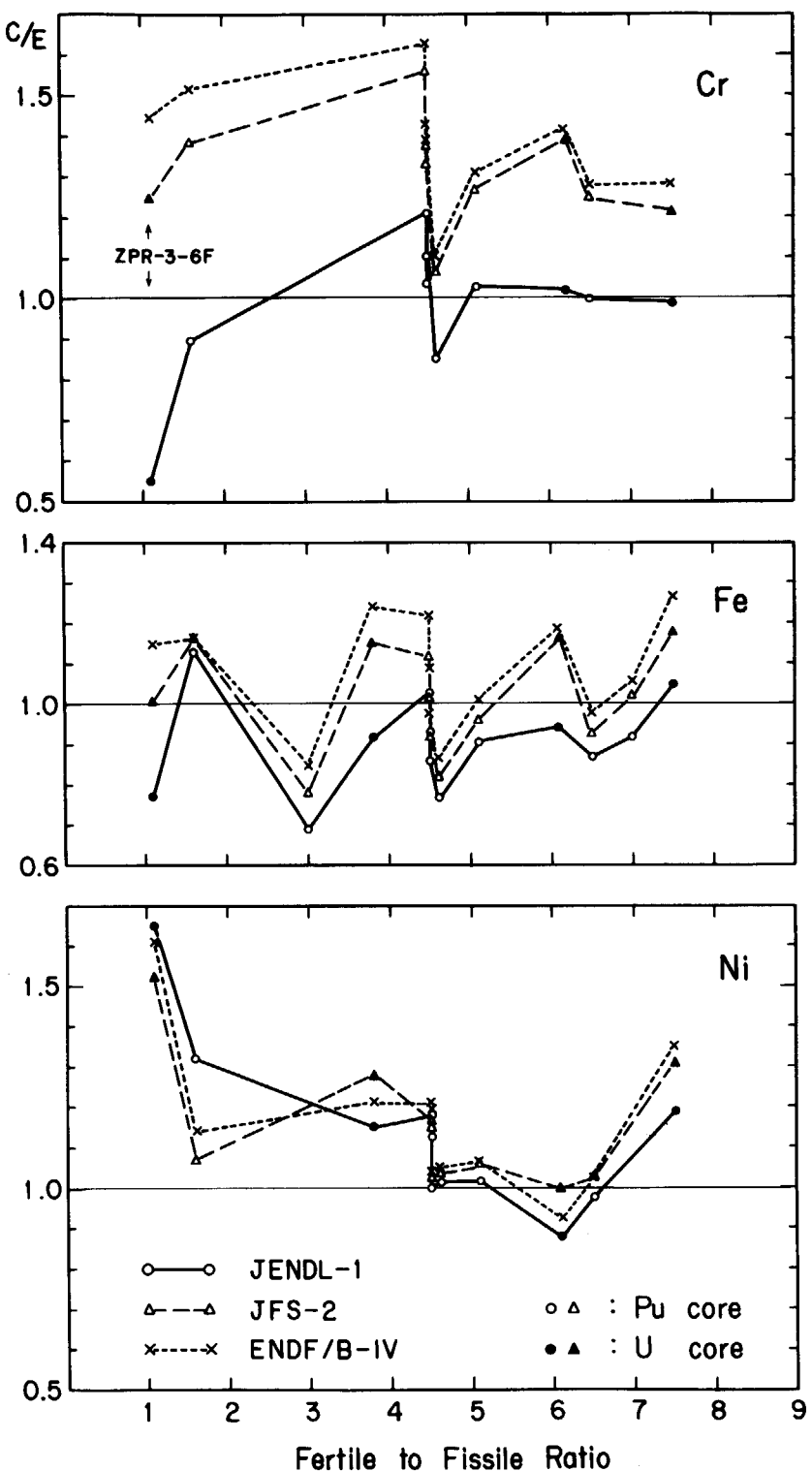


Fig. 2.4 C/E values of central reactivity worths of  $^{235}\text{U}$ ,  $^{238}\text{U}$  and  $^{10}\text{B}$  normalized to those of  $^{239}\text{Pu}$ .



**Fig. 2.5** C/E values of central reactivity worths of Cr, Fe and Ni normalized to those of  $^{239}\text{Pu}$ .

**Table 2.18** Central reactivity worths of Molybdenum normalized to those of  $^{239}\text{Pu}$ 

Fuel	Assembly	Experimental*	Calculated (C/E)		
			JENDL-1	JFS-2	ENDF/B-IV
Pu	ZPR-3-48	-0.0391	1.127	1.264	1.239
	ZPPR-2	-0.0436	1.029	1.142	1.106
	ZPR-6-7	-0.0390	1.148	1.281	1.238
	Average of C/E		1.101	1.229	1.194
	Standard deviation of C/E		0.052	0.062	0.062
U	ZPR-3-6F**	-0.0139	1.182	1.241	1.281
	ZPR-3-12	-0.0277	1.104	1.186	1.217
	ZPR-3-11	-0.0244	0.997	1.175	1.210
	Average of C/E		1.050	1.180	1.213
	Standard deviation of C/E		0.053	0.005	0.003
All	Average of C/E		1.081	1.209	1.202
	Standard deviation of C/E		0.058	0.054	0.049

\* Ratio of reactivity worths in unit of inhour/mol.

\*\* Omitted in statistical analyses.

## 2.6 Doppler Coefficient

We analyzed the small sample Doppler measurements in FCA-V-1, V-2, VI-1, VI-2, ZPPR-2 and ZPR-3-47, and the whole core Doppler measurements at SEFOR. The analysis was made with EXPANDA-70D<sup>10)</sup> on the basis of one dimensional model and the first-order perturbation approximation.

The C/E values of Doppler coefficients are given in **Table 2.19**. JENDL-1 overestimates the coefficients by 8%, while JFS-2 and ENDF/B-IV underestimate them by about 10%. The C/E-values are reported<sup>7)</sup> to increase slightly when two-dimensional model is applied. Hence the overestimation with JENDL-1 may be about 10%.

The calculated neutron spectra were compared in order to know the cause of the discrepancy of 20% between JENDL-1 and JFS-2. **Figure 2.6** shows the spectra for ZPPR-2. JENDL-1 gives higher flux in the energy range from 1 keV to 10 keV where the Doppler effects are predominant.

**Table 2.19** Doppler reactivity coefficients (C/E)

	Assembly	JENDL-1	JFS-2	ENDF/B-IV
Small Sample Doppler Experiment	FCA V-1	1.09	0.78	0.91
	V-2	0.98	0.74	0.78
	VI-1	1.13	0.94	0.93
	VI-2	1.03	0.90	0.87
	ZPPR-2 (Normal)	1.25	1.08	0.93
	(Na-voided)	0.96	0.81	0.81
Whole Core Doppler Experiment	ZPR-3-47	1.04	0.95	0.92
	SEFOR	1.12	1.05	1.04
	Average of C/E	1.08	0.91	0.90
Standard Deviation of C/E		0.09	0.12	0.08

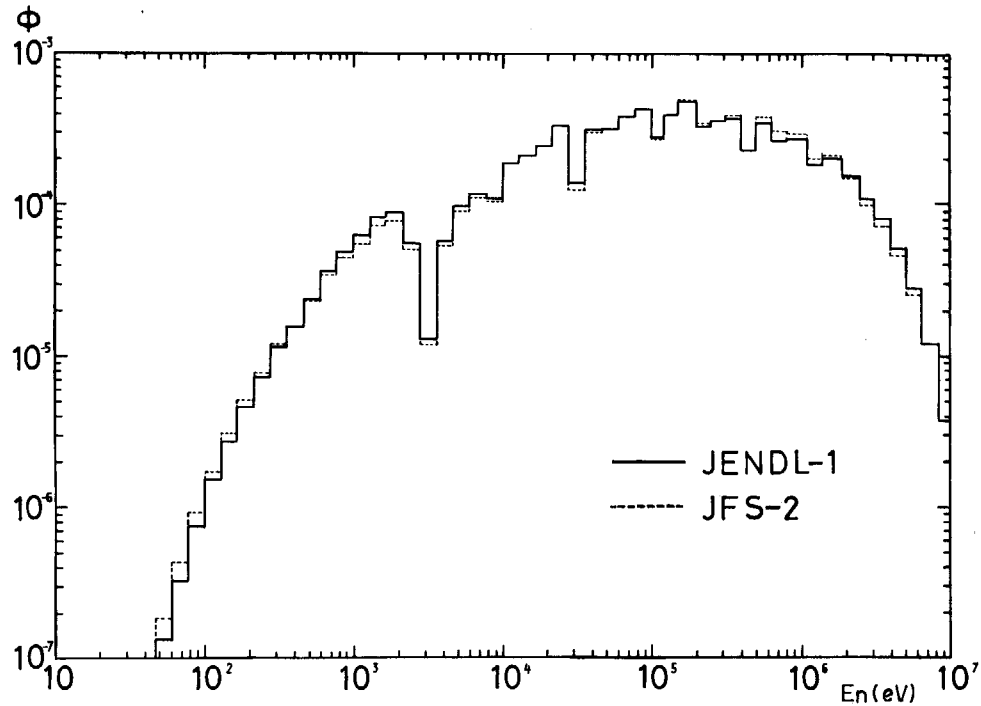


**Fig. 2.6** Spectrum at core center of ZPPR-2 calculated with JENDL-1 and JFS-2.

## 2.7 Analysis of Snell Experiments

Measurements of average cross sections in a natural uranium equilibrium spectrum were first carried out by Snell et al.<sup>16)</sup>, and this type of experiment is generally called Snell experiment. Considerable number of experimental data are now available for the average fission rate ratio of  $^{235}\text{U}$  to  $^{238}\text{U}$ ,  $^{237}\text{Np}$  to  $^{238}\text{U}$  and  $^{239}\text{Pu}$  to  $^{238}\text{U}$ . They are summarized by Chezem<sup>17)</sup>.

In the present tests, the fission rate ratios of  $^{235}\text{U}$  to  $^{238}\text{U}$  and  $^{239}\text{Pu}$  to  $^{238}\text{U}$  were calculated with the equilibrium spectrum, which were calculated at the depth of 190 cm in a hypothetical large natural uranium blanket of 200 cm thickness attached to the core of FCA-V-II.

The calculated values were compared with the experimental data compiled in Ref. (17) in **Table 2.20**. The fission rate ratio of  $^{235}\text{U}$  to  $^{238}\text{U}$  calculated with JENDL-1 agrees well with the data of Chezem<sup>17)</sup>, but the calculated ratio of  $^{239}\text{Pu}$  to  $^{238}\text{U}$  is lower than the experimental data. Both the ratios calculated with JFS-2 are about 8% lower than those with JENDL-1. The calculated ratios of  $^{235}\text{U}$  to  $^{238}\text{U}$  are larger than the ratios of  $^{239}\text{Pu}$  to  $^{238}\text{U}$ , while the experimental data show an opposite tendency except for the data of Leipunsky et al.<sup>21)</sup> which were measured in the depleted uranium. This discrepancy seems to be consistent with the underestimate of the fission rate ratio of  $^{239}\text{Pu}$  to  $^{235}\text{U}$  in the core center as discussed in section 2.4. This problem should be further investigated.

**Table 2.20** Fission rate ratios in natural uranium equilibrium spectra

	$\frac{^{235}\text{U fission}}{^{238}\text{U fission}}$	$\frac{^{239}\text{Pu fission}}{^{238}\text{U fission}}$
JENDL-1	240.8	220.0
JFS-2	226.7	206.0
ENDF/B-IV	227.7	203.4
Experiments*		
Snell et al. (1943, U Chicago) <sup>16)</sup>	200	
Brolley et al. (1943, ORNL) <sup>18)</sup>	336	
Beyer et al. (1955, ANL) <sup>19)</sup>	363 ± 40	
Neuer et al. (1955, LASL) <sup>20)</sup>	220 ± 22 <sup>a)</sup> 200 ± 10 <sup>b)</sup> 210 ± 10 <sup>c)</sup>	228 ± 12
Leipunsky et al. (1958, USSR) <sup>21)</sup>	249 ± 20	230
Campan et al. (1958, Saclay) <sup>22)</sup>	221 ± 11	
Chezem (1960, LASL) <sup>17)</sup>	239 ± 7	250 ± 16

\* Taken from Ref. (17)

a) Foil activation

b) Radiochemistry

c) Fission chambers

### 3. Benchmark Tests with Two-dimensional Model

After completion of the benchmark tests on the core center characteristics with the one-dimensional model, applicability of JENDL-1 was further tested to more sophisticated problems such as reaction rate distributions, sodium void reactivities and control rod worths. The MOZART and ZPPR-3 assemblies were selected for these tests. The analyses were made on the basis of the two-dimensional model and the first-order or exact perturbation method. The cell heterogeneity corrections were made with the integral transport theory. The anisotropy of the diffusion coefficients were considered according to Benoist's method.<sup>23)</sup>

The calculation started from the ABBN type reactor constants of 25 group structure because of limitation of codes which treat the cell heterogeneity. Hence the library of 70 group structure was collapsed to that of 25 group structure by using the reactor integrated spectrum of ZPPR-2. This collapse may cause some errors particularly in the elastic removal cross sections in the blanket region.

The analyses of MOZART and ZPPR-3 were performed by Mitsubishi Atomic Power Industries Inc. and Nippon Atomic Industry Group Co., Ltd., respectively.

#### 3.1 MOZART

The MOZART program is a Japan-U.K. joint research work for the mock-up critical experiments of the Japanese prototype fast breeder reactor "MONJU". Neutronics characteristics were studied in three core configurations; MZA, MZB and MZC. The MZA core is a one-zone core simulating the outer core of MONJU for basic studies of reactor physics. The MZB core is a mock-up of the clean two-zone core of MONJU and the MZC core is an extention of MZB by adding control rod positions.

In the present study, analyses were made for the reaction rate distributions and the sodium void reactivities in the MZB core and the control rod worths in the MZC core.

##### 3.1.1 Reaction Rate Distribution in MZB

Fission and capture reaction rate distributions were measured in the radial direction at the core midplane in MZB using the foils of  $^{235}\text{U}$ ,  $^{238}\text{U}$  and the fission chambers of  $^{235}\text{U}$ ,  $^{238}\text{U}$ ,  $^{239}\text{Pu}$  and  $^{240}\text{Pu}$ . Axial scans were also made at the core center position. The measurements were reviewed by Ingram et al.<sup>24)</sup>

The calculation of the reaction rate distributions was made on the basis of the X-Y and R-Z diffusion model with 6 groups. The six-group cross sections were reduced with the spectra obtained by one-dimensional diffusion calculations in radial and axial directions. The group structure is given in **Table 3.1**. The X-Y calculation model of MZB is shown in **Fig. 3.1**. Axial bucklings at the core midplane for the X-Y calculation were obtained from the R-Z calculation. Corrections for the group collapsing and for diffusion-versus-transport approximation were obtained from one-dimensional calculations and were applied to the results of the six-group diffusion calculations.

The calculated radial distributions of  $^{235}\text{U}$ ,  $^{238}\text{U}$ ,  $^{239}\text{Pu}$  and  $^{240}\text{Pu}$  fission rates and  $^{238}\text{U}$  capture rate are compared with the measured data in **Tables 3.2 ~ 3.6** and also shown in **Fig. 3.2**. The fission rates of  $^{235}\text{U}$  and  $^{239}\text{Pu}$  are underestimated in the outer core and the blanket. Though this underestimation is observed with other sets, it is significant with

JENDL-1. On the other hand, the fission rate of  $^{240}\text{Pu}$  is overestimated in the outer core and the blanket. The C/E values stay near unity for the fission and capture rates of  $^{238}\text{U}$ .

**Table 3.1** Energy group structure of collapsed group cross sections used for analyses of MOZART

For reaction rate distribution and control rod worth			For sodium void reactivity		
Group No.	E <sub>max</sub> (eV)	E <sub>min</sub> (eV)	Group No.	E <sub>max</sub> (eV)	E <sub>min</sub> (eV)
1	1.05 + 7*	1.4 + 6	1	1.05 + 7	6.5 + 6
2	1.4 + 6	1.0 + 5	2	6.5 + 6	4.0 + 6
3	1.0 + 5	1.0 + 4	3	4.0 + 6	2.5 + 6
4	1.0 + 4	1.0 + 3	4	2.5 + 6	1.4 + 6
5	1.0 + 3	1.0 + 2	5	1.4 + 6	8.0 + 5
6	1.0 + 2	Thermal	6	8.0 + 5	4.0 + 5
			7	4.0 + 5	2.0 + 5
			8	2.0 + 5	1.0 + 5
			9	1.0 + 5	4.65 + 4
			10	4.65 + 4	2.15 + 4
			11	2.15 + 4	1.0 + 4
			12	1.0 + 4	4.65 + 3
			13	4.65 + 3	2.15 + 3
			14	2.15 + 3	1.0 + 3
			15	1.0 + 3	4.65 + 2
			16	4.65 + 2	Thermal

\*  $1.05 + 7$  denotes  $1.05 \times 10^7$

**Table 3.2** Radial fission rate traverse of  $^{235}\text{U}$  with fission chamber in MZB

Radius (cm)	Calculation	Correction Factor		Corrected Calculation	Experiment	C/E
		Collapsing	Transport			
I/C	0.0	1.0000	1.0	1.0000	1.0000	1.000
	10.85	0.9889	1.0	0.9889	0.9866	1.002
	21.70	0.9553	1.0	0.9553	0.9532	1.002
	32.55	0.8995	1.0	0.8995	0.8955	1.004
	43.40	0.8216	1.0	0.8216	0.8110	1.014
	48.83	0.7742	1.0	0.7742	0.7669	1.010
O/C	54.25	0.7208	1.0	0.7244	0.7080	1.023
	59.68	0.6610	1.0	0.6676	0.6528	1.023
	65.11	0.5928	1.0	0.6023	0.5855	1.029
	70.53	0.5259	1.0	0.5354	0.5298	1.011
R/B	75.96	0.4671	1.0	0.4741	0.4820	0.984
	81.37	0.4452	0.989	0.4421	0.4627	0.955
	86.81	0.3928	0.984	0.3857	0.4228	0.912
	92.23	0.3217	0.990	0.3169	0.3631	0.873
	97.66	0.2555	0.997	0.2535	0.2973	0.853
	103.10	0.2032	1.009	0.2040	0.2479	0.823
	108.50	0.1755	1.006	0.1755	0.2155	0.815

**Table 3.3** Radial fission rate traverse of  $^{238}\text{U}$  with fission chamber in MZB

	Radius (cm)	Calculation	Correction Factor		Corrected Calculation	Experiment	C/E
			Collapsing	Transport			
I/C	0.0	1.0000	1.0	1.0	1.0000	1.0000	1.000
	10.85	0.9892	1.0	1.0	0.9892	0.9843	1.005
	21.70	0.9565	1.0	1.0	0.9565	0.9481	1.009
	32.55	0.9035	1.0	1.0	0.9035	0.8968	1.007
	43.40	0.8341	1.0	1.0	0.8341	0.8215	1.015
	48.83	0.7958	1.0	1.0	0.7958	0.7859	1.013
	54.25	0.7581	1.0	1.0	0.7581	0.7456	1.017
	59.68	0.7255	1.0	1.003	0.7277	0.7219	1.008
O/C	65.11	0.7098	1.0	1.040	0.7382	0.7145	1.033
	70.53	0.6271	1.0	1.047	0.6566	0.6423	1.022
	75.96	0.4908	1.0	1.054	0.5173	0.4977	1.039
R/B	81.37	0.2690	1.005	0.941	0.2544	0.2704	0.941
	86.81	0.1430	1.027	0.933	0.1370	0.1378	0.994
	92.23	0.07946	1.002	0.955	0.07604	0.0774	0.982
	97.66	0.04567	0.981	0.988	0.04426	0.0455	0.973
	103.10	0.02176	0.962	1.034	0.02702	0.0287	0.941
	108.50	0.01618	1.009	1.072	0.01750	0.0173	1.012

**Table 3.4** Radial capture rate traverse of  $^{238}\text{U}$  with foil detector in MZB

	Radius (cm)	Calculation	Correction Factor		Corrected Calculation	Experiment	C/E
			Collapsing	Transport			
I/C	0.0	1.0000	1.0	1.0	1.0000	1.0000	1.000
	10.85	0.9889	1.0	1.0	0.9889	0.9874	1.002
	21.70	0.9552	1.0	1.0	0.9552	0.9491	1.006
	32.55	0.8990	1.0	1.0	0.8990	0.8923	1.008
	43.40	0.8204	1.0	1.0	0.8204	0.8090	1.014
	48.83	0.7721	1.0	1.0	0.7721	0.7601	1.016
	54.25	0.7174	1.0	1.007	0.7224	0.7077	1.021
	59.68	0.6554	1.0	1.011	0.6626	0.6470	1.024
O/C	65.11	0.5886	1.0	1.015	0.5974	0.5861	1.019
	70.53	0.5207	1.0	1.016	0.5290	0.5171	1.023
	75.96	0.4626	1.0	1.013	0.4686	0.4652	1.007
R/B	81.37	0.3740	0.989	1.005	0.3717	0.3731	0.996
	86.81	0.3151	0.988	0.998	0.3107	0.3129	0.993
	92.23	0.2483	0.997	0.995	0.2463	0.2530	0.974
	97.66	0.1896	1.008	0.995	0.1902	0.1967	0.967
	103.10	0.1434	1.018	0.995	0.1453	0.1511	0.961
	108.50	0.1131	1.014	0.995	0.1141	0.1171	0.974

**Table 3.5** Radial fission rate traverse of  $^{239}\text{Pu}$  with fission chamber in MZB

Radius (cm)	Calculation	Correction Factor		Corrected Calculation	Experiment	C/E
		Collapsing	Transport			
I/C	0.0	1.0000	1.0	1.0000	1.0000	1.000
	10.85	0.9890	1.0	0.9890	0.9882	1.001
	21.70	0.9556	1.0	0.9556	0.9551	1.001
	32.55	0.9003	1.0	0.9003	0.8964	1.004
	43.40	0.8237	1.0	0.8237	0.8202	1.004
	48.83	0.7774	1.0	0.7774	0.7237	1.005
	54.25	0.7258	1.0	0.7302	0.7230	1.010
	59.68	0.6686	1.0	0.6753	0.6602	1.023
O/C	65.11	0.6037	1.0	0.6146	0.6009	1.023
	70.53	0.5337	1.0	0.5454	0.5403	1.010
	75.96	0.4640	1.0	0.4728	0.4834	0.978
R/B	81.37	0.4378	0.988	0.4330	0.4615	0.938
	86.81	0.3802	0.984	0.3726	0.4140	0.900
	92.23	0.3108	0.991	0.3065	0.3656	0.838
	97.66	0.2485	1.009	0.2495	0.3088	0.808
	103.10	0.2018	1.038	0.2084	0.2691	0.775
	108.50	0.1824	1.006	0.1828	0.2469	0.740

**Table 3.6** Radial fission rate traverse of  $^{240}\text{Pu}$  with fission chamber in MZB

Radius (cm)	Calculation	Correction Factor		Corrected Calculation	Experiment	C/E
		Collapsing	Transport			
I/C	0.0	1.0000	1.0	1.0000	1.0000	1.000
	10.85	0.9891	1.0	0.9891	0.9875	1.002
	21.70	0.9563	1.0	0.9563	0.9550	1.001
	32.55	0.9026	1.0	0.9026	0.8973	1.006
	43.40	0.8301	1.0	0.8301	0.8276	1.003
	48.83	0.7880	1.0	0.7880	0.7852	1.004
	54.25	0.7430	1.0	0.7467	0.7422	1.006
	59.68	0.6967	1.0	0.7016	0.7028	0.998
O/C	65.11	0.6685	1.0	0.6865	0.6669	1.029
	70.53	0.5870	1.0	0.6052	0.5914	1.023
	75.96	0.4764	1.0	0.4921	0.4713	1.044
R/B	81.37	0.3177	0.995	0.3114	0.3045	1.023
	86.81	0.2036	0.990	0.1965	0.1925	1.021
	92.23	0.1377	0.986	0.1331	0.1252	1.063
	97.66	0.09380	0.981	0.09119	0.08371	1.089
	103.10	0.06446	0.977	0.06304	0.05543	1.137
	108.50	0.04437	1.000	0.04481	0.03788	1.183

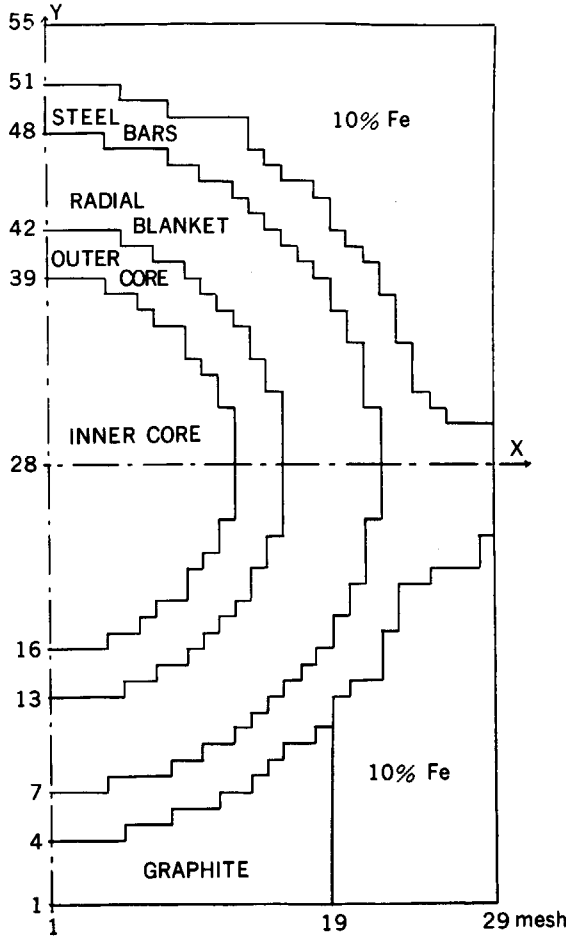


**Fig. 3.1** X-Y calculational model of MZB for reaction rate distribution analysis.

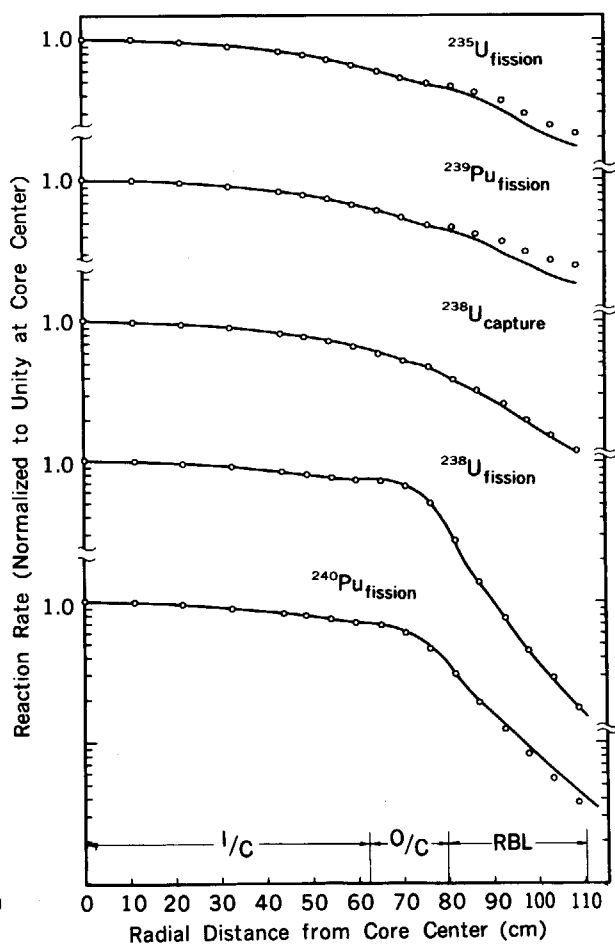


**Fig. 3.2** Reaction rate distributions in MZB.

### 3.1.2 Sodium Void Reactivity in MZB

Sodium void reactivities in MZB were measured at various positions in the axial and radial directions. Axial traverse measurements were made in the central nine elements at the core center. Radial traverse measurements were made by removing sodium of 9 elements in the core at six different positions shown in **Fig. 3.3**. The experimental condition and results are given in Ref. (25).

The calculated worths of sodium removal were obtained using a two-dimensional R-Z diffusion code with 16-group cross sections whose group structure is also given in **Table 3.1**. Both exact and first-order perturbation calculations were made to obtain reactivity components. The calculation model is shown in **Fig. 3.4**. Mesh arrangement and typical plate cells were indicated in the figure.

The calculated results are compared with the measured ones in **Tables 3.7** and **3.8**. The comparison is also shown in **Fig. 3.5**.

The following are observed:

- 1) The C/E value is 1.1 for void in the core center.
- 2) The calculation well predicts the sodium void worths in the axial direction.
- 3) The calculation overestimates the negative sodium void reactivities, when sodium is removed from the outer core. By examining the perturbation components, we considered that this might be caused by overestimation of the radial leakage component.

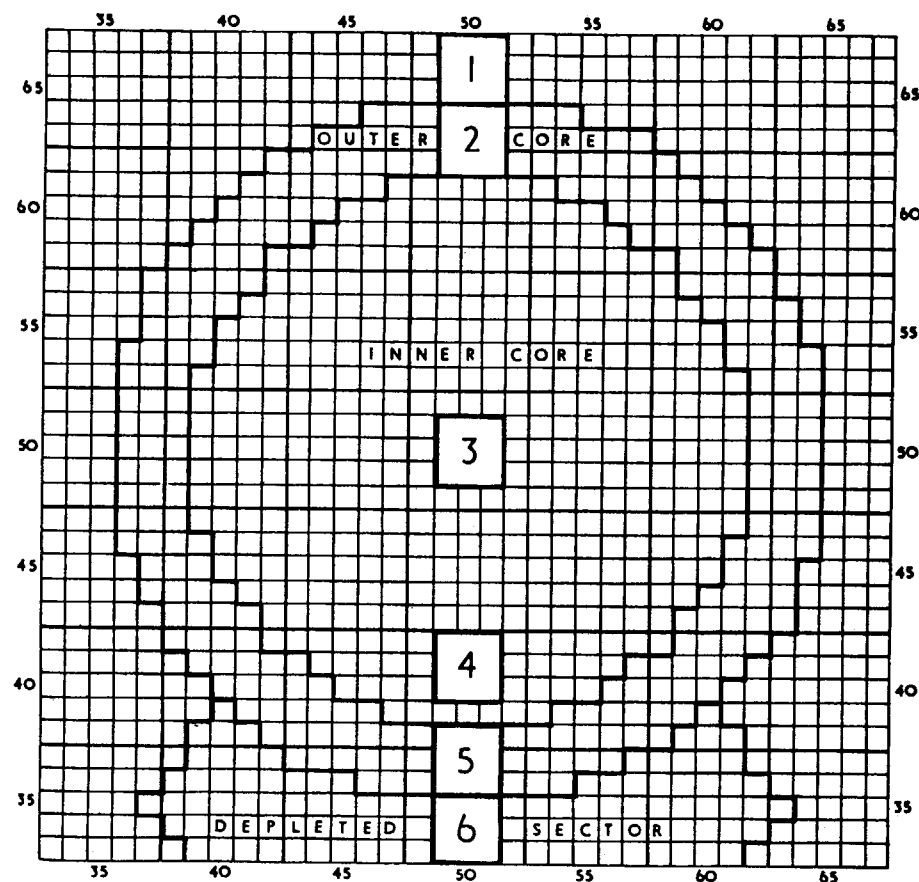


**Fig. 3.3** Positions of sodium removal measurements in MZB. Taken from Ref. (25).

**Table 3.7** Radial traverse of sodium void worth in 9 elements of MZB assembly

Void Position	Measured Worth	Perturbation Calculation						Direct Calc.	
		Total	Fission	Absorption	Moderation	Radial Leakage	Axial Leakage		
#3 Core Center	+231 ± 5	+223 +244	-97 -102	+167 +162	+478 +498	-2 -2	-323 -312	FP EP	+243
#4 I.C. Edge	+50 ± 5	+10	-58	+94	+269	-103	-191	FP	
#2 O.C.	-201 ± 5	-437 -335	-28 -32	+41 +40	+120 +126	-450 -360	-120 -109	FP EP	-335
#1 Rad. Bl.	-129 ± 2	-135 -118	-2 -3	+7 +7	+38 +39	-168 -151	-10 -10	FP EP	-120

\* FP: First order perturbation

EP: Exact perturbation

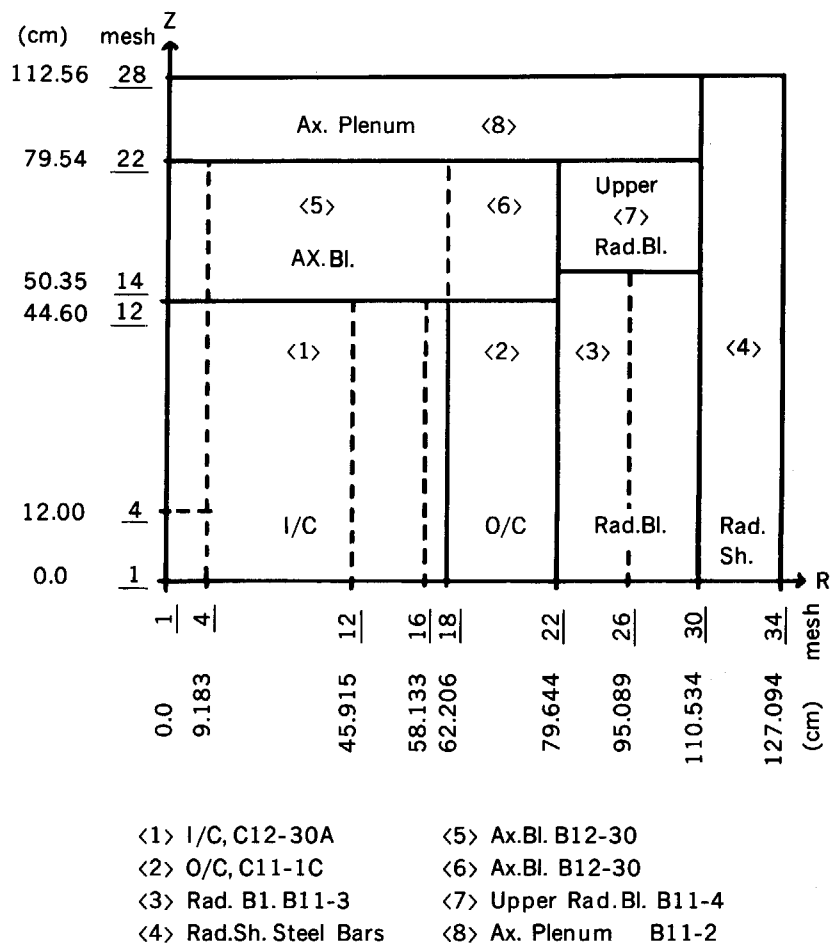


**Fig. 3.4** R-Z calculational model of MZB for sodium void worth analysis.

**Table 3.8** Axial traverse of sodium void worth in plate-type central 9 elements of MZB assembly

(in unit of  $10^{-6} \Delta\rho$ )

Void Position	Measured Worth	Perturbation Calculation							Direct Calc.
		Total	Fission	Absorption	Moderation	Radial Leakage	Axial Leakage	*	
0-12 cm Core Center	$+175 \pm 2$	+194	-38	+63	+178	-1	-8	FP	$+190$
		+198	-40	+62	+184	-1	-8	EP	
12-45 cm Core Edge	$+56 \pm 4$	+29	-59	+104	+300	-1	-315	FP	
		+29	-59	+104	+300	-1	-315	FP	
0-45 cm Core Height	$+231 \pm 5$	+223	-97	+167	+478	-2	-323	FP	$+243$
		+244	-102	+162	+498	-2	-312	EP	
45-80 cm Axial Bl.	$-76 \pm 3$	-86	-1	+13	+71	0	-169	FP	
0-80 cm All Element	$+149 \pm 6$	+137	-98	+180	+549	-2	-492	FP	$+181$
		+153	-103	+175	+572	-2	-487	EP	

\* FP: First order perturbation

EP: Exact perturbation

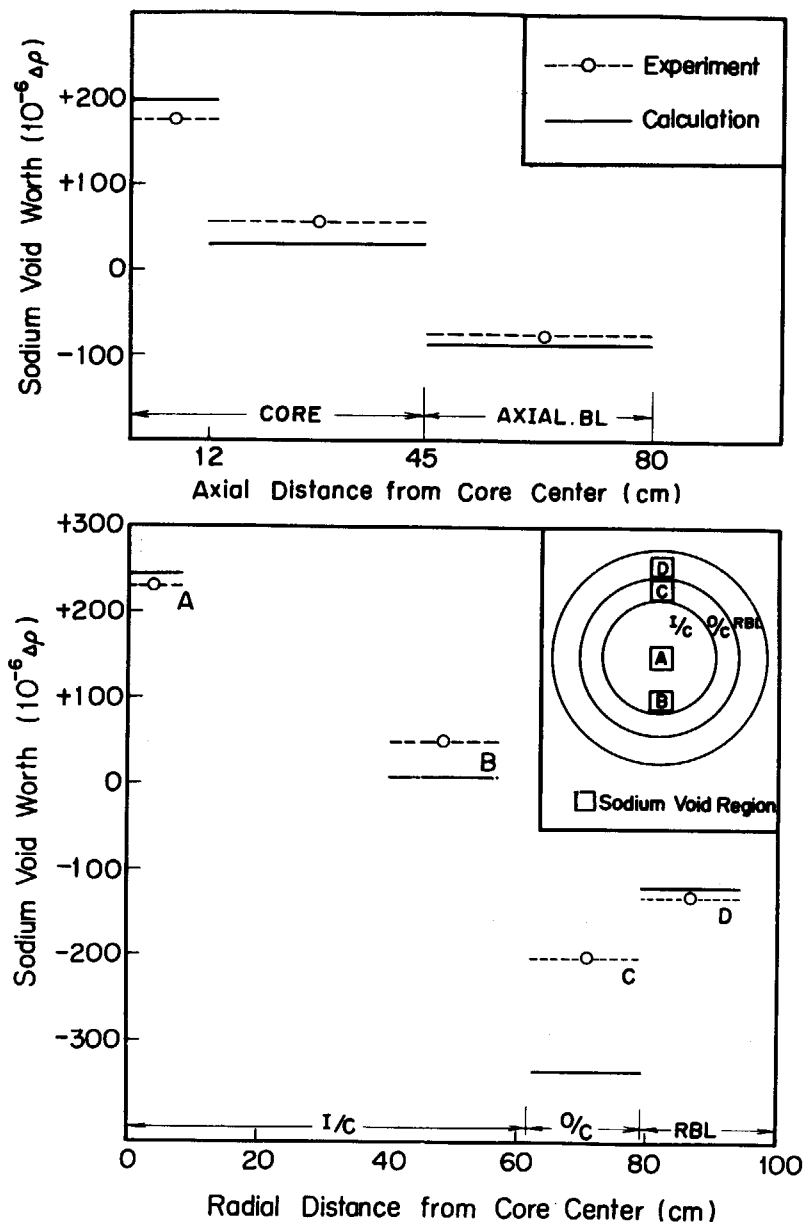


Fig. 3.5 Axial and radial traverses of sodium void worth in MZB.

### 3.1.3 Control Rod Worth in MZC

Analysis of control rod worths was made for a control rod inserted at the center of the MZC core. In the experiment, worths were measured for four types of control rod with different  $^{10}\text{B}$  enrichments (natural, 30% (weight), 80% (weight) and 90% (weight)) to study the C/E dependence on  $^{10}\text{B}$  content. The detail of measurements is given in Ref. (26).

The six-group cross sections for the fuel regions were prepared using 26-group flux spectra obtained with one-dimensional diffusion calculations in radial and axial directions. In producing the six-group cross sections for control rods, one-dimensional transport calculations were used to take into consideration the heterogeneous arrangement of  $\text{B}_4\text{C}$  pins in a control rod.

The basic calculations for the control rod worths were made with two-dimensional six-group diffusion calculation in the R-Z model containing a central control rod position shown in Fig. 3.6. Several correction factors listed in Table 3.9 were applied to the calculated rod worths.

Comparison between calculation and experiment is shown in **Table 3.10**. The C/E values are nearly 0.95, and show no apparent dependence on the enrichment of  $^{10}\text{B}$ , while the  $^{10}\text{B}$  enrichment dependence was often observed in analyses with other cross section sets except JFS-2.

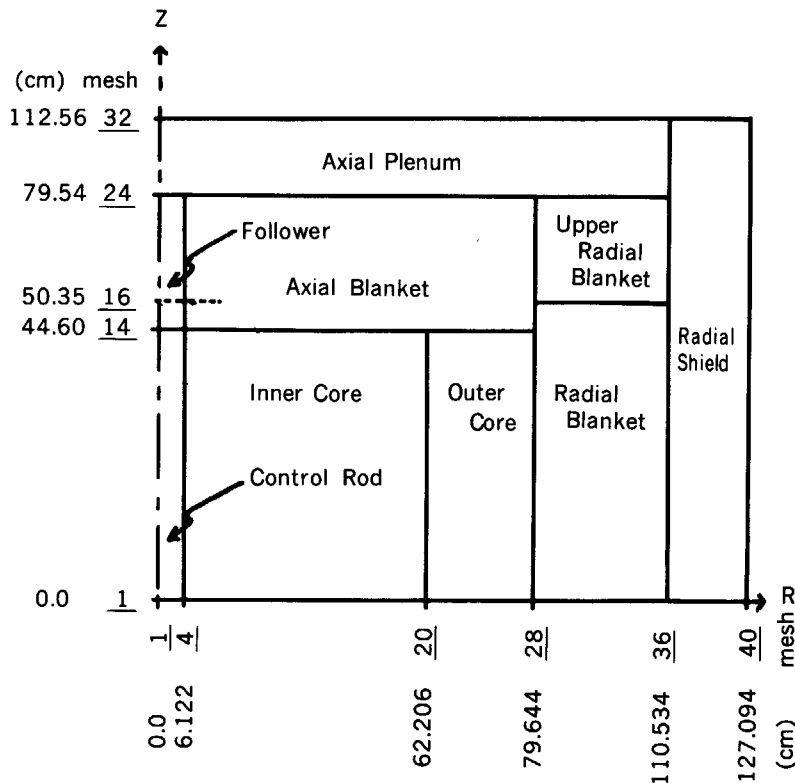


**Fig. 3.6** R-Z calculational model of MZC for control rod worth analysis.

**Table 3.9** Correction factors for MZC central control rod worth analysis

Rod Pattern	Pin ( $^{10}\text{B}$ ) Absorber Heterogeneity*	26 gr. to 6 gr.	2 reg. to 1 reg.*	$S_N$ **	Mesh	Total
BN	0.990	0.997	0.976	0.958	1.009	0.931
B30	0.989	0.997	0.973	0.949	1.011	0.920
B80	0.976	0.994	0.966	0.938	1.015	0.892
B90	0.977	0.994	0.964	0.930	1.016	0.885

\* Corrections for heterogeneity in control rods ( $\text{B}_4\text{C}$  mass lumping and pin heterogeneity)

\*\* Transport theory correction ( $S_4$  approximation was used.)

**Table 3.10** Results of MZC central control rod worth analysis

Rod Pattern	Experiment % $\Delta k/kk'$	Calculation with JENDL-1			
		without Correction % $\Delta k/kk'$	Correction Factor	with Correction % $\Delta k/kk'$	C/E
BN	$0.808 \pm 1.3\%$	0.822	0.931	0.765	0.947
B30	$0.993 \pm 1.4\%$	1.028	0.920	0.946	0.952
B80	$1.525 \pm 1.8\%$	1.638	0.892	1.461	0.958
B90	$1.629 \pm 1.9\%$	1.740	0.885	1.540	0.945

### 3.2 ZPPR-3

Items included in the present analysis are single and multiple control rod worth experiments in ZPPR-3 Phase 1B core and  $^{235}\text{U}$  fission rate distribution experiments in ZPPR-3 Phase 2 core.

The method of calculation is basically two-dimensional (X-Y) 7 group anisotropic diffusion theory. Spatial self-shielding calculations for plate heterogeneities were done using an integral transport theory code, and anisotropic diffusion coefficients were obtained with Benoist's first approximation<sup>23)</sup>. The cross sections for the control rod positions were calculated with the homogeneous model. The bucklings were calculated at  $Z = 6.1$  cm with the R-Z model. The group reduction from 25 to 7 groups was made with one-dimensional flux of ZPPR-3 Phase 1B or Phase 2 core. The group structure of 7 groups is given in **Table 3.11**.

**Table 3.11** Energy group structure of collapsed group cross sections used for analyses of ZPPR-3

Group No.	$E_{\min}$ (eV)	$E_{\max}$ (eV)
1	$1.05 + 7^*$	$1.4 + 6$
2	$1.4 + 6$	$4.0 + 5$
3	$4.0 + 5$	$1.0 + 5$
4	$1.0 + 5$	$1.0 + 4$
5	$1.0 + 4$	$1.0 + 3$
6	$1.0 + 3$	$1.0 + 2$
7	$1.0 + 2$	Thermal

\*  $1.05 + 7$  denotes  $1.05 \times 10^{+7}$

#### 3.2.1 Worth of Multiple Control Rods in Phase 1B Core

Phase 1B of ZPPR assembly 3 is the end-of-cycle configuration for the US demonstration plant. The assembly has 19 simulated control rod positions (CRP), all of which are sodium-filled channels. The control rod configuration is shown in **Fig. 3.7**. The control rod worth measurements were made by three different methods, i.e., inverse multiplication method, polarity coherence method and rod drop method. Details of measurements are given in Ref. (27).

Three different designs were adopted for the simulated control rods. The principal difference of design is the mass of  $\text{B}_4\text{C}$  loaded. Design H has 0.78 kg of natural  $\text{B}_4\text{C}$ , design I has 1.85 kg, and design J has 1.21 kg. Control rods of design H are inserted at the CRP's 2, 3, 4, 5, 6 and 7, design I at CRP's 8, 10, 12, 14, 16 and 18, and design J at CRP's 9, 11, 13, 15, 17 and 19.

The analysis was made with the two-dimensional diffusion model, and corrections were made for the transport, mesh and transverse buckling effects. **Table 3.12** shows the results of analysis for various control rod patterns in Phase 1B core. Results<sup>28)</sup> with JFS-2 set are also shown in the table for comparison. The C/E values show little dependence on the control rod pattern as seen in the table. The average of C/E is 0.96 with standard deviation of 2%, which agrees with the results for MZC.

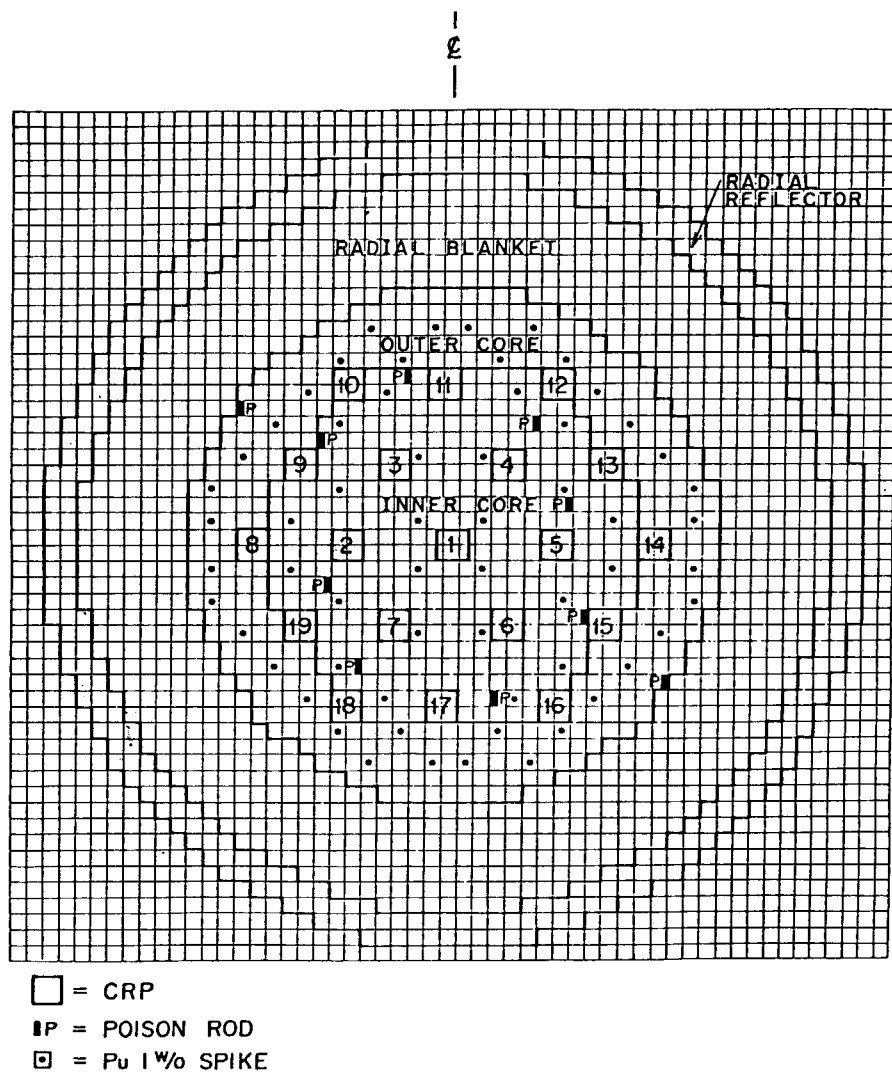


Fig. 3.7 ZPPR assembly 3, phase 1B, reference core.

Table 3.12 C/E values for control rod worth of ZPPR-3 phase 1B core

No.	Control Rod Positions Inserted	No. of C.R.	Measured Worth \$	$\beta_{\text{eff}}$	C/E Values	
					JFS-2	JENDL-1
$\times 10^{-3}$						
1 8		1	1.94	3.51	0.96	0.94
2 2		1	2.02	3.51	1.00	0.98
3 2, 8		2	3.58	3.51	—	0.95
4 Type-I in CRP-1		1	4.14	3.51	0.96	0.96
5 8, 14		2	4.24	3.51	0.97	0.99
6 2, 5		2	4.26	3.51	0.99	0.98
7 2, 4, 6		3	6.51	3.52	0.99	0.98
8 2, 4, 6, 10, 14, 18		6	14.33	3.54	0.97	0.98
9 8, 10, 12, 14, 16, 18		6	14.88	3.54	0.97	0.93
10 2, 3, 4, 5, 6, 7, 10, 14, 18		9	20.75	3.55	—	0.97
11 2, 4, 6, 8, 10, 12, 14, 16, 18		9	22.65	3.55	—	0.98
12 8, 9, 10, 11, 12, 13, 14, 15, 16, 17, 18, 19		12	28.96	3.57	0.99	0.97
13 2, 4, 6, 9, 10, 11, 13, 14, 15, 17, 18, 19		12	28.99	3.57	—	0.95
14 2, 3, 4, 5, 6, 7, 8, 10, 12, 14, 16, 18		12	30.12	3.57	—	0.95
15 All except CRP-1		18	44.76	3.61	—	0.95
Average and one standard deviation of C/E values					0.98 ± 0.01	0.96 ± 0.02

### 3.2.2 Fission Rate Distribution of $^{235}\text{U}$ in Phase 2 Core

Phase 2 core of ZPPR assembly 3 is the middle-of-cycle configuration for the US demoplant. Six simulated control rods are fully inserted in this core. The foil measurements were performed for the following three control rod patterns: (1) Three rods are inserted in the inner ring and three in the outer ring (Phase 2 Reference), (2) all of the six control rods are inserted in the inner ring (A.I.R), and (3) all of the six are inserted at the CRP positions of even numbers in the outer ring. (E.O.R.).

Analysis was made for the radial fission rate distribution measurements, in which foils are placed on the X-Y plane at about  $Z = 7.7$  cm. No correction was performed for the structure of in-cell flux distribution. The error due to neglect of this effect is estimated to be less than 1%. Transport effect was not taken into account in the present analysis.

**Figures 3.8 ~ 3.10** show the C/E distributions of  $^{235}\text{U}$  fission rate for the three rod patterns in Phase 2 core. The C/E values along X axis are shown in **Fig. 3.11**. The following are concluded as to the applicability of JENDL-1 library in the fission rate distribution prediction:

- 1) The calculation underestimates the fission rate in the outer core.
- 2) The underestimation is much enhanced when the control rods are inserted in the outer ring. The average C/E value is decreased down to 0.88.
- 3) The control rods have little effect on the C/E value of reaction rate distribution when inserted in the inner ring.

It is interesting to compare the present results with those obtained by using different cross section library sets. **Table 3.13** shows the maximum and minimum, and average C/E values obtained using the JENDL-1, JFS-2, and NNS-5<sup>29)</sup> sets for the above three core configurations. The average C/E values with JENDL-1 are relatively smaller than those with JFS-2 and NNS-5. Note that the C/E value with JENDL-1 is 0.92 in the case of E.O.R., while those with JFS-2 and NNS-5 are 0.98 and 0.97, respectively. The poor prediction of reaction rate distribution with JENDL-1 seems to come from too small diffusion coefficient and too large slowing down cross sections of JENDL-1 in the energy range from 10 keV to 1.4 MeV. The detailed discussion on this point will be made in Chapter 4 and Appendix 3.

**Table 3.13** Comparison of C/E values of  $^{235}\text{U}$  ( $n, f$ ) reaction rate distribution in outer core by using three different library sets

Case	JENDL-1			JFS-2			NNS-5		
	Max.	Min.	C/E $\pm\sigma$	Max.	Min.	C/E $\pm\sigma$	Max.	Min.	C/E $\pm\sigma$
<b>Phase 2</b>									
Reference Core	0.99	0.91	0.95 $\pm$ 0.02	1.02	0.96	0.98 $\pm$ 0.01	1.01	0.96	0.98 $\pm$ 0.01
A.I.R. Core	1.00	0.92	0.96 $\pm$ 0.02	1.03	0.94	0.98 $\pm$ 0.02	1.00	0.94	0.98 $\pm$ 0.01
E.O.R. Core	0.97	0.88	0.92 $\pm$ 0.02	1.02	0.94	0.98 $\pm$ 0.02	1.01	0.95	0.97 $\pm$ 0.02

Note:

- 1) Normalization between calculation and measurement is done at the position specified in Figs. 3.8 ~ 3.10. The C/E values at control rod channels are excluded in the statistical procedure.

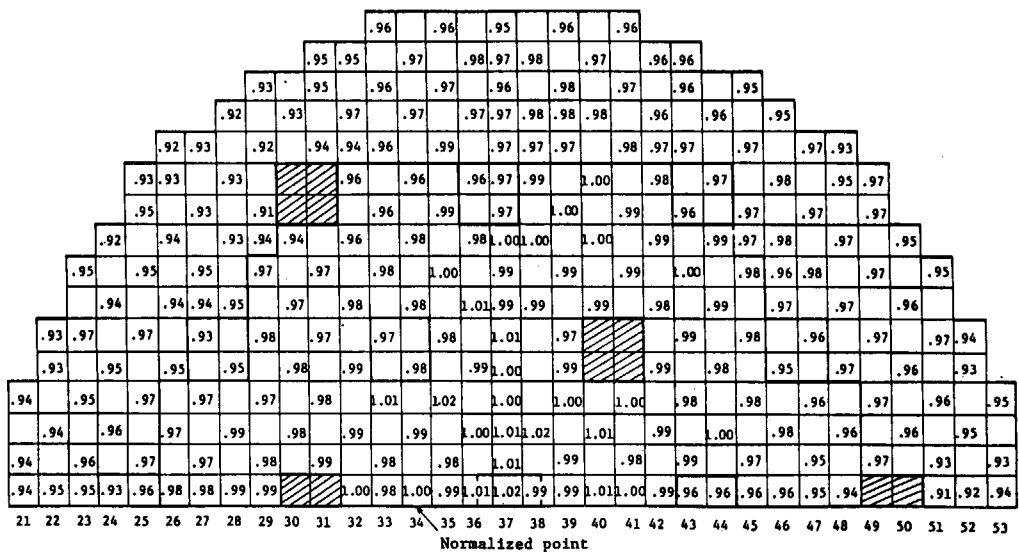


**Fig. 3.8** C/E values of  $^{235}\text{U}$  fission rate distribution in ZPPR-3 phase 2 reference core.

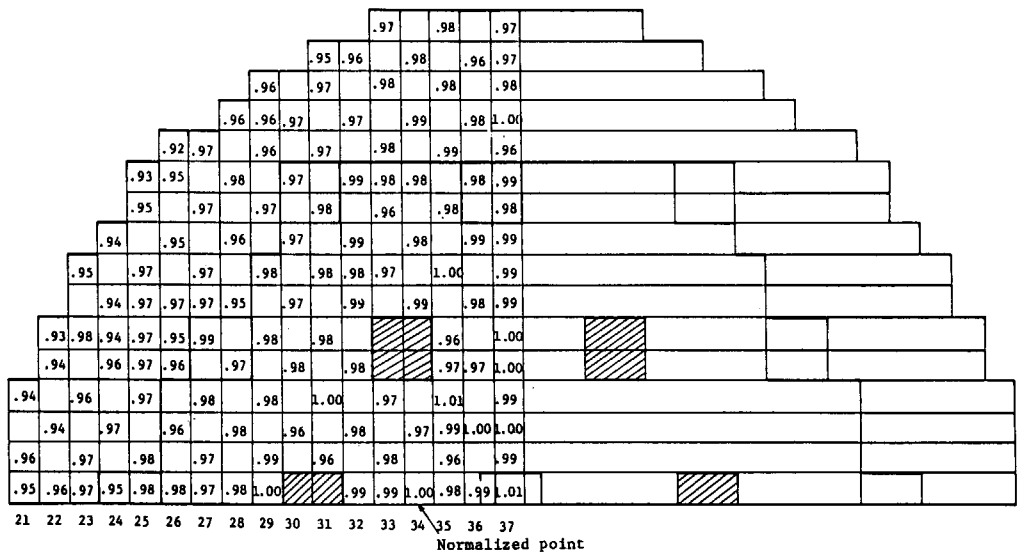


**Fig. 3.9** C/E values of  $^{235}\text{U}$  fission rate distribution in ZPPR-3 phase 2 A.I.R. core.

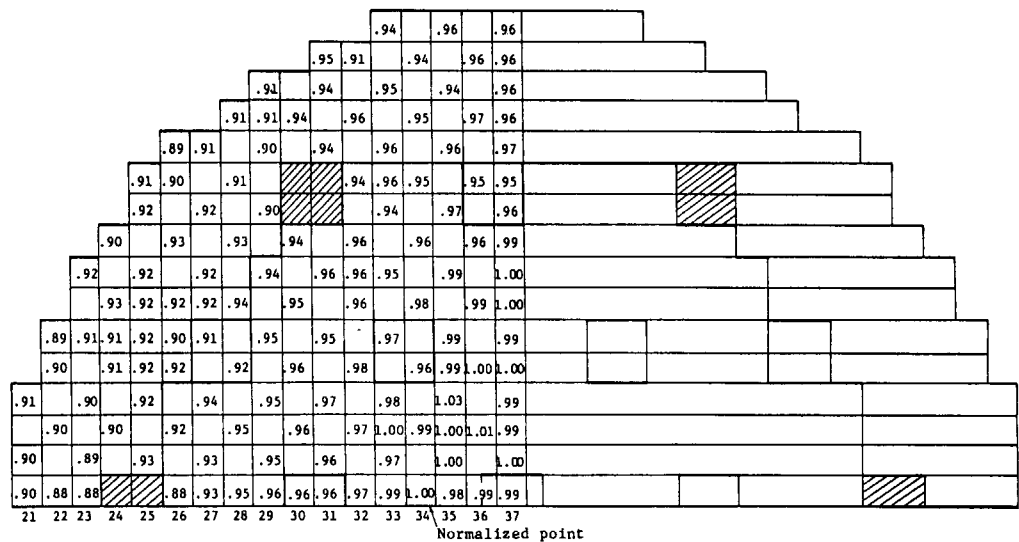


**Fig. 3.10** C/E values of  $^{235}\text{U}$  fission rate distribution in ZPPR-3 phase 2 E.O.R. core.

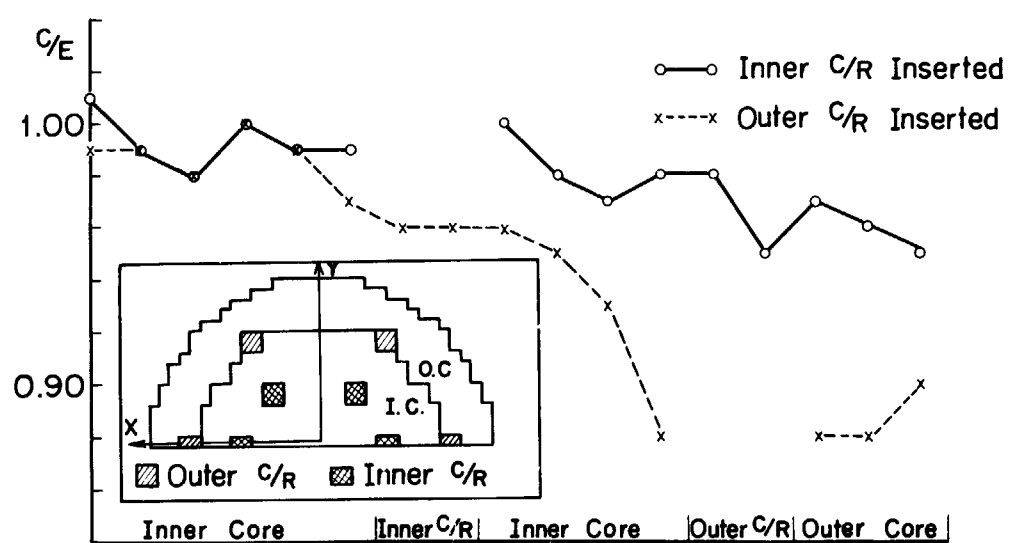


Fig. 3.11 Fission rate distribution along X-axis in ZPPR-3 phase 2 core.

## 4. Summary and Discussion

It has been proved through benchmark tests that JENDL-1 predicts various quantities of fast reactors satisfactorily as a whole. However, some problems have been pointed out through the tests. In this chapter, these problems are discussed, the possible drawbacks in the evaluation are pointed out and the way to their improvement is suggested.

### 4.1 Problems Encountered through Benchmark Tests

The following problems have been pointed out:

- 1) There exists discrepancy of 0.9% in the  $k_{\text{eff}}$ -values between the Pu- and U-cores. Most of this discrepancy comes from inconsistent  $\nu_p$ -values of  $^{252}\text{Cf}$  used as the standard in the evaluation.
- 2) The fission rate ratio of  $^{239}\text{Pu}$  to  $^{235}\text{U}$  is underestimated by 3%. This underestimate is also observed in JFS-2 and ENDF/B-IV.
- 3) Apparent discrepancies are observed in the central reactivity worths between the Pu- and U-cores. There might be some inconsistency in the delayed neutron parameters.
- 4) The Doppler reactivity coefficients are overestimated by about 10%.
- 5) The control rod worths are underestimated a little, but little dependence are observed on the  $^{10}\text{B}$  enrichment and on the number of the inserted rods.
- 6) The fission rates of  $^{235}\text{U}$  and  $^{239}\text{Pu}$  are underestimated considerably in the outer core and radial blanket regions. In the case of ZPPR-3, this underestimation is much enhanced, when the control rods are inserted in the outer core.
- 7) The sodium void reactivities are well predicted, but the negative reactivities are overestimated, when the sodium is removed from the outer core. This might be caused by the overestimation of radial leakage.

As a whole, most of problems of JENDL-1 occur in the outer core and blanket regions, and are related to the leakage and neutron spectrum.

### 4.2 Intercomparison of Macroscopic Cross Sections

The macroscopic cross sections were compared with other sets in some selected assemblies, in order to know the causes affecting the neutron leakage and spectrum. **Table A3.9** and **Figs. A3.12 ~ A3.14** in Appendix 3 should be referred as examples. It was pointed out that JENDL-1 had

- 1) smaller diffusion coefficient above 100 keV,
- 2) smaller inelastic removal cross section,
- 3) larger elastic removal cross section above 100 keV  
and
- 4) smaller elastic removal cross section below 1 keV.

From graphical comparison of group cross sections of JENDL-1, JFS-2 and ENDF/B-IV given in Appendix 4, it is seen that most of the differences in the macroscopic cross section come from the differences in the cross sections of structural materials such as chromium, iron and nickel. It has been pointed out<sup>30)</sup> through reevaluation work for JENDL-2 that JENDL-1 overestimated the total and elastic scattering cross sections of chromium, iron and

nickel in the energy range from a few hundred keV to a few MeV and underestimated the inelastic scattering cross sections of these nuclei. The overestimation of the total cross section was caused by adopting the calculated cross section with the optical model instead of following the fine structure of the cross section obtained from high resolution experiments. The optical model parameters adopted in JENDL-1 overestimate the total cross section below 1 MeV for these nuclei. Furthermore, ignorance of the fine structure up to a few MeV causes ignorance of the self-shielding effects. Hence the total and elastic scattering cross sections are doubly overestimated from a few hundred keV to a few MeV.

### 4.3 Discussion

As pointed out in the preceding section, one of the most significant problems exists in the cross sections of the structural materials. In order to know whether the cross sections of structural materials significantly affect the problems pointed out in section 4.1, some analyses were made by replacing the cross sections of chromium, iron and nickel by those of ENDF/B-IV. The detailed discussion is given in Appendix 3.

The  $k_{\text{eff}}$ -values are decreased by about 1% by the replacement, resulting in underestimate of  $k_{\text{eff}}$  by more than 1%. This suggests that JENDL-1 underestimates the  $k_{\infty}$ -values and that this underestimation is considerably compensated by underestimation of neutron leakage due to overestimation of the elastic scattering cross sections of structural materials.

By the replacement, the neutron flux is enhanced between 100 keV and 1 MeV and suppressed above 1 MeV and below a few tens of keV. This can be explained by larger inelastic scattering and larger amount of leakage with ENDF/B-IV cross sections. It can be said that JENDL-1 gives too flat neutron spectra because of its too small inelastic scattering and too small neutron leakage. This causes overestimate of the neutron flux below a few tens of keV, resulting in overestimate of the Doppler reactivity coefficients. The overestimate of the neutron flux below 10 keV was also pointed out<sup>31)</sup> in the analyses of leakage spectrum from an iron block measured<sup>32)</sup> at Research Reactor Institute, Kyoto University.

On the other hand, the fission rate becomes more underestimated in the outer core and radial blanket regions with the replaced library. Thus the underestimate of the fission rate in these regions is not due to the cross sections of the structural materials but may be attributed to the underestimation of the  $k_{\infty}$ -values in the core.

### 4.4 Feedback on Nuclear Data Evaluation

Various problems of JENDL-1 have been revealed through the benchmark tests. The following are pointed out on the evaluation of JENDL-1 from the view point of the integral tests.

- 1) The  $\nu_p$ -value of  $^{252}\text{Cf}$  should be evaluated more carefully.
- 2) Delayed neutron parameters should be reevaluated.
- 3) The total and elastic scattering cross sections of chromium, iron and nickel should be reevaluated in the energy region between a few hundred keV and a few MeV, by taking account of the fine structure observed in the high resolution experiments.
- 4) The inelastic scattering cross sections of iron and nickel should be increased.
- 5) The inelastic scattering cross section of  $^{238}\text{U}$  should be checked with the relation of the inelastic scattering cross sections of iron and nickel.
- 6) The fission and capture cross sections of the main fissile and fertile materials should be investigated carefully, because JENDL-1 underestimates the  $k_{\infty}$ -values.

These points were taken into consideration in the reevaluation work for JENDL-2.

## Acknowledgment

The authors wish to thank members of working group on JENDL integral tests of JNDC and members of JAERI Nuclear Data Center for their helpful discussion. They acknowledge T. Narita for his aid in production of group constants and K. Kaneko for his advice in improving the benchmark test system. Careful typewriting by H. Terakado is much appreciated.

## References

- 1) Iijima S., Nakagawa T., Kikuchi Y., Kawai M., Matsunobu H., Maki K. and Igarasi S.: *J. Nucl. Sci. Technol.*, **14**, 161 (1977).
- 2) Kikuchi Y., Nakagawa T., Matsunobu H., Kawai M., Igarasi S. and Iijima S.: "Neutron Cross Sections of 28 Fission Product Nuclides Adopted in JENDL-1", JAERI-1268 (1981).
- 3) Igarasi S., Nakagawa T., Kikuchi Y., Asami T. and Narita T.: "Japanese Evaluated Nuclear Data Library, Version-1, JENDL-1", JAERI-1261 (1979).
- 4) Kikuchi Y., Hasegawa A., Hojuyama T., Sasaki M., Seki Y., Kamei T. and Otake I.: "Nuclear Cross Sections for Technology", Proc. Int. Conf., Knoxville, Oct. 22-26, 1979, p. 581. NBS Special Publication 594 (1980).
- 5) Kikuchi Y., Hasegawa A., Nishimura H. and Tasaka K.: "Fission Product Fast Reactor Constants System of JNDC", JAERI-1248 (1976).
- 6) Iijima S., Watanabe T., Yoshida T., Kikuchi Y. and Nishimura H.: Proc. NEA Specialists' Meeting on Neutron Cross Sections of Fission Product Nuclei, Bologna, Dec. 12-14, 1979, p. 317, RIT/FIS-LDN(80)1, NEANDC(E)209 "L" (1980).
- 7) Takano H., Hasegawa A., Nakagawa M., Ishiguro Y. and Katsuragi S.: "JAERI Fast Reactor Group Constants Set, Version II", JAERI-1255 (1978).
- 8) Hasegawa A. et al.: To be published.
- 9) Takano H., Ishiguro Y. and Matsui Y.: "TIMS-1: A Processing Code for Production of Group Constants of Heavy Resonant Nuclei", JAERI-1267 (1980).
- 10) Hasegawa A., Katsuragi S. and Tone T.: "A One-dimensional Diffusion Code for Multi-group Criticality and Perturbation Calculations with JAERI-Fast Sets of 70-group Structure: EXPANDA-70D", JAERI-M 4953 (1972) [in Japanese].
- 11) Hasegawa A.: Private Communication.
- 12) Hardie R.W., Schenter R.E. and Wilson R.E.: *Nucl. Sci. Eng.* **57**, 222 (1975).
- 13) Ingram G., Stevenson J.M., Smith R.W., Ichimori T. and Konishi T.: Proc. Int. Symp. Physics of Fast Reactors, Tokyo, Oct. 16-19, 1973, Vol. I, p. 269 (1973).
- 14) Kamei T. and Kikuchi Y.: "Compilation of FCA Experimental Data for Integral Tests of Group Constants Set", Private Communication, (1978).
- 15) LeSage L.G. and McKnight R.D.: "Nuclear Cross Sections for Technology", Proc. Int. Conf., Knoxville, Oct. 22-26, 1979, p. 297, NBS Special Publication 594 (1980).

- 16) Snell A.H., Brolley J.E., Levinger J.S. and Wilkinson R.: "Studies in a Five Ton Metal Pile", University of Chicago Metallurgical Report CF-589 (1943).
- 17) Chezem C.G.: Nucl. Sci. Eng., **8**, 652 (1960).
- 18) Brolley J.E., Byerley F.J., Feld B., Olds A.E., Schalettar R., Slotin L. and Stewart R.B.: "Neutron Multiplication in a Mass of Uranium Metal", University of Chicago Metallurgical Project Report CF-1627 (1944).
- 19) Beyer F.C., Bryan R.H., Hummel H.H., Lennox D.H., Martens F.H., Reardon W.A., Rosenzweig N., Smith A.B. and Spinrad B.I.: Proc. 1st U.N. Int. Conf. Peaceful Uses Atomic Energy, Geneva, **5**, 342 (1956).
- 20) Neuer J.J. and Stewart, C.B.: "Preliminary Survey of Uranium Metal Exponential Columns", LA-2023 (1956).
- 21) Leipunsky A.I., Abramov A.I., Andreev V.N., Baryshnikov A.I., Bondarenko I.I., Galkov V.I., Golubev V.I., Gulko A.D., Guseinov A.G., Kazachkovsky O.D., Kozlova N.V., Krasnoyarov N.V., Kuzminov B.D., Morozov V.N., Nikolaev M.N., Smirenkin G.N., Stavissky Yu. Ya., Ukrantsev F.I., Usachev L.N., Fetisov N.I. and Sherman L.E.: Proc. 2nd U.N. Int. Conf. Peaceful Uses Atomic Energy, Geneva, **12**, 3 (1958).
- 22) Campan J.L., Clauzon P., Kirchner B., Ribon P. and Zaleski C.P.: "Experience Exponentielle Rapide, Resultats Preliminaires", Report S.N.E. No. 13 (1958).
- 23) Benoist P.: "Théorie du Coefficient des Diffusion des Neutrons dans un Réseau Comportant des Cavités", CEA-R 2278 (1964).
- 24) Ingram G., Hardiman J.P., Smith R.W., Konishi T. and Nakano M.: Proc. Int. Symp. Physics of Fast Reactors, Tokyo, Oct. 16–19, 1973, Vol. I, p. 289 (1973).
- 25) Stevenson J.M., Hardiman J.P. and Yoshida H.: Proc. Int. Symp. Physics of Fast Reactors, Tokyo, Oct. 16–19, 1973, Vol. I, p. 355 (1973).
- 26) Broomfield A.M., Collins P.J., Carter M.D., Marshall J., Sugawara A., Sekiguchi Y. and Konishi T.: Proc. Int. Symp. Physics of Fast Reactors, Tokyo, Oct. 16–19, 1973, Vol. I, p. 312 (1973).
- 27) Carpenter S.G.: "Measurement of Control Rod Worths Using ZPPR", Paper presented at Specialists' Meeting on Control Rod Measurement Technique: Reactivity Worths and Power Distributions, Cadarache, 12–22 April 1976, NEACRP-U-75L (1976).
- 28) Osugi T., Yoshida H., Iijima S., Shinhama K. and Hirata M.: "Analysis of Simulated Control Rod Worth Experiments Made in Phase 1A and Phase 1B Cores of ZPPR Assembly 3", Private Communication, (1976).
- 29) Iijima S., Iida M., Kawai M., Yamamoto M., Yoshida T. and Sano J.: Proc. 3rd Seminar Neutron Cross Sections, 9 – 11 Nov., 1972, JAERI, JAERI-1228, p. 183 (1973) [in Japanese].
- 30) Asami T., Kikuchi Y., Nakagawa T. and Igarasi S.: "Neutron Data of Structural Materials for Fast Reactors", Proc. NEANDC, NEACRP Specialists' Meeting, Geel, 5–8 Dec. 1977, p. 118, Pergamon Press (1979).
- 31) Otake I.: "Neutron Data of Structural Materials for Fast Reactors", Proc. NEANDC, NEACRP Specialists' Meeting, Geel, 5–8 Dec. 1977, p. 105, Pergamon Press (1979).
- 32) Kimura I., Kobayashi K., Hayashi S.A., Yamamoto S., Nishihara H., Ando M., Kanazawa S. and Nakagawa M.: "Nuclear Cross sections and Technology", Proc. Conf. Washington, D.C., March 3–7, 1975, Vol. 1, p. 184, NBS Special Publication 425 (1975).

## Appendices

### Appendix 1 Production of Reactor Constants

The library of multigroup constants of the JAERI-Fast set<sup>1~3)</sup> type was produced from JENDL-1 data by using two processing codes PROF-GROUCH-G-II<sup>4)</sup> and TIMS-1<sup>5)</sup>. The PROF-GROUCH-G-II code produces the group constants of light and intermediate nuclides in the full energy range and those of heavy nuclides in the smooth region above resonance energy. The TIMS-1 code calculates the temperature dependent group constants of heavy nuclides in the resonance energy region. The produced library contains both cross sections and self-shielding factors of 70 groups whose structure is given in **Table A1.1**. The thermal group is not contained in this library.

**Table A1.1** 70-group structure

Group	Upper energy	Lower energy	Lethargy width	Group	Upper energy	Lower energy	Lethargy width
1	10.5 (MeV)	8.3	0.2351	36	1.66 (keV)	1.29	0.2522
2	8.3 (MeV)	6.5	0.2445	37	1.29 (keV)	1.0	0.2546
3	6.5 (MeV)	5.1	0.2426	38	1000 (eV)	773	0.2575
4	5.1 (MeV)	4.0	0.2429	39	773 (eV)	598	0.2567
5	4.0 (MeV)	3.1	0.2549	40	598 (eV)	465	0.2516
6	3.1 (MeV)	2.5	0.2151	41	465 (eV)	360	0.2559
7	2.5 (MeV)	1.9	0.2744	42	360 (eV)	278	0.2585
8	1.9 (MeV)	1.4	0.3054	43	278 (eV)	215	0.2570
9	1.4 (MeV)	1.1	0.2412	44	215 (eV)	166	0.2587
10	1.1 (MeV)	0.8	0.3185	45	166 (eV)	129	0.2522
11	0.8 (MeV)	0.63	0.2389	46	129 (eV)	100	0.2546
12	0.63 (MeV)	0.50	0.2311	47	100 (eV)	77.3	0.2575
13	0.50 (MeV)	0.4	0.2231	48	77.3 (eV)	59.8	0.2567
14	0.4 (MeV)	0.31	0.2549	49	59.8 (eV)	46.5	0.2516
15	0.31 (MeV)	0.25	0.2151	50	46.5 (eV)	36.0	0.2559
16	0.25 (MeV)	0.2	0.2231	51	36.0 (eV)	27.8	0.2585
17	0.2 (MeV)	0.15	0.2877	52	27.8 (eV)	21.5	0.2570
18	0.15 (MeV)	0.12	0.2231	53	21.5 (eV)	16.6	0.2587
19	0.12 (MeV)	0.1	0.1823	54	16.6 (eV)	12.9	0.2522
20	100 (keV)	77.3	0.2575	55	12.9 (eV)	10.0	0.2546
21	77.3 (keV)	59.8	0.2567	56	10.0 (eV)	7.73	0.2575
22	59.8 (keV)	46.5	0.2516	57	7.73 (eV)	5.98	0.2567
23	46.5 (keV)	36.0	0.2559	58	5.98 (eV)	4.65	0.2516
24	36.0 (keV)	27.8	0.2585	59	4.65 (eV)	3.60	0.2559
25	27.8 (keV)	21.5	0.2570	60	3.60 (eV)	2.78	0.2585
26	21.5 (keV)	16.6	0.2587	61	2.78 (eV)	2.15	0.2570
27	16.6 (keV)	12.9	0.2522	62	2.15 (eV)	1.66	0.2587
28	12.9 (keV)	10.0	0.2546	63	1.66 (eV)	1.29	0.2522
29	10.0 (keV)	7.73	0.2575	64	1.29 (eV)	1.0	0.2546
30	7.73 (keV)	5.98	0.2567	65	1.0 (eV)	0.773	0.2575
31	5.98 (keV)	4.65	0.2516	66	0.773 (eV)	0.598	0.2567
32	4.65 (keV)	3.60	0.2559	67	0.598 (eV)	0.465	0.2516
33	3.60 (keV)	2.78	0.2585	68	0.465 (eV)	0.360	0.2559
34	2.78 (keV)	2.15	0.2570	69	0.360 (eV)	0.278	0.2585
35	2.15 (keV)	1.66	0.2587	70	0.278 (eV)	0.215	0.2570

In the group constants system of JAERI-Fast set, the group-averaged cross section of reaction  $x$  for energy group  $g$  is defined as

$$\bar{\sigma}_x^g(\sigma_0, T) = \frac{\int_{\Delta E_g} \sigma_x(E, T) \phi(E, T, \sigma_0) dE}{\int_{\Delta E_g} \phi(E, T, \sigma_0) dE},$$

where  $\phi(E, T, \sigma_0)$  is the weighting spectrum depending on the energy  $E$ , temperature  $T$ , and admixture cross section  $\sigma_0$ . Furthermore, a special total cross section used to calculate the diffusion coefficient is defined as

$$\bar{\sigma}_t^g(\sigma_0, T) = \frac{\int_{\Delta E_g} \phi(E, T, \sigma_0) dE}{\int_{\Delta E_g} \frac{\phi(E, T, \sigma_0)}{\sigma_t(E, T) + \sigma_0} dE} - \sigma_0.$$

The elastic removal cross section is given by

$$\begin{aligned} \bar{\sigma}_{\sigma}^g(\sigma_0, T) &= \frac{\int_{\Delta E'} \sigma_s(E, T) \phi(E, T, \sigma_0) \frac{E_L - \alpha E}{1-\alpha} dE}{\int_{\Delta E_g} \phi(E, \sigma_0, T) dE} \\ \Delta E' &= \frac{E_L}{\alpha} - E_L, \\ \alpha &= \left( \frac{A-1}{A+1} \right)^2, \end{aligned}$$

where  $E_L$  is the lower energy boundary of integration interval  $\Delta E_g$ ,  $\sigma_s(E, T)$  the elastic scattering cross section and  $A$  the atomic mass of the resonant element. The self-shielding factor is defined as the ratio to the effective cross section of an infinitely dilute system at 300°K:

$$f_x^g(\sigma_0, T) = \frac{\bar{\sigma}_x^g(\sigma_0, T)}{\bar{\sigma}_x^g(\infty, 300)}.$$

As to the weighting spectrum, the PROF-GROUGH-G-II code uses the conventional form as

$$\phi(E, T, \sigma_0) = \frac{\phi^0(E)}{\sigma_t(E, T) + \sigma_0},$$

where the global spectrum  $\phi^0(E)$  is assumed to be  $1/E$  up to 1 MeV and to be fission spectrum with nuclear temperature of 200 keV above 1 MeV. In the TIMS-1 code, on the other hand, the weight function  $\phi(E, T, \sigma_0)$  are numerically calculated by solving the neutron slowing down equation by the use of a recurrence formula for neutron slowing down source.

The presently processed nuclides are H, Be,  $^{10}\text{B}$ ,  $^{11}\text{B}$ , C, O, Na, Al, Si, Cr, Mn, Fe, Ni, Cu, Mo,  $^{234}\text{U}$ ,  $^{235}\text{U}$ ,  $^{238}\text{U}$ ,  $^{239}\text{Pu}$ ,  $^{240}\text{Pu}$ ,  $^{241}\text{Pu}$ ,  $^{242}\text{Pu}$  and  $^{241}\text{Am}$ . Among them, data of Be,  $^{11}\text{B}$ , O and  $^{242}\text{Pu}$  were taken from ENDF/B-IV, because they are not contained in JENDL-1. The temperature dependent self-shielding factors<sup>6)</sup> were produced for five heavy resonant nuclides,  $^{235}\text{U}$ ,  $^{238}\text{U}$ ,  $^{239}\text{Pu}$ ,  $^{240}\text{Pu}$  and  $^{241}\text{Pu}$  at 300, 900 and 2100°K. The admixture cross sections were selected appropriately from the range between 0 and  $10^4$  barns. Detailed specifications are given for each nuclide in **Table A1.2**.

**Table A1.2** Materials processed with PROF-GROUGH-G-II and TIMS-1

Material	PROF-GROUGH-G-II	TIMS-1	Temperature (°K)	$\sigma_0$ -values (barn)
$^{235}\text{U}$	10.5MeV–21.5keV	21.5keV–0.215eV	300, 900, 2100	0, 10, $10^2$ , $10^3$
$^{238}\text{U}$	10.5MeV–46.5keV	46.5keV–0.215eV	300, 900, 2100	0, 1, 10, $10^2$ , $10^3$
$^{239}\text{Pu}$	10.5MeV–21.5keV	21.5keV–0.215eV	300, 900, 2100	0, 10, $10^2$ , $10^3$
$^{240}\text{Pu}$	10.5MeV–46.5keV	46.5keV–0.215eV	300, 900, 2100	0, $10^2$ , $10^3$ , $10^4$
$^{241}\text{Pu}$	10.5MeV–21.5keV	21.5keV–0.215eV	300, 900, 2100	0, 10, $10^2$ , $10^3$ , $10^4$
H	10.5MeV–0.215eV		0	0, 1, 10, $10^2$ , $10^3$ , $10^4$
Be	"		0	"
$^{10}\text{B}$	"		0	"
$^{11}\text{B}$	"		0	"
C	"		0	"
O	"		0	"
Na	"		0	"
Al	"		0	"
Si	"		0	"
Cr	"		0	"
Mn	"		0	"
Fe	"		0	"
Ni	"		0	"
Cu	"		0	"
Mo	"		0	"
$^{234}\text{U}$	"		0	"
$^{242}\text{Pu}$	"		0	"
$^{241}\text{Am}$	"		0	"

**References**

- 1) Katsuragi S., Tone T. and Hasegawa A.: "JAERI Fast Reactor Group Constants Systems Part I", JAERI 1195 (1970).
- 2) Katsuragi S., Ishiguro Y., Takano H. and Nakagawa M.: "JAERI Fast Reactor Group Constants Systems Part II-1", JAERI 1199 (1970).
- 3) Takano H., Hasegawa A., Nakagawa M., Ishiguro Y. and Katsuragi S.: "JAERI Fast Reactor Group Constants Set, Version II", JAERI 1255 (1978).
- 4) Hasegawa A. et al.: to be published.
- 5) Takano H., Ishiguro Y. and Matsui Y.: "TIMS-1: A Processing Code for Production of Group Constants of Heavy Resonant Nuclei", JAERI 1267 (1980).
- 6) Takano H., Matsui Y. and Ishiguro Y.: "Effect of Difference between group Constants Processed by Codes TIMS and ETOX on Integral Quantities", JAERI-M 7724 (1978).

## Appendix 2 Benchmark Specification

### A2.1 Twenty-seven Assemblies with One-dimensional Model

#### A2.1.1 Eighteen Assemblies Selected by Hardie et al.

Hardie *et al.*<sup>1)</sup> selected 18 critical assemblies for benchmark tests of ENDF/B. We adopted all of them. One-dimensional spherical model was adopted in the present work except for ZPPR-2 in which case the model was a 1-D cylinder. The precise specifications are given in Ref. (1). In the present model, number densities of some minor nuclides were included to those of analogous nuclides because of limitation on number of nuclides for EXPANDA-70D<sup>2)</sup>. The specifications adopted in the present calculations are given in **Table A2.4** as the input format for EXPANDA-70D.

#### A2.1.2 MZA and MZB

The MOZART experiments were performed for mock-up of Japanese proto-type fast reactor "MONJU" as a joint work between Japan and the United Kingdom. The measurements were made very carefully and the detailed analyses were made for the calculational model. Hence we adopted the physics mock-up cores, MZA and MZB, for the present benchmark tests.

One-dimensional spherical model was adopted for both MZA and MZB, though 1-D cylinder model may be more adequate for MZB of pancake shape. The specifications are given in **Table A2.1**. The input format for EXPANDA-70D is given in **Table 2.4**.

#### A2.1.3 FCA Assemblies

Number of critical experiments have been made at FCA facility in JAERI since 1967. Kamei and Kikuchi<sup>3)</sup> made the benchmark problems concerning FCA assemblies. Examining the quality and quantity of the measured data and abandoning cores for complicated engineering mock-up experiments, they selected 13 assemblies for the benchmark tests of nuclear data: I-1, I-4, I-6, II-4S, II-5S, III-1, III-2S, IV-1, IV-1-P', V-1, V-2, VI-1 and VI-2.

Two-dimensional R-Z model and one-dimensional spherical model were made for most cores. One-dimensional cylinder model was applied for FCA VI-2 assembly because of its pancake shape. Assemblies II-4S, II-5S and III-2S are spherical cores and therefore only 1-D spherical model was applied. Assemblies IV-1 and IV-1-P' are special cores whose  $k_{\infty}$ -value is unity. As the EXPANDA-70D code has no option to treat completely reflective boundaries, we assume a very large spherical core with radius of 20 m so that the leakage becomes negligible. The transport corrections were calculated by using JENDL-1 with a 1-D transport code DTF-IV<sup>4)</sup>. The cell heterogeneity corrections were obtained by solving the integral transport equation with the EXPANDA-75 code<sup>5)</sup> by using JENDL-1. The benchmark specifications and the corrections are given in **Table A2.2**.

The benchmark calculation was made for all the 13 assemblies, but we considered only the results of I-1, I-6, III-2S, V-1, V-2, VI-1 and VI-2, taking account of the quality and quantities of the measured data and of the reliability of modeling. Particularly we abandoned FCA-II series and -IV series in the present work from the following reasons.

FCA-II series (II-4S and II-5S) contain large amount of polyethylene to soften the spectrum. It was found that the  $k_{\text{eff}}$ -values of these assemblies were very sensitive to the method used in calculating the self-shielding factors. The sensitivity of the method was investigated by Takano *et al.*<sup>6)</sup> by using two sets of the self-shielding factors; one is obtained with

**Table A2.1** Benchmark Specifications of MZA and MZB Assemblies

Assembly	MZA						MZB						
	Model Region	Sphere: 4 region core + blanket + reflector			R.B.	Reflector	Sphere: 4 region inner core + outer core + blanket + reflector			O.C.	R.B.	Reflector	
Thickness (cm)	Core-1	Core-2	Core-3	Core-4	R.B.	Reflector	I.C.-1	I.C.-2	I.C.-3	I.C.-4	O.C.	R.B.	Reflector
Number density ( $10^{22}/\text{cc}$ )							44.55	8.71	8.79	7.54	11.41	38.24	26.33
Pu-239	0.1361	0.1343	0.1347	0.1348			0.0892	0.0894	0.0894	0.0892	0.0892	0.1346	
Pu-240	0.0323	0.0350	0.0332	0.0330			0.0183	0.0183	0.0183	0.0183	0.0184	0.0332	
Pu-241	0.0046	0.0055	0.0053	0.0053			0.0027	0.0027	0.0027	0.0027	0.0027	0.0052	
U-235	0.0039	0.0039	0.0039	0.0039	0.0070		0.0043	0.0043	0.0043	0.0043	0.0043	0.0055	
U-238	0.5357	0.5354	0.5357	0.5357	0.9718		0.5926	0.5925	0.5925	0.5925	0.5351	0.7644	
B-10	1.14-6*			1.14-4*									1.75-5*
B-11	4.01-6*			1.34-6*									4.63-7*
C	0.3123	0.3126	0.3127	0.3117	1.4437	0.0485	0.0111	0.0111	0.0106	0.0105	0.3119	1.1257	0.0461
O	1.0799	1.0793	1.0800	1.0797	0.3318		1.2551	1.2551	1.2551	1.2551	1.0789	0.0512	
Na	0.8580	0.8515	0.8520	0.8520	0.5067	0.0185	0.9242	0.9244	0.9257	0.9257	0.8584	0.9099	0.0169
Al	0.0026	0.0026	0.0026	0.0025	0.4246	1.1503	0.0027	0.0027	0.0027	0.0027	0.0026	0.0683	1.3724
Cr	0.3464	0.3448	0.3449	0.3448	0.2030	0.0345	0.3447	0.3455	0.3552	0.3552	0.3403	0.3355	0.0412
Mn	0.0250	0.0271	0.0271	0.0271	0.0141	0.0401	0.0259	0.0259	0.0253	0.0253	0.0268	0.0236	0.0358
Fe	1.2520	1.2613	1.2609	1.2596	1.3951	5.3110	1.2532	1.2512	1.2349	1.2518	1.2891	4.9574	
Ni	0.1739	0.1715	0.1715	0.1714	0.1027	0.0193	1.1811	0.1819	0.1882	0.1881	0.1693	0.1678	0.0230
Cu	0.0996	0.0496	0.0496	0.0496	0.0007	0.0002	0.0232	0.0236	0.0236	0.0236	0.0054	0.0010	0.0004
Mo	0.0011	0.0011	0.0011	0.0011	0.0003	0.0003	0.0011	0.0011	0.0011	0.0011	0.0011	0.0016	0.0004
Corrections ( $\% \Delta k/k$ )	1D → 2D: -1.96, $S_n$ : 0.75, Hetero: 1.40						1D → 2D: -1.86, $S_n$ : 0.36, Hetero: 1.23						

\* 1.1 – 6 denotes  $1.1 \times 10^{-6}$

**Table A2.2** Benchmark specifications of FCA assemblies

Assembly Name		I-1	I-4	I-6	II-4S	II-5S	III-1	III-2S	IV-1	IV-1-P*	V-1	V-2	VI-1	VI-2
Fuel Type	20% EU	EU/C	EU	EU/C/CH <sub>4</sub>	EU/CH <sub>4</sub>	EU/AI	EU/C	EU/NU	Pu/EU/ Na/Al <sub>2</sub> O <sub>3</sub>	Pu/EU/Na	Pu/DUO <sub>2</sub> /Na/Al <sub>2</sub> O <sub>3</sub>			
Benchmark model	Geometry Number of Region	Sphere 2	Sphere 2	Sphere 2	Sphere 2	Sphere 2	Sphere $\infty$	1	2	2	2	2	2 (core) + R.B. R1=29.38, R2=46.70	
	Core Radius (cm)	19.24	23.442	17.88	31.9	38.15	36.91	38.8	32.34	36.30	46.59	91.44		
	Core Height (cm)												V1=247.96, V2=378.54	
	Core Volume (l)	29.81	53.96	23.94	135.98	232.58	210.63	244.67	141.66	200.36	423.63	422.0 (1st & 2nd Reg.)		
	Critical Mass:U	91.1	123.8	73.2	95.1	162.6	281.5	256.2	k <sub>in</sub> =1.024	k <sub>in</sub> =0.9963	108.3	114.9	2.51	
	Pu-fiss.								59.3	84.0	266.6	103.8 (1st Reg.)		
Core													1st region	2nd region
Pu-239													0.10446	0.10458
Pu-240									0.0112	0.009325	0.01400	0.00933		
Pu-241									0.0010	0.009427	0.001124	0.001069	0.00142	0.000927
U-235	0.7836	0.588	0.7836	0.1792*	0.1792*	0.3428	0.2685*	0.2407	0.0261	0.1960	0.1470	0.0152	0.28483	
U-238	3.113	2.3344	3.113	0.7114*	0.7114*	1.362	1.0670*	3.677	3.598	0.7781	0.58359	0.69057	0.68915	
H														
C ( $\times 10^{22}/\text{cc}$ )		1.8361												
O														
Na														
Al														
Cr	0.1827	0.1827	0.1827	0.2814*	0.2814*	1.216	0.3553	0.2814*	0.183	0.217	1.6476	1.3101	1.5598	1.7286
Fe	0.6652	0.6652	0.6652	1.0233*	1.0233*	1.292	0.1233*	0.6665	0.788	0.10975	0.81341	0.7656	0.7656	0.9079
Ni	0.07964	0.07964	0.07964	0.1214*	0.1214*	0.1527	0.1214*	0.080	0.098	0.14275	0.30335	0.32734	0.3552	0.3413
B <sub>g</sub> <sup>2</sup> (cm <sup>-2</sup> )														
Blanket or Reflector	30cm NU	30cm NU	25.5 cm Carbon	30.6cm NU	28.4cm NU	20cm NU	27.8cm NU				30cm NU	30cm NU	26.47cm NU	
* U-235	0.02891	0.02891									0.02891	0.0086	0.02891	
U-238	3.989	3.989									3.989	4.0070	3.989	
C														
Cr ( $\times 10^{-22}/\text{cc}$ )	0.1827	0.1827		0.1827							0.1827	0.1827		
Fe	0.6652	0.6652		0.6652							0.6652	0.6652		
Ni	0.07964	0.07964		0.07964							0.07964	0.07964		
B <sub>g</sub> <sup>2</sup>														
Heterogeneity Effect** % $\Delta k/k$	0.0	0.1	0.0	1.5	1.4	0.1	0.4	0.0	0.6	0.3†	0.4†	0.7	0.6	
Transport Effect** % $\Delta k/k$	1.9	1.4	3.4	0.7	0.5	0.9	0.6	0.0	0.0	1.1	1.0	0.8	0.4	
Comment														

\* Private communication from Dr. H. Kuroi (1976)

\*\* Calculated with JENDL-1

at March 1973

TIMS-1<sup>7)</sup> and the others with ETOX<sup>8)</sup>. Little difference was observed<sup>6)</sup> between the two sets for most cases. For FCA-II series, however, there exist discrepancies of 3 ~ 4% in the  $k_{\text{eff}}$ -values as seen in **Table A2.3**, though the differences are less than 0.3% for the other FCA assemblies. TIMS-1 solves the slowing down equation in the medium of  $A = 30$ , while ETOX assumes the narrow resonance approximation. It is not easy to say which method is more adequate, and we concluded that FCA-II series were not appropriate to benchmark tests of nuclear data.

FCA-IV series consist of the test region with  $k_{\infty} = 1$  sustained by the surrounding driver region. In the present analysis, hypothetical large cores were assumed to make the leakage negligible. But this makes the mesh interval very large and causes the errors due to rough meshes. Hence FCA-IV-1 and -IV-1-P' were abandoned in the benchmark tests.

The input format for EXPANDA-70D is given in **Table A2.4**.

**Table A2.3** Effects of difference in processing  
the self-shielding factors on  $k_{\text{eff}}$   
values

Assemblies	TIMS	ETOX
FCA-I-1	1.0120	1.0122
I-4	1.0113	1.0116
I-6	1.0093	1.0106
II-4S	0.9764	1.0180
I-5S	0.9981	1.0266
III-1	1.0163	1.0178
III-2S	1.0026	1.0028
IV-1	0.9960	0.9958
IV-1-P	0.9548	0.9544
V-1	1.0061	1.0083
V-2	1.0108	1.0129
VI-1	0.9945	0.9967
VI-2	1.0071	1.0101







## A2.2 Doppler Analysis

Analyses of Doppler measurements are required in order to test the temperature dependence of group cross sections. For this purpose, we adopted the Doppler experiments performed in eight critical assemblies, FCA-V-1, FCA-V-2, FCA-VI-1, FCA-VI-2, ZPPR-2 (normal core), ZPPR-2 (Na-voided core), ZPR-3-47 and SEFOR. Main characteristics of these assemblies are shown in **Table A2.5**.

**Table A2.5** Main characteristics of fast critical assemblies used for benchmark calculation of Doppler effects

Assembly	Fuel	$R = \frac{\text{Fertile N}}{\text{Fertile N}}$	Doppler sample	Sample size (cm)
FCA-V-1	Pu, U	2.6	NUO <sub>2</sub>	2.5φ, 15L
FCA-V-2	Pu, U	2.3	NUO <sub>2</sub>	2.5φ, 15L
FCA-VI-1	Pu, U	$R_I=4.3, R_o=3.0$	NUO <sub>2</sub>	2.5φ, 15L
FCA-VI-2	Pu, U	$R_I=6.9, R_o=2.5$	NUO <sub>2</sub>	2.5φ, 15L
ZPPR-2	Pu	$R_I=6.5, R_o=4.0$	NUO <sub>2</sub>	2.54φ, 30, 48L
ZPR-3-47	Pu	5.1	NUO <sub>2</sub>	1.27φ, 15.24L
SEFOR	Pu	4.3	All core on power	

$R_I$  and  $R_o$  mean the density ratio of fertile to fissile materials in the inner and outer cores, respectively.

In SEFOR assembly, the Doppler measurement was performed by measuring the reactivity change due to the power increase from zero to 20 MW, while holding the coolant temperature constant<sup>9)</sup>. This experimental isothermal Doppler coefficient was  $T$  ( $dk/dT$ ) =  $-0.0081 \pm 0.001$  and the experimental uncertainty is  $\pm 12\%$ . Though three models (spherical, slab and R-Z geometries) are recommended as the benchmark specification problem in Ref. (9), the present benchmark claculation was performed only for one-dimensional spherical model.

In the other seven assemblies the <sup>238</sup>U Doppler reactivity effect was measured for natural UO<sub>2</sub> (NUO<sub>2</sub>) sample. The sample oscillation reactivity difference technique was used at JAERI and ANL. In this technique, a Doppler sample and a reference sample are periodically exchanged at some point in a reactor where the Doppler effect is to be measured. The Doppler samples are 2.5 cm in diameter and 15 cm long at FCA assemblies, 2.54 cm in diameter and 30.48 cm long at ZPPR assembly 2, and 1.27 cm and 15.24 cm at ZPR-3-47. The Doppler measurement was made in both the normal and Na-voided inner cores in ZPPR-2. The compositions and configurations for these fast critical assemblies are detailed in Ref. (10).

In the present benchmark calculation, one-dimensional spherical model was adopted for these assemblies. Resonance heterogeneity effect was considered by the usual equivalent relation  $\sigma_{ex} = a(1-C)/(NI)$ , where  $N$  and  $I$  stand for the atomic number density of the resonant material and the mean chord length of the sample, and the Dancoff factor  $a(1-C)$  was assumed to be 1.35. However, the heterogeneity effect, the buffer effect of steel-environment of the sample and the two-dimensional to one-dimensional effect were not considered in the present calculation. These effects contribute significantly to Doppler effect. It was found<sup>10)</sup> that the <sup>238</sup>U Doppler effect was underestimated considerably by ignoring these effects. The input data for EXPANDA-70D are given in **Table A2.6**.





### References

- 1) Hardie R.W., Schenter R.E. and Wilson R.E.: Nucl. Sci. Eng., **57**, 222 (1975).
- 2) Hasegawa A., Katsuragi S. and Tone T.: "A One-dimensional Diffusion Code for Multi-group Criticality and Perturbation Calculations with JAERI-Fast Sets of 70-group Structure: EXPANDA-70D", JAERI-M 4953 (1972) [in Japanese].
- 3) Kamei T. and Kikuchi Y.: "Compilation of FCA Experimental Data for Integral Tests of Group Constants Set", Private Communication (1978).
- 4) Lathrop K.D.: "DTF-IV: a FORTRAN-IV Program for Solving the Multi-group Transport Equation with Anisotropic Scattering", LA-3373 (1965).
- 5) Kikuchi Y., Katsuragi S., Ogitsu M. and Suzuki T.: "EXPANDA-75: One-dimensional Diffusion Code for Multi-region Plate Lattice Heterogeneous System", JAERI 1239 (1975).
- 6) Takano H., Matsui Y. and Ishiguro Y.: "Effect of Difference between Group Constants Processed by Codes TIMS and ETOX on Integral Quantities", JAERI-M 7724 (1978).
- 7) Takano H., Ishiguro Y. and Matsui Y.: "TIMS-1: A Processing Code for Production of Group Constants of Heavy Resonant Nuclei", JAERI 1267 (1980).
- 8) Schenter R.E., Baker J.L. and Kidman R.B.: "ETOX: a Code to Calculate Group Constants for Nuclear Reactor Calculations", BNWL-1002 (1969).
- 9) Freeman D.D.: "SEFOR Experimental Results and Applications to LMFBRs", GEAP-13929 (1973).
- 10) Takano H. and Matsui Y.: "Analysis of Doppler Effects with JAERI-Fast Sets", JAERI-M 7195 (1977) [in Japanese].

### Appendix 3 Effects of Structural Material Cross Sections

It has been pointed out from the benchmark tests on JENDL-1 that JENDL-1 may have too small diffusion coefficients and too large removal cross sections above 100 keV. On the other hand, it has been pointed out through reevaluation work for JENDL-2 that the total and elastic scattering cross sections of chromium, iron and nickel may be overestimated in JENDL-1 in the energy range from a few hundred keV to a few MeV. This is consistent with the observation on the diffusion coefficients and the removal cross sections. The total, capture and inelastic scattering cross sections of chromium, iron and nickel are shown in **Figs. A3.1 ~ A3.9** with those of ENDF/B-IV as well as some selected experimental data. Overestimation of the total cross sections in JENDL-1 is evident in the energy region above resolved resonances up to a few MeV. This is caused by our adopting the calculated values with the optical model instead of following the structure appeared in the experimental data. Considerable differences are observed between JENDL-1 and ENDF/B-IV in the other cross sections for these nuclides.

Hence the effects of the cross sections of structural materials were investigated by replacing the cross sections of chromium, iron and nickel in JENDL-1 with those in ENDF/B-IV. This replaced group cross section library is called JENDL-B4 in this appendix. This study was made on the 27 assemblies mentioned in Chapter 2 with the 1-D model, and on MZB assembly and a large fast breeder reactor of 1000 MWe with the 2-D R-Z model.

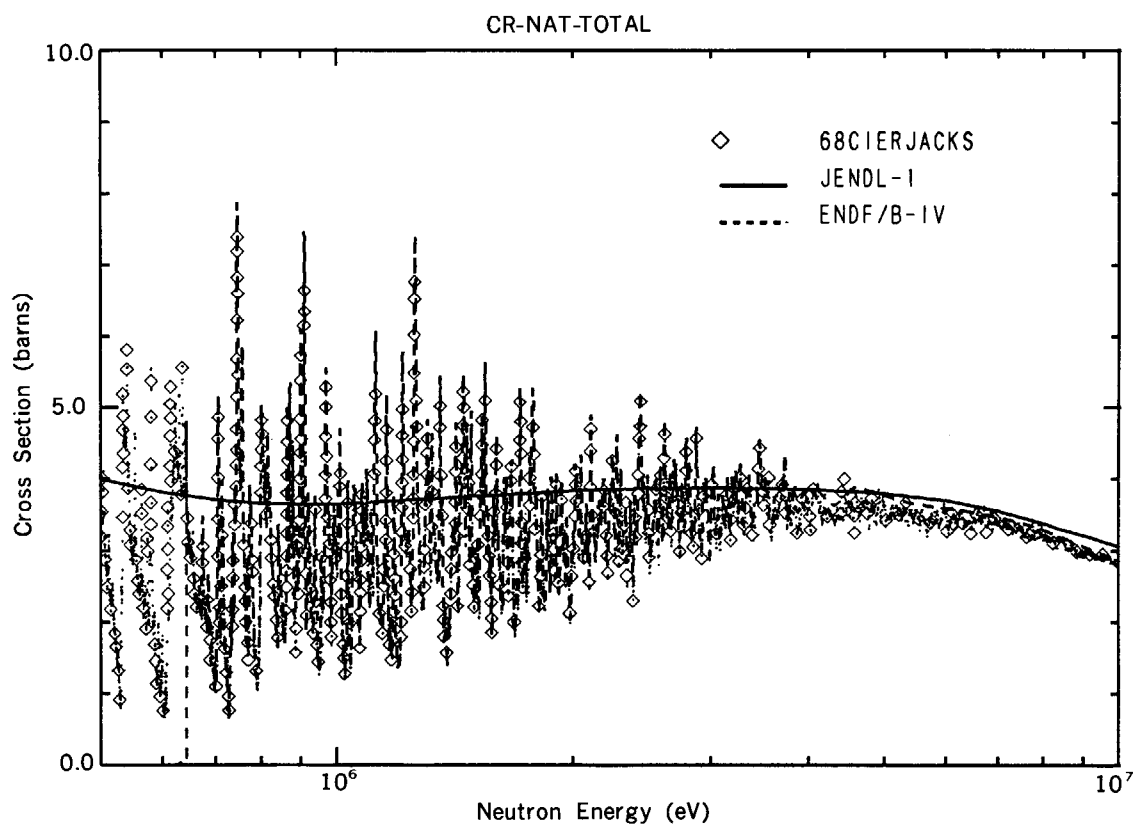


**Fig. A3.1** Total cross sections of chromium.

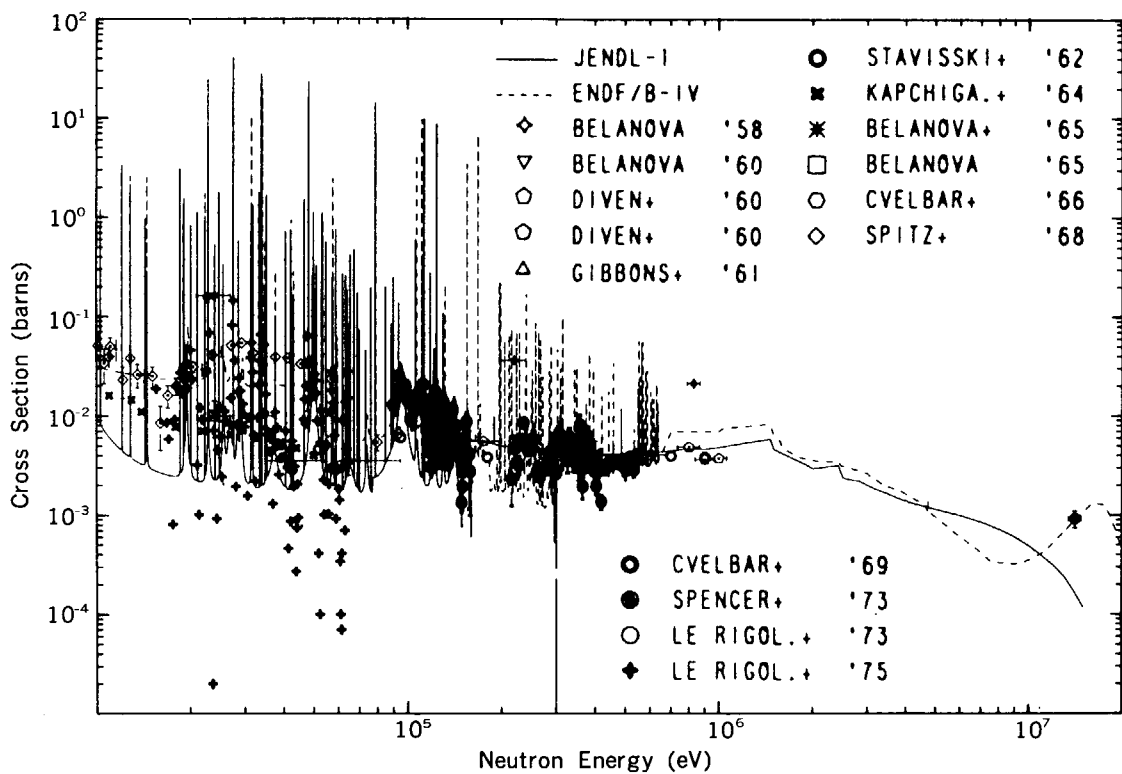


**Fig. A3.2** Capture cross sections of chromium.

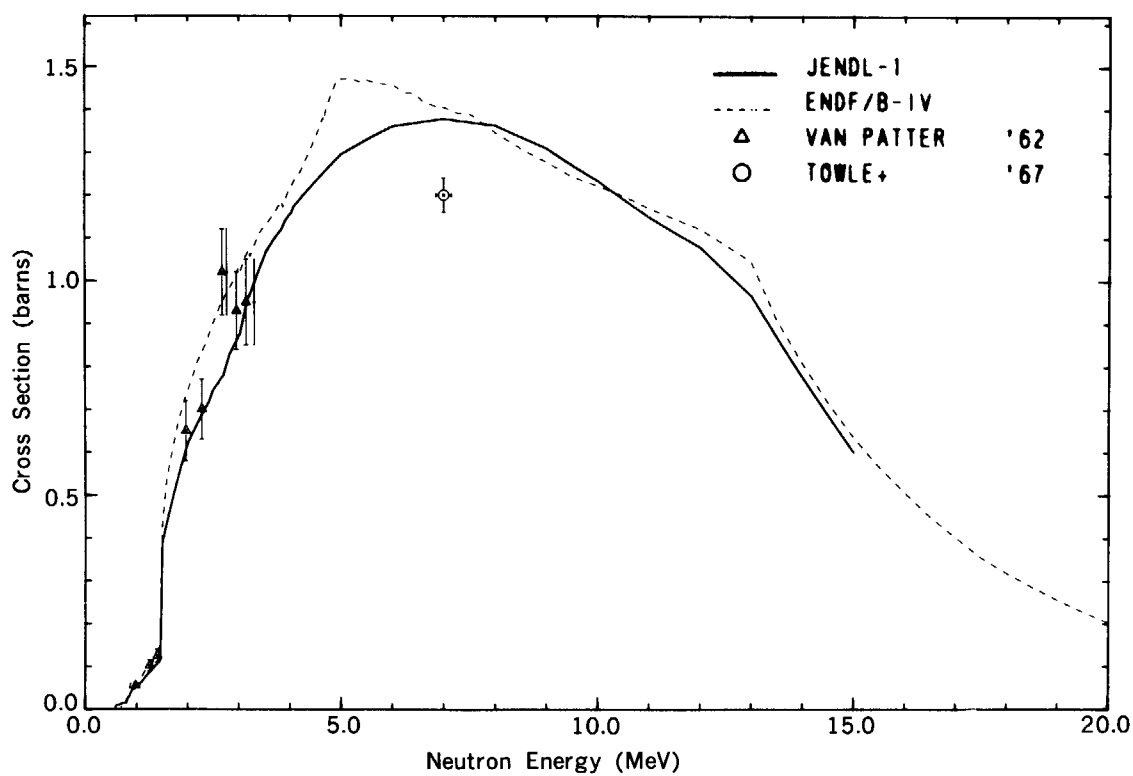


**Fig. A3.3** Inelastic scattering cross sections of chromium.

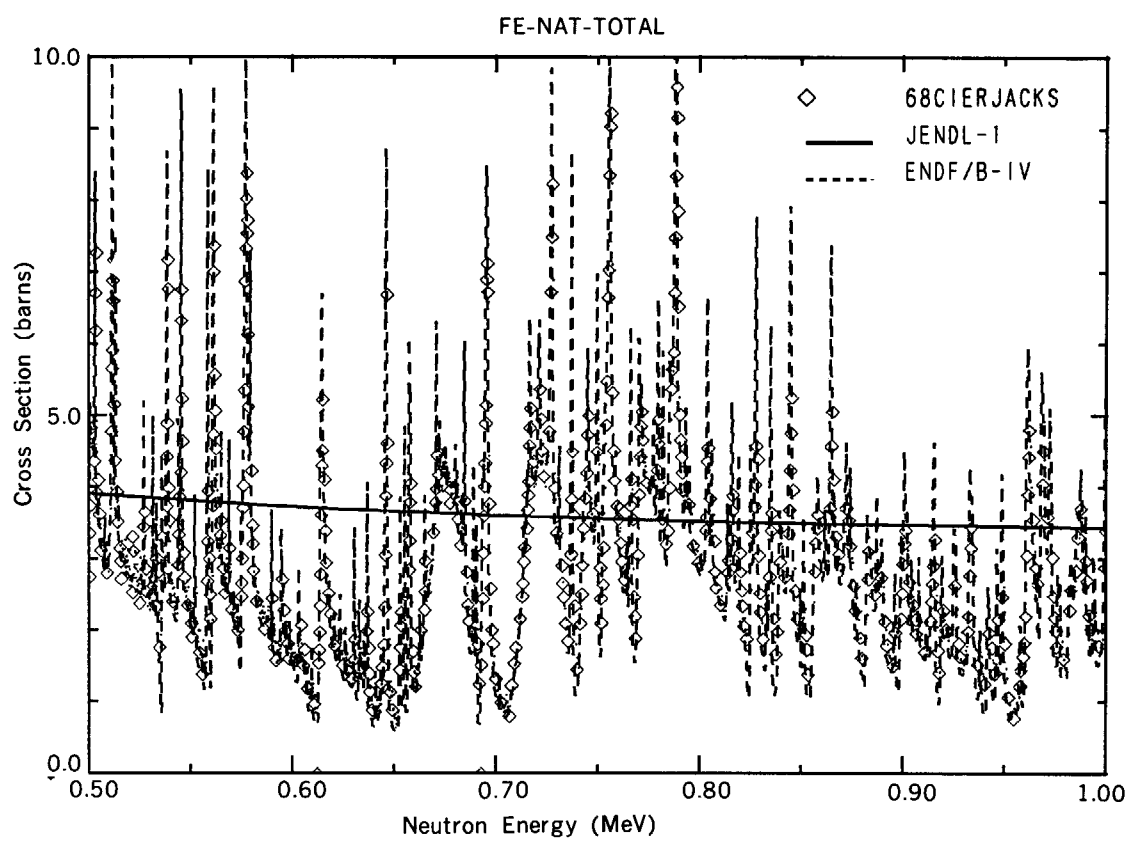


**Fig. A3.4 (a)** Total cross sections of ion.

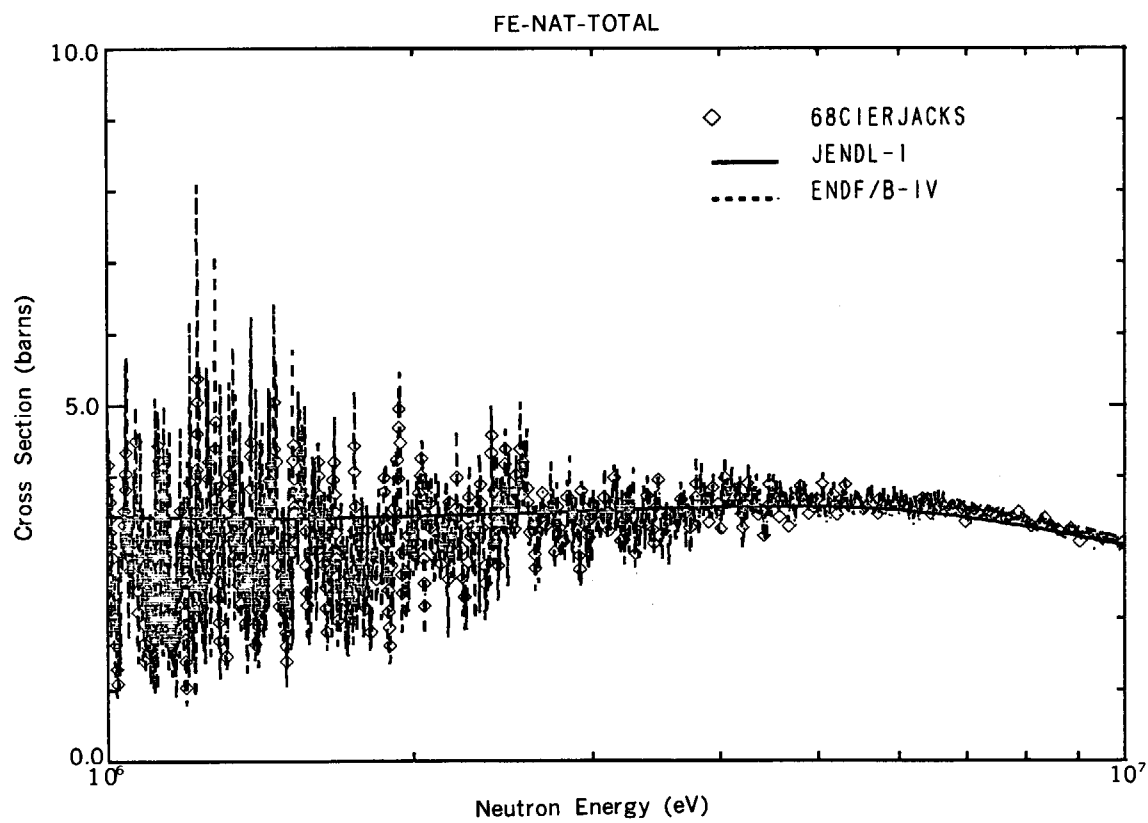


**Fig. A3.4 (b)** Total cross sections of iron.

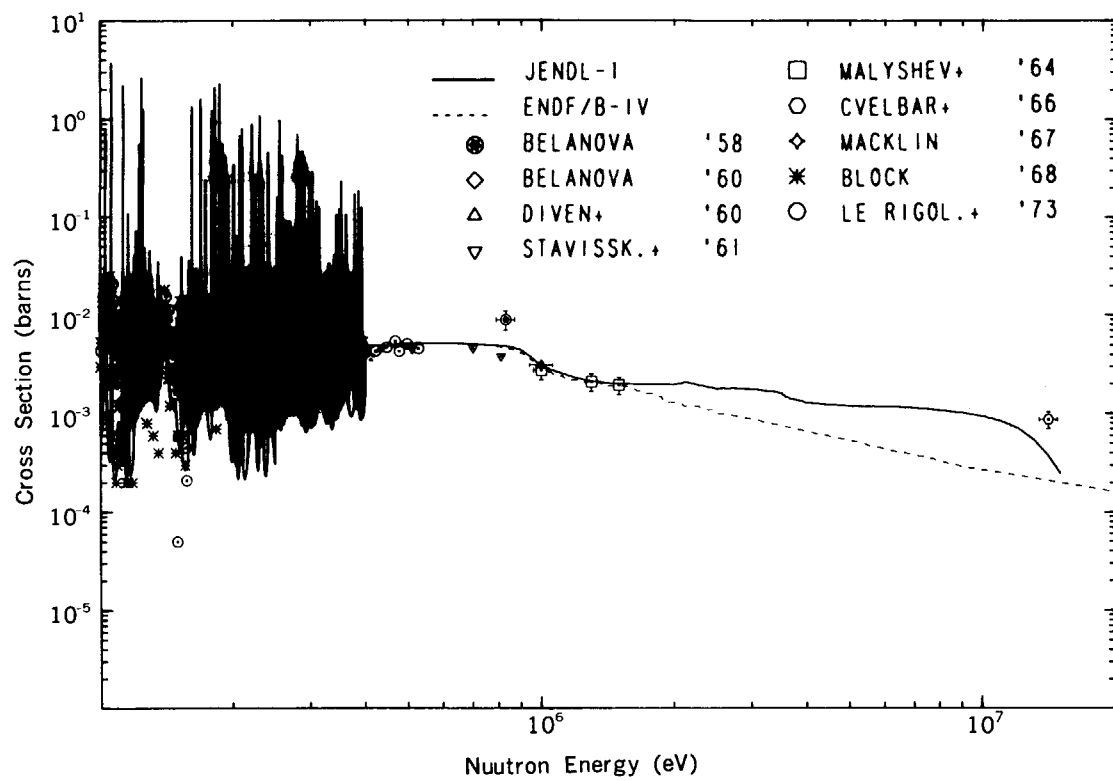


**Fig. A3.5** Capture cross sections of iron.

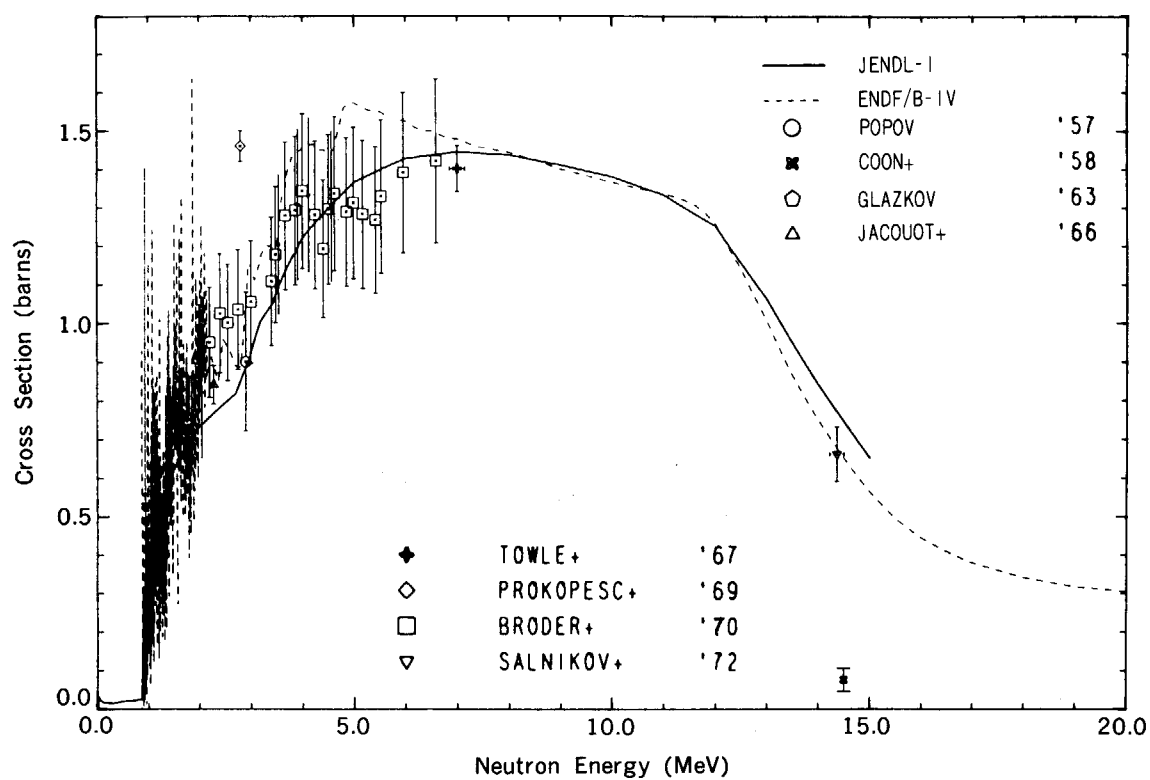


**Fig. A3.6** Inelastic scattering cross sections of iron.

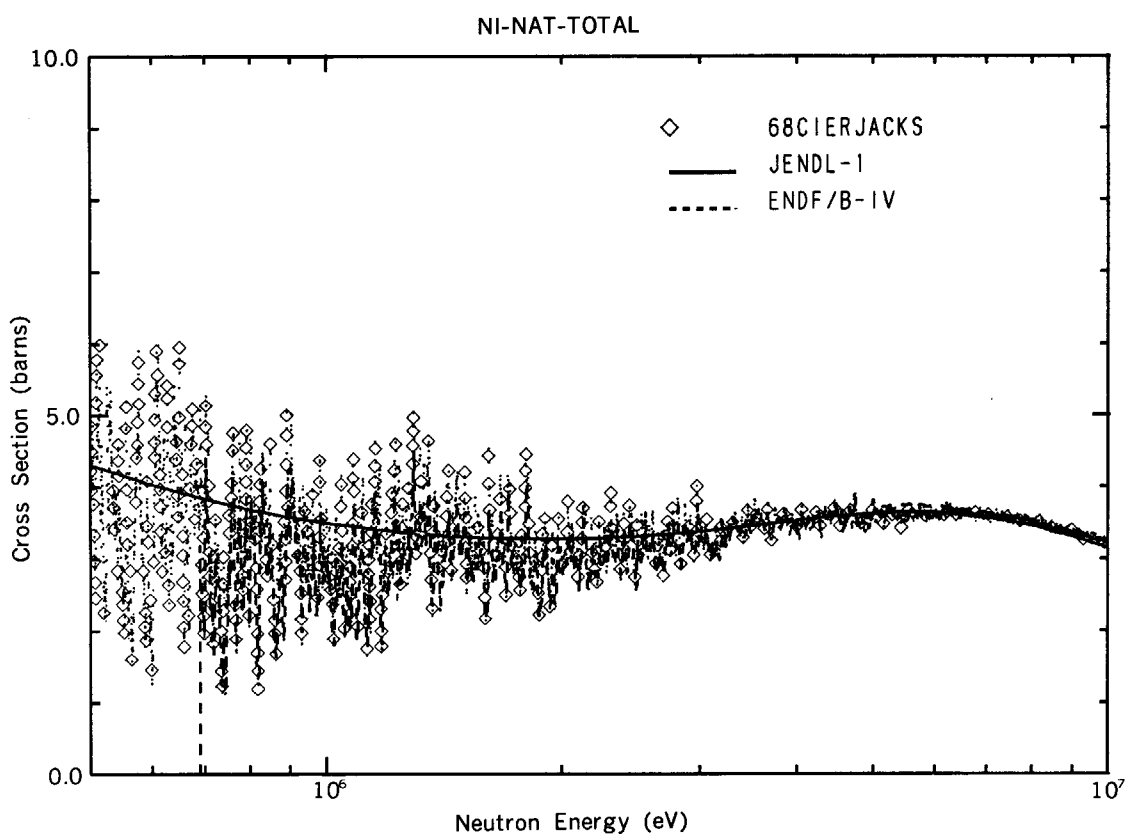


**Fig. A3.7** Total cross sections of nickel.

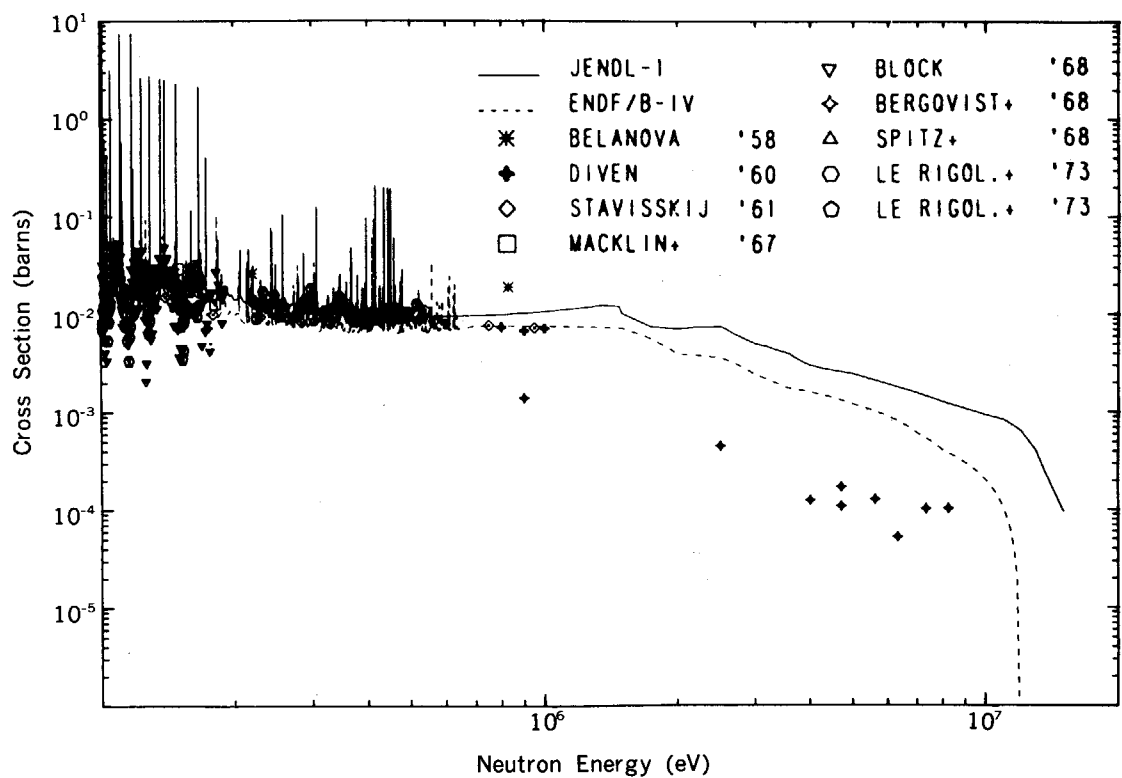


Fig. A3.8 Capture cross sections of nickel.

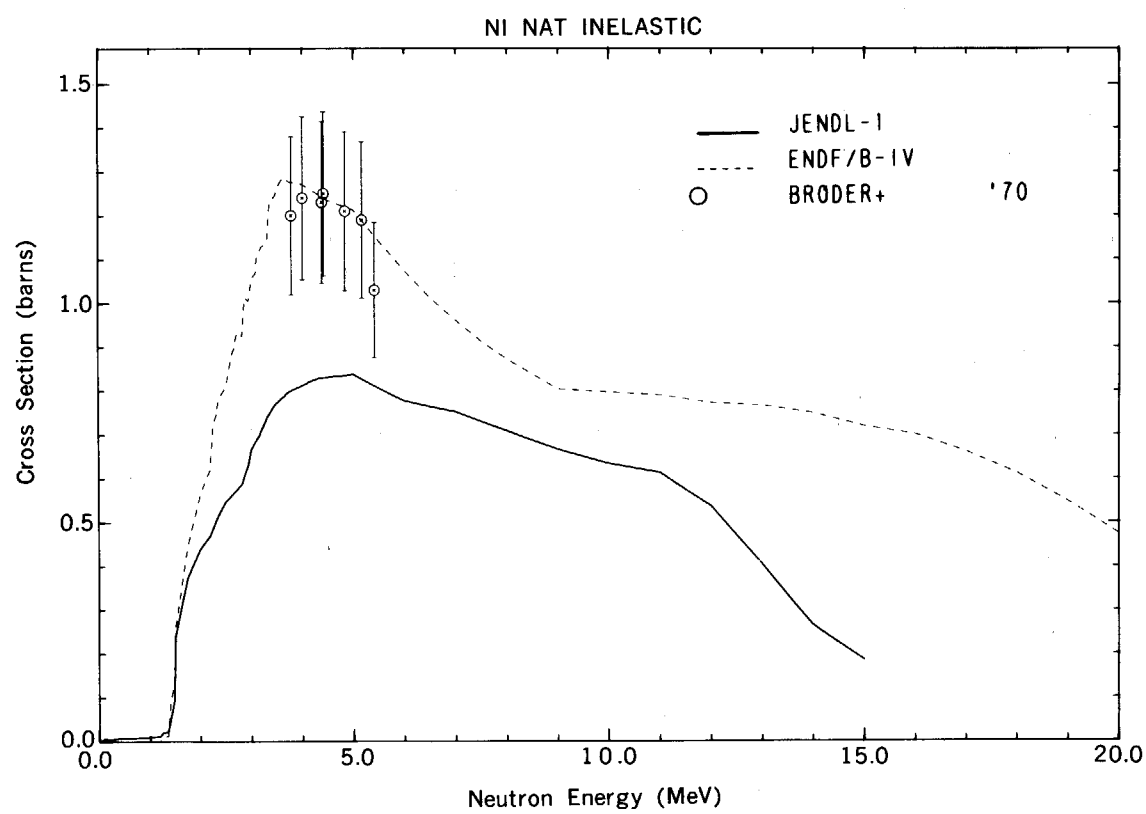


Fig. A3.9 Inelastic scattering cross sections of nickel.

### A3.1 Analysis with One-dimensional Model

The same calculations were made as done in the benchmark tests described in Chapter 2. We mainly discuss on the statistical average values.

#### A3.1.1 Effective Multiplication Factor

The effects of the replacement are shown in **Table A3.1**. The C/E values of  $k_{\text{eff}}$  are decreased by 0.7% on an average. Particularly the average C/E value is underestimated more than 1% for the Pu-cores with JENDL-B4. The  $k_{\text{eff}}$ -value of ZPR-3-54 is 4% lower than ZPR-3-53 with JENDL-B4 as the cases with JFS-2 and ENDF/B-IV. It could be concluded from these facts that the  $k_{\infty}$ -values are underestimated with JENDL-1 and that this underestimate is cancelled by underestimate of leakage effect due to overestimate of the elastic scattering cross sections of the structural materials.

**Table A3.1** Effective multiplication factors (C/E)

Assembly	*	JENDL-1	JENDL-B4	JFS-2	ENDF/B-IV
16 Pu-cores	A	0.9978	0.9894	1.0017	0.9859
	B	0.0074	0.0062	0.0044	0.0057
10 U-cores	A	1.0067	1.0011	1.0033	0.9960
	B	0.0077	0.0065	0.0100	0.0104
All cores	A	1.0012	0.9939	1.0023	0.9898
	B	0.0087	0.0085	0.0071	0.0093
ZPR-3-53		0.9994	0.9948	0.9965	0.9772
ZPR-3-54		1.0217	0.9572	0.9544	0.9335

\* A: Average of C/E  
B: Standard deviation of C/E

#### A3.1.2 Central Reaction Rate Ratio

The C/E values of central reaction rate ratio are given in **Table A3.2**. The fission rate ratio of  $^{238}\text{U}$  to  $^{235}\text{U}$  is decreased by 2 ~ 3% by replacing JENDL-1 with JENDL-B4. Little changes are observed in the other reaction rate ratio by the replacement. As shown in **Fig. A3.15** in the next section, the neutron flux above 1 MeV is decreased by the replacement.

#### A3.1.3 Central Reactivity Worth

**Table A3.3** compares the averages and standard deviations of the central reactivity worths normalized to those of  $^{239}\text{Pu}$ . By the replacement, the C/E values for  $^{238}\text{U}$  and  $^{10}\text{B}$  becomes slightly lower. The C/E values for chromium and iron increase by 25% and by 6%, respectively, while the C/E value decreases by 5% for nickel.

Components of the perturbation cross section are compared in **Table A3.4** in order to further investigate the changes in the worths of structural materials. It is evident from the table that the dominant components are capture and inelastic scattering, and that the elastic scattering has a minor role.

Both capture and inelastic scattering components of chromium are lower in JENDL-1 than ENDF/B-IV. It was pointed out by Asami et al.<sup>1)</sup> that the capture cross section might be overestimated in ENDF/B-IV. The inelastic scattering cross section of JENDL-1 is also lower than that of ENDF/B-IV. By comparing with the experimental data, the data of JENDL-1 look more reasonable.

The capture component of iron decreases by 5% by the replacement, while the inelastic

scattering components increases by 20%. As a whole, the total reactivity worth increases by several percents. There exist differences in the capture and inelastic scattering cross sections between JENDL-1 and ENDF/B-IV. By comparing with the measured data in **Fig. A3.4** and **A3.5**, it is difficult to say which one is better.

As to nickel, the capture component of ENDF/B-IV is 13% lower than that of JENDL-1, while the inelastic scattering component of ENDF/B-IV is about 60% higher. The difference in the total worth is much smaller because of compensation. We conclude from **Figs. A3.8** and **A3.9** that the capture cross section is overestimated and the inelastic scattering cross section is underestimated in JENDL-1.

**Table A3.2** Central reaction rate ratios

Quantity	Number of Assemblies	*	JENDL-1	JENDL-B4	JFS-2	ENDF/B-IV
<u><math>^{238}\text{U}</math> Fission</u> <u><math>^{235}\text{U}</math> Fission</u>	Pu-cores	A	1.008	0.980	1.021	1.031
	16	B	0.076	0.078	0.072	0.068
	U-cores	A	0.954	0.941	1.002	1.022
	9	B	0.073	0.076	0.074	0.080
	All cores	A	0.988	0.965	1.014	1.028
	25	B	0.079	0.080	0.073	0.073
	Pu-cores	A	0.964	0.964	0.974	0.975
	15	B	0.031	0.031	0.031	0.031
<u><math>^{239}\text{Pu}</math> Fission</u> <u><math>^{235}\text{U}</math> Fission</u>	U-cores	A	0.972	0.972	0.985	0.990
	8	B	0.041	0.041	0.038	0.039
	All cores	A	0.967	0.967	0.977	0.980
	23	B	0.035	0.035	0.034	0.034
	Pu-cores	A	1.009	1.007	1.058	1.063
	9	B	0.127	0.125	0.117	0.127
	U-cores	A	1.008	1.007	1.061	1.083
	4	B	0.082	0.080	0.069	0.077
<u><math>^{240}\text{Pu}</math> Fission</u> <u><math>^{235}\text{U}</math> Fission</u>	All cores	A	1.009	1.007	1.059	1.069
	13	B	0.115	0.113	0.105	0.114
	Pu-cores	A	0.997	1.001	0.995	1.021
	6	B	0.028	0.029	0.027	0.029
	U-cores	A	0.983	0.984	0.981	0.984
	6	B	0.013	0.014	0.014	0.023
	All cores	A	0.990	0.993	0.988	1.003
	12	B	0.023	0.024	0.023	0.032
<u><math>^{238}\text{U}</math> Capture</u> <u><math>^{235}\text{U}</math> Fission</u>	Pu-cores	A	1.042	1.046	1.030	1.052
	6	B	0.031	0.031	0.030	0.032
	U-cores	A	0.983	0.984	0.981	0.984
	6	B	0.013	0.014	0.014	0.023
	All cores	A	0.990	0.993	0.988	1.003
	12	B	0.023	0.024	0.023	0.032
	Pu-cores	A	1.042	1.046	1.030	1.052
	6	B	0.031	0.031	0.030	0.032
<u><math>^{238}\text{U}</math> Capture</u> <u><math>^{239}\text{Pu}</math> Fission</u>	U-cores	A	0.985	0.987	0.972	0.965
	5	B	0.040	0.039	0.036	0.030
	All cores	A	1.016	1.019	1.004	1.012
	11	B	0.045	0.045	0.044	0.053

\* A: Average of C/E

B: Standard deviation of C/E

**Table A3.3** Central reactivity worths normalized to those of  $^{239}\text{Pu}$ 

Sample	Number of Assemblies	*	JENDL-1	JENDL-B4	JFS-2	ENDF/B-IV
$^{235}\text{U}$	14	A	1.046	1.047	1.011	1.037
		B	0.037	0.037	0.039	0.038
$^{238}\text{U}$	13	A	1.041	1.036	0.982	0.965
		B	0.094	0.091	0.080	0.087
$^{10}\text{B}$	13	A	0.919	0.914	0.910	0.852
		B	0.095	0.092	0.089	0.086
Cr	9	A	1.014	1.265	1.316	1.375
		B	0.098	0.132	0.129	0.143
Fe	12	A	0.916	0.979	1.019	1.113
		B	0.113	0.139	0.134	0.201
Ni	10	A	1.084	1.036	1.116	1.119
		B	0.123	0.115	0.105	0.117

\* A: Average of C/E

B: Standard deviation of C/E

**Table A3.4** Components of perturbation cross section for chromium, iron and nickel

Assembly	Com- ponent	Cr			Fe			Ni		
		JENDL -1	JENDL -B4	Ratio*	JENDL -1	JENDL -B4	Ratio*	JENDL -1	JENDL -B4	Ratio*
VERA-11A	Capture	-8.05	-11.44	1.42	-8.42	-7.84	0.93	-49.45	-43.06	0.87
	Inelastic	1.41	1.19	0.85	3.39	2.25	0.66	1.19	1.32	1.11
	Elastic	6.86	6.72	0.98	3.42	2.77	0.81	9.01	9.98	1.11
	Total	0.22	-3.52	-15.96	-1.61	-2.81	1.75	-39.25	-31.75	0.81
VERA-1B	Capture	-9.34	-13.23	1.42	-8.54	-7.87	0.92	-42.39	-36.47	0.86
	Inelastic	14.08	16.56	1.18	18.46	19.58	1.06	10.23	15.93	1.56
	Elastic	14.38	13.66	0.95	11.68	10.84	0.93	17.26	17.49	1.01
	Total	19.12	16.99	0.89	21.59	22.55	1.04	-14.91	-3.06	0.21
ZPR-3-6F	Capture	-5.58	-8.02	1.44	-7.18	-6.67	0.93	-39.83	-33.90	0.85
	Inelastic	-6.36	-7.83	1.23	-4.06	-6.76	1.66	-4.21	-6.97	1.66
	Elastic	8.29	7.47	0.90	2.87	2.21	0.77	10.40	12.37	1.19
	Total	-3.65	-8.38	2.30	-8.37	-11.23	1.34	-33.64	-28.50	0.85
ZPR-3-54	Capture	-17.22	-21.75	1.26	-12.77	-12.86	1.01	-42.69	-37.45	0.88
	Inelastic	0.81	2.76	3.40	1.68	3.54	2.11	0.55	2.46	4.44
	Elastic	7.48	9.00	1.20	5.65	6.74	1.19	12.52	14.98	1.20
	Total	-8.92	-9.99	1.12	-5.44	-2.59	0.48	-29.62	-20.01	0.68
ZPR-3-53	Capture	-17.24	-21.94	1.27	-12.80	-13.01	1.02	-42.87	-37.75	0.88
	Inelastic	0.67	0.86	1.28	1.57	1.35	0.86	0.48	0.69	1.42
	Elastic	7.92	8.16	1.03	6.02	6.12	1.02	13.23	13.82	1.04
	Total	-8.65	-12.92	1.49	-5.21	-5.54	1.06	-29.15	-23.24	0.80
FCA-V-2	Capture	-8.72	-12.91	1.48	-8.15	-7.61	0.93	-38.78	-33.24	0.86
	Inelastic	-4.97	-5.79	1.16	-4.66	-5.92	1.27	-3.39	-5.39	1.59
	Elastic	3.85	4.37	1.14	2.15	1.99	0.93	13.23	14.69	1.11
	Total	-9.85	-14.32	1.45	-10.66	-11.54	1.08	-28.94	-23.94	0.83
FCA-V-1	Capture	-8.34	-12.46	1.49	-8.04	-7.39	0.92	-38.13	-32.65	0.86
	Inelastic	-5.96	-6.92	1.16	-5.58	-7.05	1.27	-4.09	-6.47	1.58
	Elastic	3.69	4.06	1.10	1.94	1.62	0.84	12.96	14.17	1.09
	Total	-10.61	-15.32	1.44	-11.67	-12.82	1.10	-29.26	-24.94	0.85

Table A3.4 (cont.)

Assembly	Com- ponent	Cr			Fe			Ni		
		JENDL -1	JENDL -B4	Ratio*	JENDL -1	JENDL -B4	Ratio*	JENDL -1	JENDL -B4	Ratio*
SNEAK-7A	Capture	-12.04	-16.48	1.37	-10.05	-9.58	0.95	-44.75	-39.11	0.87
	Inelastic	-9.75	-11.25	1.15	-10.17	-12.16	1.20	-6.75	-10.80	1.60
	Elastic	3.43	3.98	1.16	1.74	1.84	1.06	9.16	9.83	1.07
	Total	-18.36	-23.74	1.29	-18.47	-19.90	1.08	-42.35	-40.08	0.95
FCA-VI-2	Capture	-12.31	-17.18	1.40	-9.88	-9.55	0.97	-38.55	-33.34	0.87
	Inelastic	-9.38	-10.27	1.10	-10.32	-11.32	1.10	-6.59	-9.78	1.48
	Elastic	-1.56	-0.87	0.56	-0.91	-0.55	0.61	4.51	4.68	1.04
	Total	-23.25	-28.32	1.22	-21.11	-21.42	1.02	-40.63	-38.44	0.95
ZPR-3-12	Capture	-8.00	-11.87	1.48	-8.60	-7.70	0.90	-41.32	-36.08	0.87
	Inelastic	-14.17	-16.44	1.16	-13.14	-16.76	1.28	-9.63	-15.45	1.60
	Elastic	5.25	4.97	0.95	4.62	4.59	0.99	11.65	12.04	1.03
	Total	-16.92	-23.34	1.38	-17.11	-19.87	1.16	-39.30	-39.49	1.01
MAZ	Capture	-10.35	-14.65	1.42	-8.90	-8.60	0.97	-38.77	-33.20	0.86
	Inelastic	-9.30	-10.38	1.12	-10.43	-11.58	1.11	-6.50	-9.83	1.51
	Elastic	-1.81	-0.77	0.42	-1.43	-0.91	0.63	3.97	4.90	1.24
	Total	-21.46	-25.79	1.20	-20.77	-21.08	1.02	-41.31	-38.13	0.92
FCA-I-6	Capture	-5.70	-8.01	1.41	-7.73	-7.06	0.91	-40.24	-34.84	0.87
	Inelastic	-19.40	-22.83	1.18	-18.62	-23.71	1.27	-13.13	-21.37	1.63
	Elastic	4.40	3.24	0.74	2.51	2.90	1.15	4.65	5.84	1.26
	Total	-20.70	-27.59	1.33	-23.84	-27.87	1.17	-48.73	-50.38	1.03
FCA-I-1	Capture	-5.62	-7.90	1.41	-7.73	-7.04	0.91	-39.80	-34.45	0.87
	Inelastic	-19.84	-23.26	1.17	-19.20	-24.28	1.26	-13.39	-21.74	1.62
	Elastic	3.93	2.77	0.70	2.26	2.63	1.16	4.26	5.39	1.27
	Total	-21.53	-28.40	1.32	-24.67	-28.69	1.16	-48.94	-50.80	1.04
FCA-3-2S	Capture	-12.76	-17.59	1.38	-9.83	-9.33	0.95	-40.79	-35.62	0.87
	Inelastic	-7.72	-8.65	1.12	-6.78	-8.61	1.27	-5.26	-8.18	1.56
	Elastic	7.22	7.30	1.01	5.84	5.83	1.00	14.83	15.26	1.03
	Total	-13.26	-18.94	1.43	-10.77	-12.11	1.12	-31.22	-28.54	0.91
FCA-VI-1	Capture	-10.06	-14.36	1.43	-8.78	-8.42	0.96	-39.27	-33.71	0.86
	Inelastic	-10.23	-11.46	1.12	-11.20	-12.61	1.13	-7.14	-10.90	1.53
	Elastic	-1.40	-0.33	0.24	-1.21	-0.83	0.68	6.03	7.05	1.17
	Total	-21.69	-26.16	1.21	-21.20	-21.86	1.03	-40.38	-37.56	0.93
ZPR-3-50	Capture	-15.82	-20.54	1.30	-11.98	-11.90	0.99	-44.17	-38.95	0.88
	Inelastic	-11.25	-12.78	1.14	-11.67	-13.84	1.19	-7.77	-12.23	1.58
	Elastic	5.15	5.76	1.12	3.49	3.88	1.11	12.12	12.77	1.05
	Total	-21.93	-27.57	1.26	-20.16	-21.85	1.08	-39.82	-38.41	0.97
ZPR-3-48	Capture	-11.90	-16.40	1.38	-9.83	-9.54	0.97	-41.67	-36.17	0.87
	Inelastic	-12.13	-13.67	1.13	-12.84	-14.85	1.16	-8.39	-13.02	1.55
	Elastic	1.26	2.11	1.67	0.80	1.20	1.50	8.60	9.44	1.10
	Total	-22.76	-27.96	1.23	-21.87	-23.19	1.06	-41.46	-39.75	0.96
ZPR-3-49	Capture	-10.92	-15.14	1.39	-8.95	-8.58	0.96	-42.44	-36.71	0.87
	Inelastic	-14.27	-16.08	1.13	-15.19	-17.46	1.15	-9.86	-15.32	1.55
	Elastic	0.15	0.96	6.55	0.85	0.44	0.51	5.64	6.59	1.17
	Total	-25.05	-30.26	1.21	-25.00	-26.48	1.06	-46.66	-45.43	0.97
ZPR-3-56B	Capture	-11.06	-15.53	1.41	-9.03	-8.74	0.97	-39.23	-33.74	0.86
	Inelastic	-10.10	-11.21	1.11	-11.19	-12.41	1.11	-7.07	-10.67	1.51
	Elastic	-2.39	-1.49	0.62	-1.70	-1.34	0.97	4.66	5.41	1.16
	Total	-23.54	-28.23	1.20	-21.91	-22.49	1.03	-41.65	-39.00	0.94

**Table A3.4** (cont.)

Assembly	Com- ponent	Cr			Fe			Ni		
		JENDL -1	JENDL -B4	Ratio*	JENDL -1	JENDL -B4	Ratio*	JENDL -1	JENDL -B4	Ratio*
ZPR-6-6A	Capture	-12.37	-17.50	1.42	-9.48	-9.15	0.97	-36.75	-31.82	0.87
	Inelastic	-6.01	-6.47	1.08	-5.94	-6.82	2.36	-4.18	-6.13	1.47
	Elastic	3.06	3.47	1.14	2.89	2.88	1.00	12.46	13.04	1.05
	Total	-15.32	-20.50	1.34	-12.52	-13.08	1.05	-28.48	-24.91	0.88
ZPPR-2	Capture	-12.81	-17.67	1.38	-9.97	-9.77	0.98	-38.53	-33.31	0.86
	Inelastic	-10.33	-11.20	1.09	-11.50	-12.48	1.09	-7.26	-10.66	1.47
	Elastic	-2.60	-1.63	0.63	-1.13	-0.68	0.60	5.47	5.93	1.08
	Total	-25.74	-30.50	1.19	-22.60	-22.93	1.01	-40.32	-38.04	0.94
MZB	Capture	-12.07	-16.82	1.39	-9.81	-9.56	0.97	-37.96	-32.70	0.86
	Inelastic	-10.31	-11.19	1.09	-11.60	-12.55	1.08	-7.24	-10.62	1.47
	Elastic	-3.31	-2.31	0.70	-1.79	-1.30	0.73	3.84	4.18	1.09
	Total	-25.70	-30.32	1.18	-23.20	-23.40	1.01	-41.37	-39.14	0.95
ZEBRA-2	Capture	-12.51	-17.35	1.39	-10.79	-10.01	0.93	-42.50	-37.63	0.89
	Inelastic	-14.84	-17.17	1.16	-14.63	-18.18	1.24	-10.12	-16.26	1.61
	Elastic	6.13	6.28	1.02	5.87	6.07	1.03	15.50	15.48	1.00
	Total	-21.22	-28.24	1.33	-19.54	-22.12	1.13	-37.13	-38.41	1.42
ZPR-6-7	Capture	-12.84	-17.70	1.38	-9.96	-9.76	0.98	-38.52	-33.29	0.86
	Inelastic	-10.27	-11.13	1.08	-11.42	-12.40	1.09	-7.22	-10.59	1.47
	Elastic	-2.44	-1.51	0.62	-1.02	-0.59	0.58	5.69	6.09	1.07
	Total	-25.55	-30.34	1.19	-22.40	-22.75	1.02	-40.05	-37.79	0.94
SNEAK-7B	Capture	-10.03	-14.40	1.44	-9.09	-8.37	0.92	-42.62	-37.17	0.87
	Inelastic	-17.62	-19.91	1.13	-19.03	-21.89	1.15	-12.18	-19.18	1.58
	Elastic	-3.33	-2.62	0.79	-3.68	-3.42	0.93	2.39	2.76	1.15
	Total	-30.98	-36.93	1.19	-31.80	-33.69	1.06	-52.41	-53.59	1.02
ZPR-3-11	Capture	-5.88	-8.41	1.43	-7.90	-7.08	0.90	-36.29	-31.37	0.86
	Inelastic	-20.91	-24.32	1.16	-21.63	-26.28	1.22	-14.20	-22.98	1.62
	Elastic	-3.59	-4.17	1.16	-2.68	-2.55	0.95	-1.11	-0.83	0.75
	Total	-30.38	-36.90	1.22	-32.21	-35.91	1.12	-51.60	-55.18	1.07
ZEBRA-3	Capture	-5.81	-8.21	1.41	-8.14	-7.35	0.90	-41.17	-36.08	0.88
	Inelastic	-27.13	-31.78	1.17	-29.21	-35.08	1.20	-18.38	-30.18	1.64
	Elastic	-11.20	-11.16	1.00	-10.02	-10.23	1.02	-12.01	-11.72	0.98
	Total	-44.14	-51.14	1.16	-47.37	-52.65	1.11	-71.56	-77.98	1.09
Average	Capture	-10.57	-14.65	1.39	-9.35	-8.90	0.95	-40.72	-35.33	0.87
	Inelastic	-9.83	-11.13	1.13	-9.81	-11.79	1.20	-6.72	-10.53	1.57
	Elastic	2.18	2.50	1.15	1.38	1.53	1.11	7.81	8.58	1.10
	Total	-18.22	-23.28	1.28	-17.77	-19.16	1.08	-39.63	-37.28	0.94

\* JENDL-B4/JENDL-1

**A3.1.4 Doppler Coefficient**

The C/E values of Doppler coefficients are given in **Table A3.5**. The C/E values decrease by about 2% with JENDL-B4.

**Table A3.5** Doppler reactivity coefficients (C/E)

	Assembly	JENDL-1	JENDL-B4	ENDF/B-IV
Small Sample Doppler Experiment	FCA V-1	1.09	1.07	0.91
	V-2	0.98	0.96	0.78
	VI-1	1.13	1.10	0.93
	VI-2	1.03	1.01	0.87
	ZPPR-2 (Normal)	1.25	1.22	0.93
	(Na-voided)	0.96	0.92	0.81
	ZPR-3-47	1.04	1.04	0.92
Whole Core Doppler Experiment	SEFOR	1.12	1.12	1.04
Average of C/E		1.08	1.06	0.90
Standard Deviation of C/E		0.09	0.09	0.08

### A3.1.5 Snell Experiments

The fission rate ratios of  $^{235}\text{U}$  to  $^{238}\text{U}$  and of  $^{239}\text{Pu}$  to  $^{238}\text{U}$  in natural uranium equilibrium spectra are given in **Table A3.6**. Both ratios decrease by 1% with JENDL-B4.

**Table A3.6** Fission rate ratios in natural uranium equilibrium spectra

Library	$\frac{^{235}\text{U} \text{ fission}}{^{238}\text{U} \text{ fission}}$	$\frac{^{239}\text{Pu} \text{ fission}}{^{238}\text{U} \text{ fission}}$
	$\frac{^{235}\text{U} \text{ fission}}{^{238}\text{U} \text{ fission}}$	$\frac{^{239}\text{Pu} \text{ fission}}{^{238}\text{U} \text{ fission}}$
JENDL-1	240.8	220.0
JENDL-B4	238.2	217.8
ENDF/B-IV	227.7	203.4

### A3.2 Analysis of MZB with Two-dimensional Model

Effects of cross sections of the structural materials were studied on MZB core characteristics. Effective multiplication factor, central reaction rate ratios and reaction rate distributions were calculated with the two-dimensional R-Z model as shown in **Fig. A3.10**. The calculation was performed with the 25 group macroscopic cross sections collapsed with the 1-D diffusion code EXPANDA-70D. The difference in the 70 group elastic removal cross sections between ENDF/B-IV and JENDL-1 is shown in **Fig. A3.11**. The discrepancies are specially remarkable in the energy range from 500 keV to 4 MeV. **Figures A3.12, A3.13** and **A3.14** compare the 25 group macroscopic capture cross sections, diffusion coefficients and removal cross sections, respectively, in the steel reflector of MZB. It is seen from these figures that the discrepancies between ENDF/B-IV and JENDL-1 are remarkable. The discrepancy of the diffusion coefficients in the important energy range from 10 keV to 4 MeV must have considerable effects on the calculation of neutron leakage.

**Table A3.7** shows comparison of the effective multiplication factors and central reaction rate ratios calculated with JENDL-1, JENDL-B4 and JFS-2. The effective multiplication factor  $k_{\text{eff}}$  with JENDL-B4 becomes about 1.3% smaller than that with JENDL-1 as observed in the 1-D calculation described in Section A3.1. This must be mainly caused by the difference in the neutron leakage. As to the central reaction rate ratios, the difference is seen only for the ratio of  $^{238}\text{U}$  fission to  $^{235}\text{U}$  fission. This can be understood from the core center neutron

spectra shown in **Fig. A3.15**. The spectra calculated with JENDL-B4 are softer than those for JENDL-1, because the removal cross sections of JENDL-B4 are larger than those of JENDL-1 in the energy range above 1.4 MeV. This is caused by the difference in the inelastic scattering cross sections as shown in **Fig. A3.6**.

The reaction rate distribution for  $^{235}\text{U}$  fission,  $^{239}\text{Pu}$  fission,  $^{238}\text{U}$  fission,  $^{238}\text{U}$  capture and iron capture are shown in **Figs. A3.16 ~ A3.20**, respectively, as the ratio of the result with JENDL-B4 to that with JENDL-1. It is seen from these figures that the results with JENDL-B4 become smaller than those with JENDL-1 in the radial blanket and reflector regions except for the capture rate distribution of iron  $\alpha_c(\text{Fe})$ . This depression with JENDL-B4 is caused by the larger neutron leakage due to the larger diffusion coefficients in the reflector above 10 keV as seen in **Fig. A3.13**. The larger capture rate of iron in the blanket region can be understood by the larger capture cross section of ENDF/B-IV in the energy region below 10 keV as is seen in **Fig. A4.10**.

**Table A3.7** Effective multiplication factors and central reaction rate ratios for MZB

	JENDL-1	JENDL-B4	JFS-2
$k_{\text{eff}}$	0.98824	0.97548	0.98749
$^{238}\text{U}$ fission/ $^{235}\text{U}$ fission	0.02218	0.02128	0.02244
$^{235}\text{U}$ fission/ $^{239}\text{Pu}$ fission	1.09341	1.09123	1.08502
$^{238}\text{U}$ capture/ $^{239}\text{Pu}$ fission	0.15009	0.15063	0.14831
$^{241}\text{Pu}$ fission/ $^{239}\text{Pu}$ fission	1.37445	1.37279	1.3788

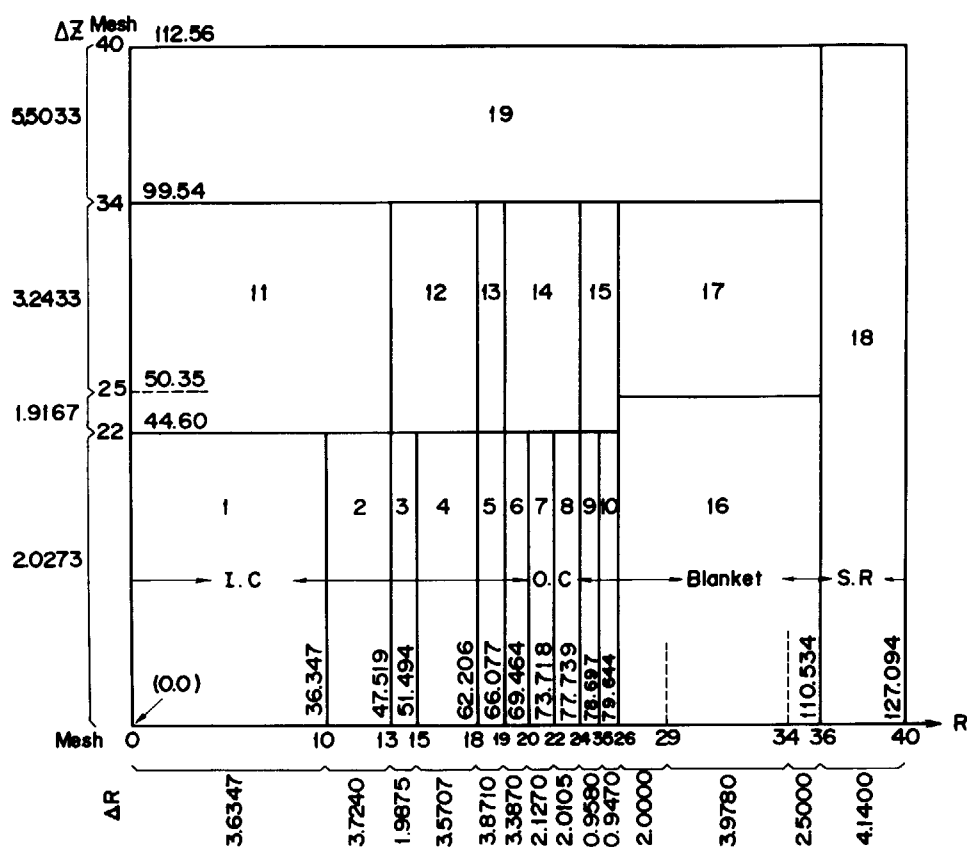


**Fig. A3.10** Two-dimensional R-Z calculational model for MZB critical assembly.

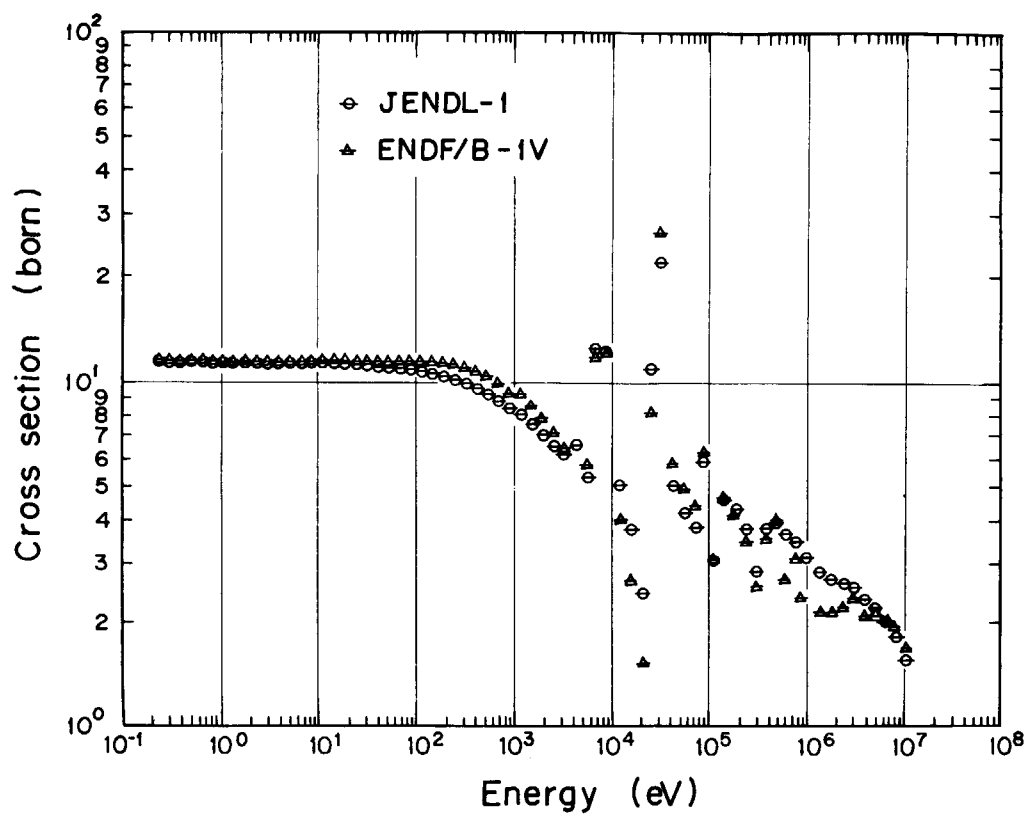


**Fig. A3.11** 70-group elastic removal cross sections of iron.

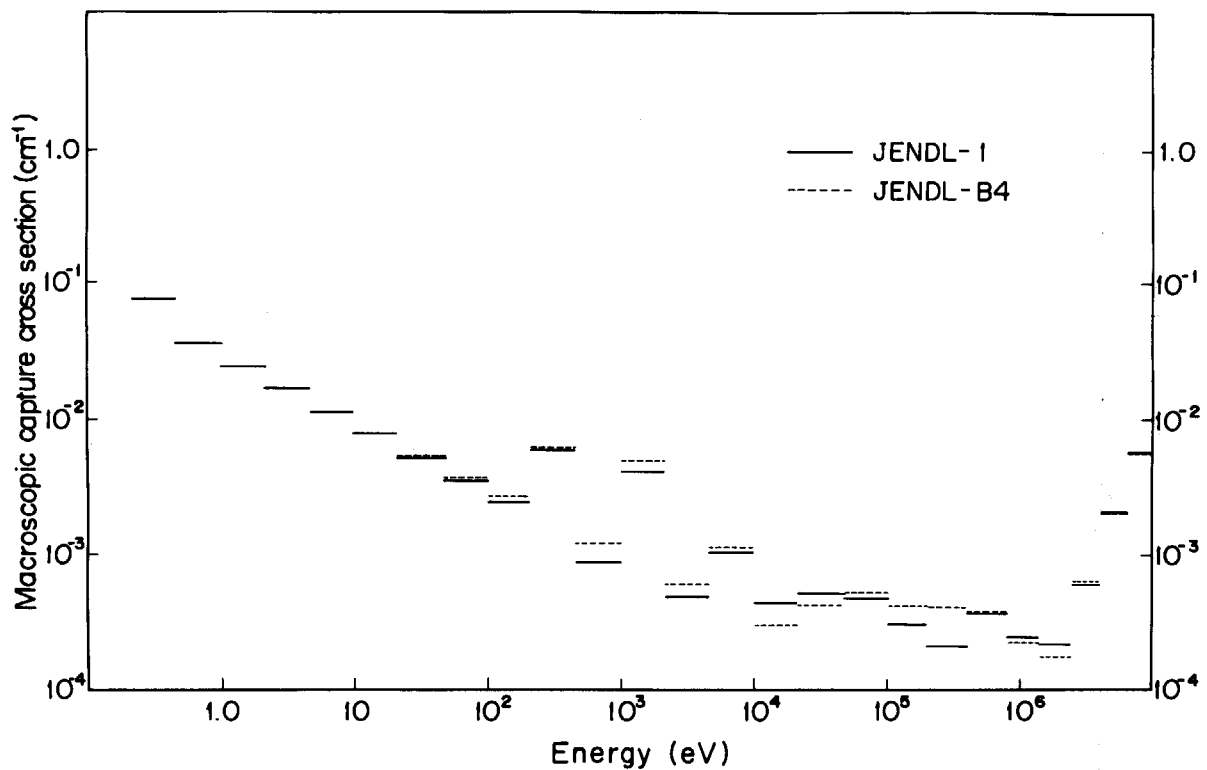


**Fig. A3.12** 25-group macroscopic capture cross sections in the steel reflector of MZB.

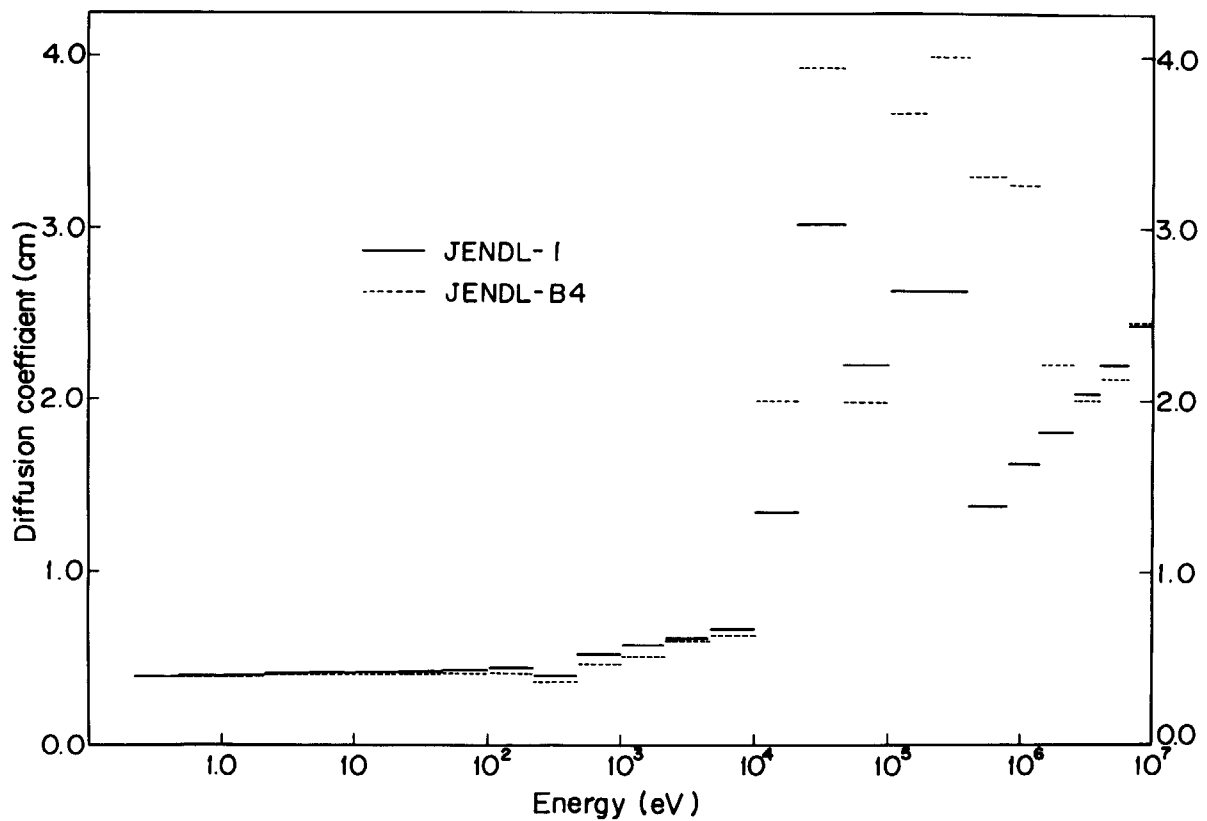


**Fig. A3.13** 25-group diffusion coefficients in the steel reflector of MZB.

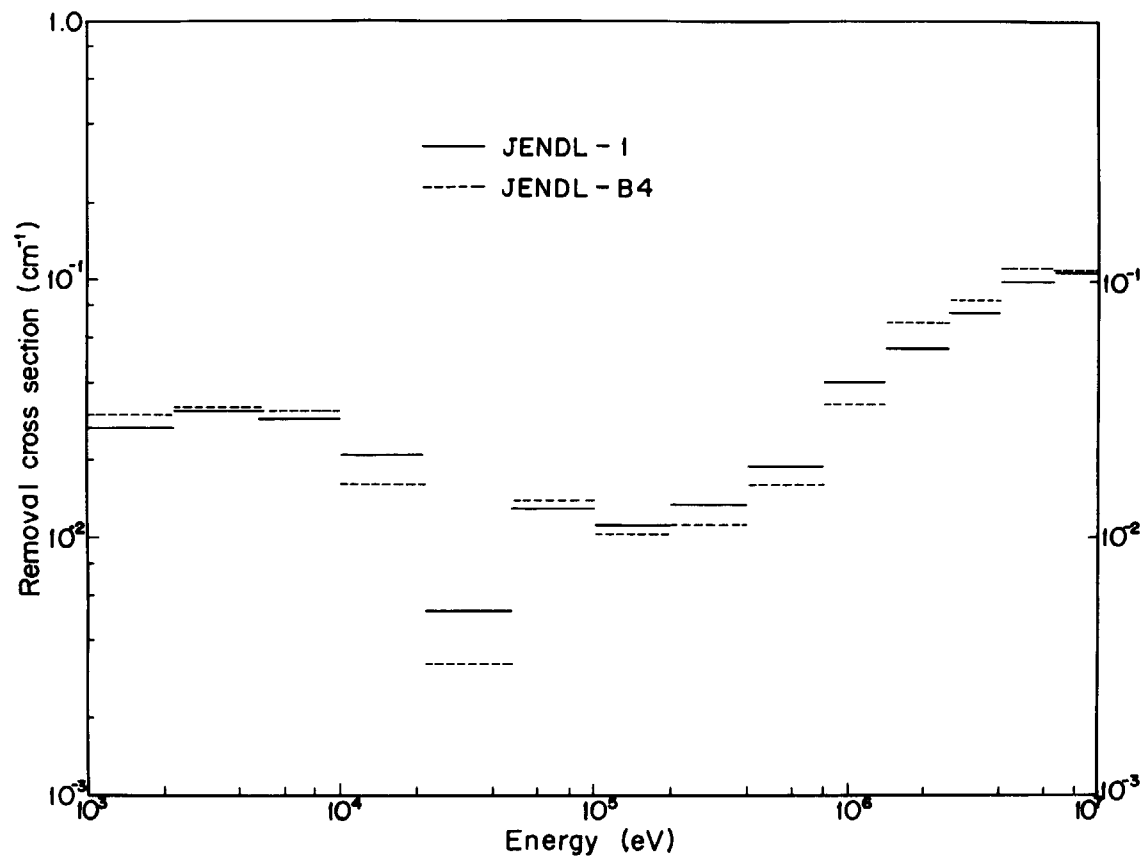


**Fig. A3.14** 25-group macroscopic removal cross sections in the steel reflector of MZB.

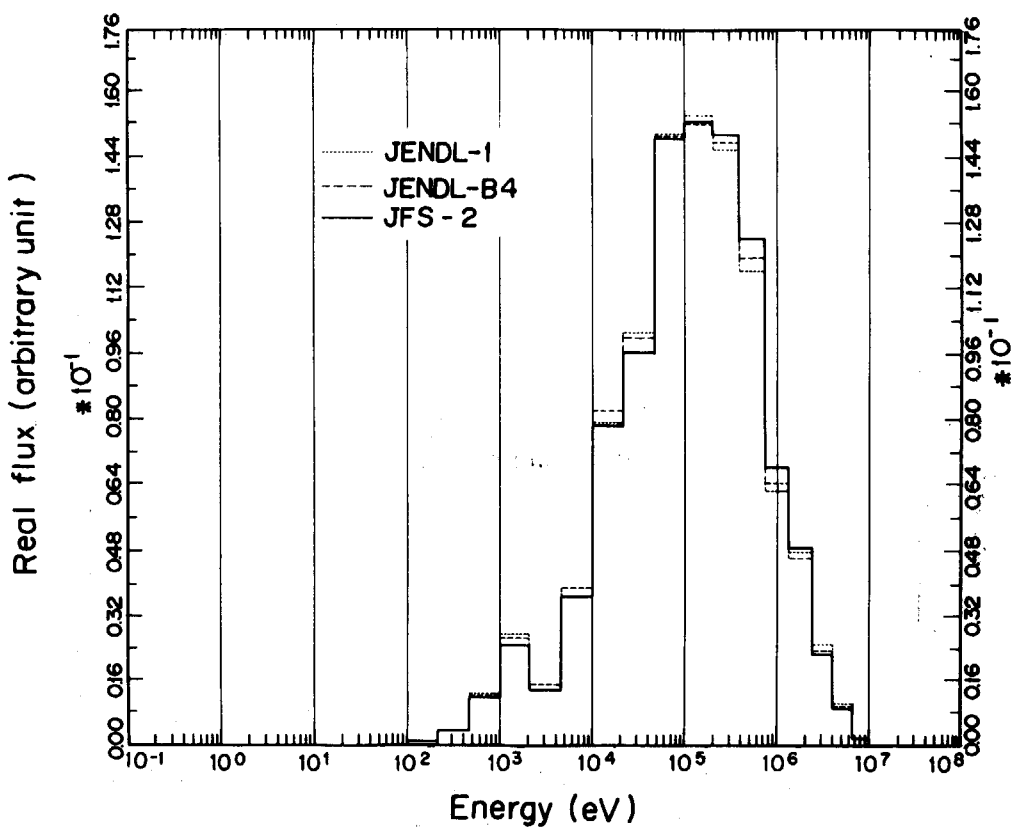
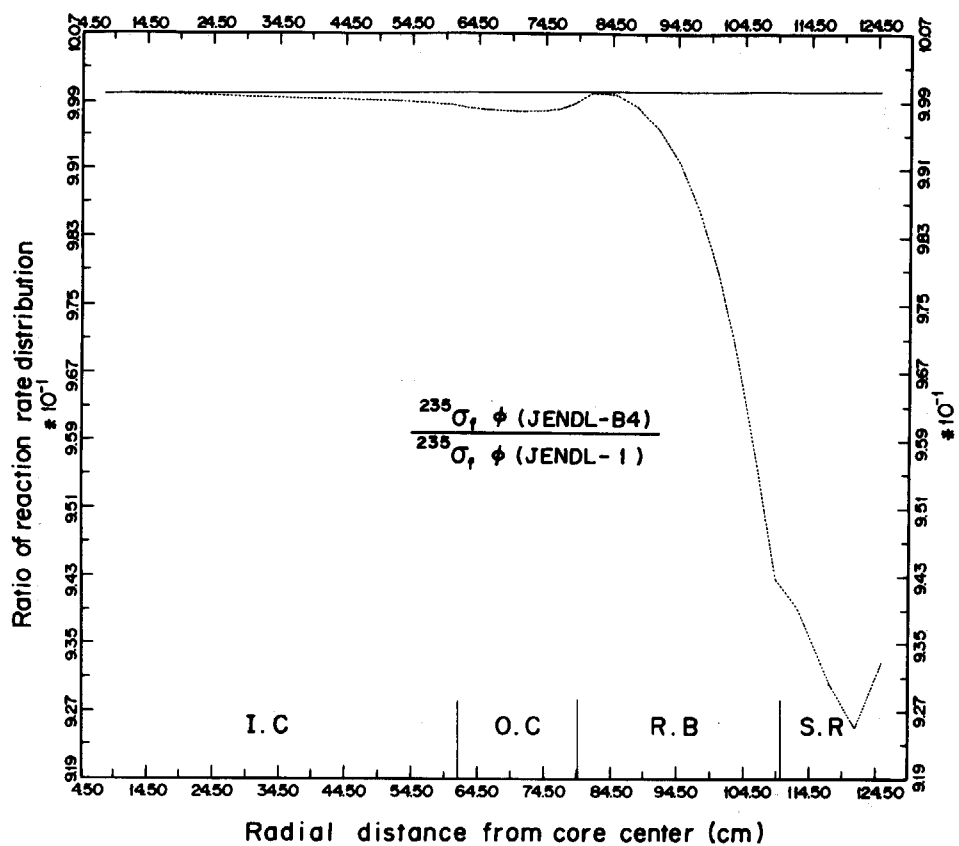
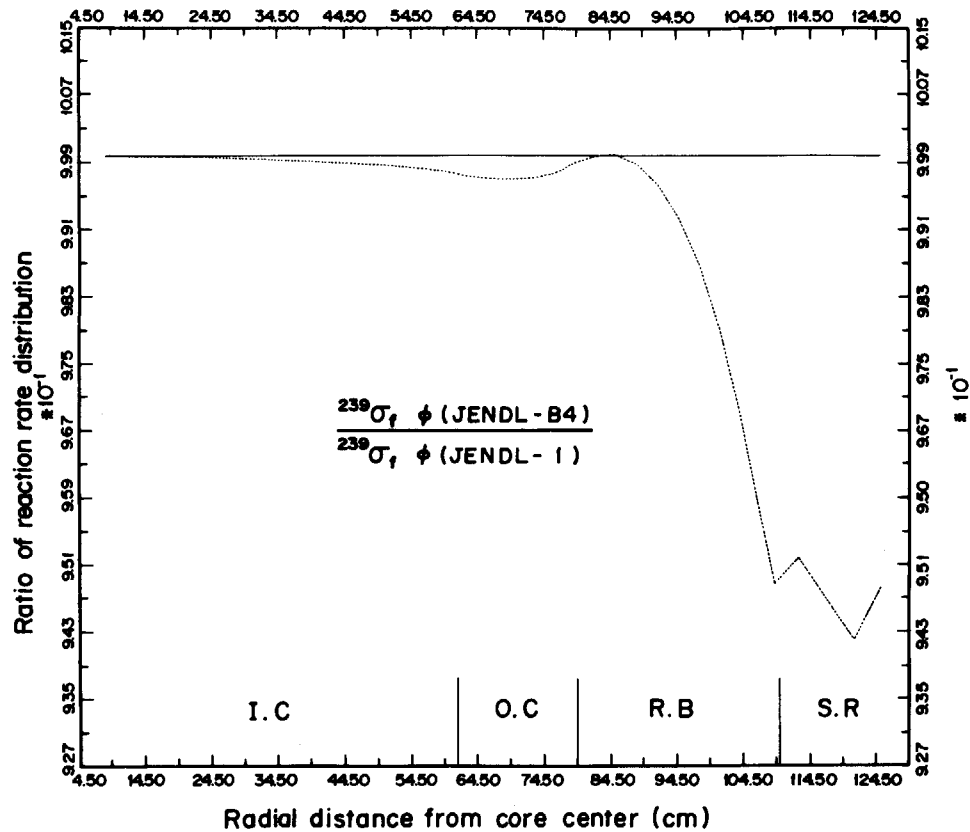
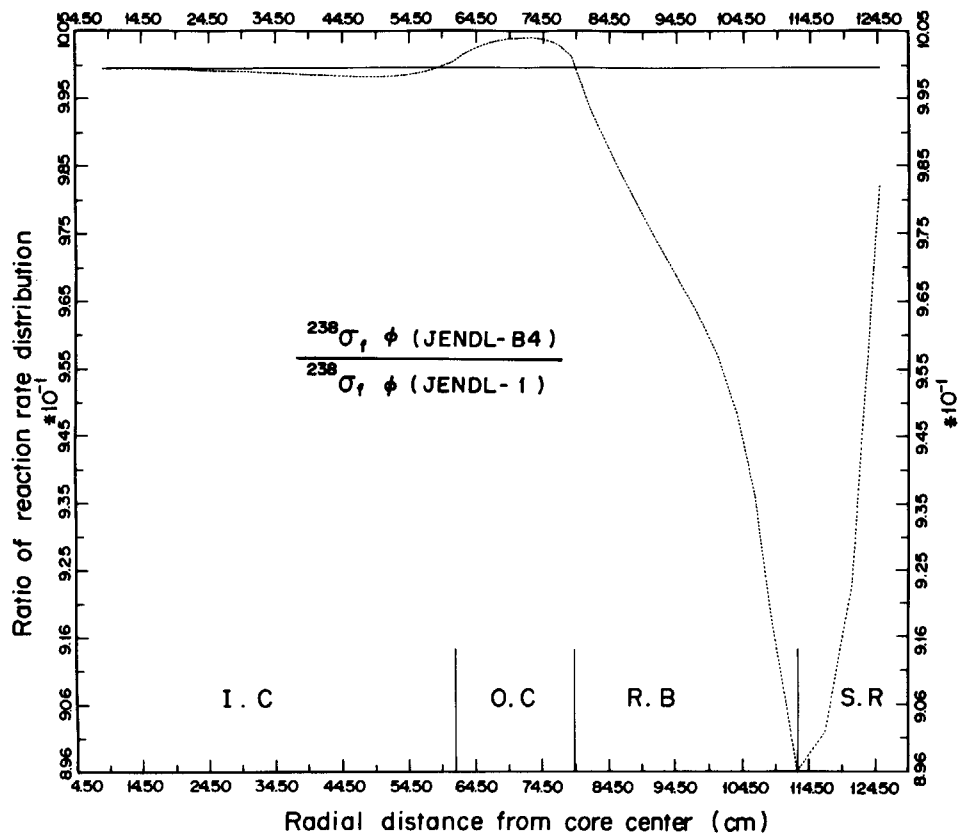


Fig. A3.15 Neutron spectra at the core center of MZB.

Fig. A3.16 Ratio of  $^{235}\text{U}$  fission rate distribution calculated with JENDL-B4 to that with JENDL-1.



**Fig. A3.17** Ratio of  $^{239}\text{Pu}$  fission rate distribution calculated with JENDL-B4 to that with JENDL-1.



**Fig. A3.18** Ratio of  $^{238}\text{U}$  fission rate distribution calculated with JENDL-B4 to that with JENDL-1.

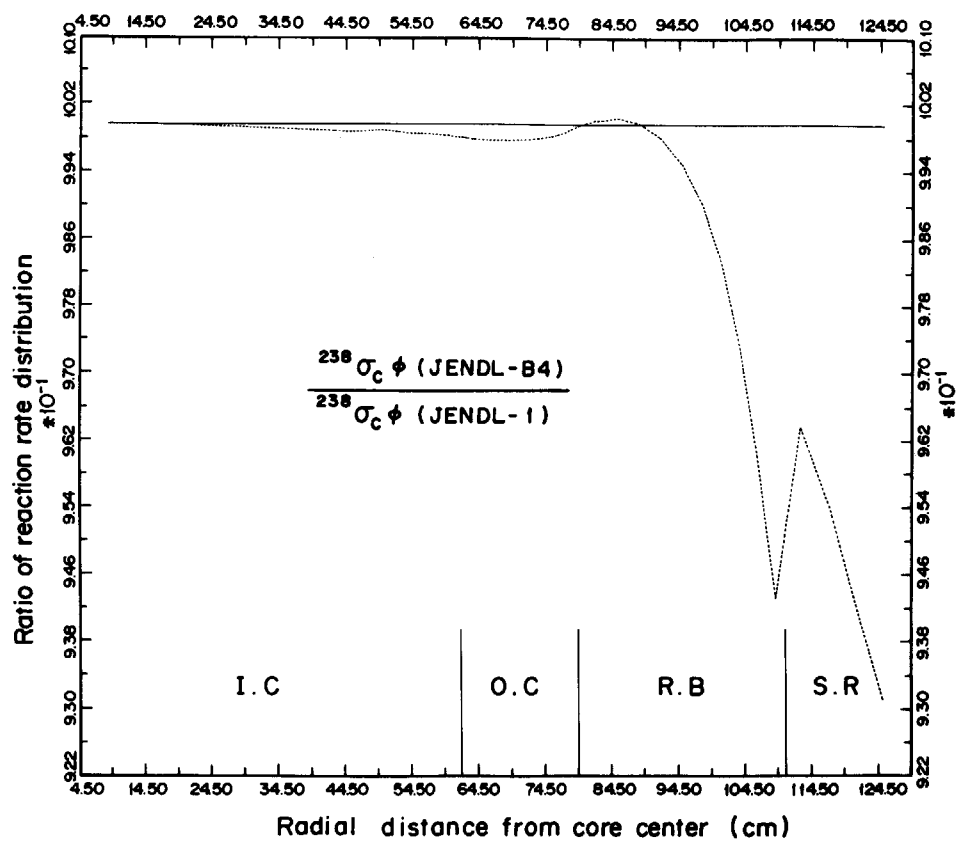


**Fig. A3.19** Ratio of  $^{238}\text{U}$  capture rate distribution calculated with JENDL-B4 to that with JENDL-1.

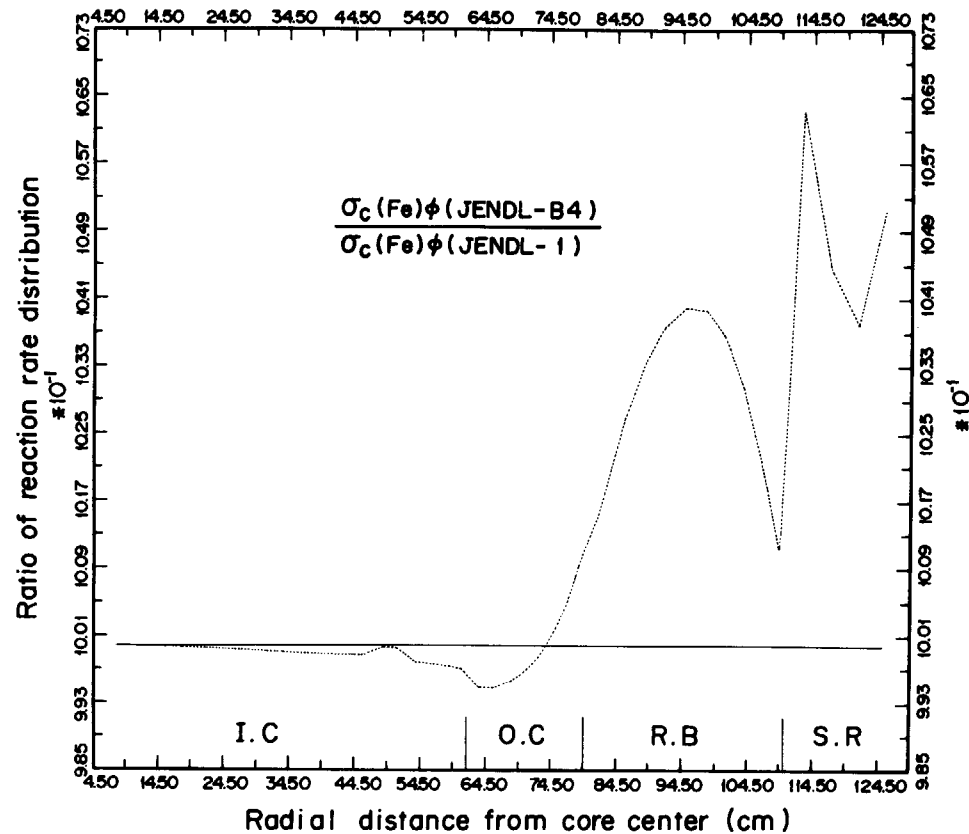


**Fig. A3.20** Ratio of iron capture rate distribution calculated with JENDL-B4 to that with JENDL-1.

### A3.3 Analysis of Large Fast Breeder Reactor

Effects of the structural material cross sections were studied on core characteristics of a large fast breeder reactor under conceptual design, in order to know the core size dependence of the effects. The design specification and characteristics of the reactor are given in **Table A3.8**. The analysis was made with the 2-D R-Z diffusion model and six group cross section collapsed with the 1-D diffusion calculation. The R-Z model is shown in **Fig. A3.21**. We replaced not only the cross sections of chromium, iron and nickel but also those of sodium by those of ENDF/B-IV in this study. It was proved, however, that the latter replacement

**Table A3.8** Design specifications and characteristics of  
1000 MWe LMFBR

Reactor thermal output	2600	(MW)
Reactor electric out put	1000	(MW)
Core height	98	(cm)
Core diameter	345	(cm)
Axial blanket thickness (upper/lower)	35/35	(cm)
Radial blanket thickness	40	(cm)
Pu enrichment (inner core/outer core)	11.3/14.5	(a/o Pu-fiss)
Pu isotope ratio (239/240/241/242)	58/24/14/4	
Fuel pellet density (core/blanket)	90/93	(% T.D.)
Burn up (average)	80,000	(MWD/T)
Number of refueling batches (core/blanket)	3/6	
Breeding ratio (MOEC)	1.30	
Reactivity swing	2.89	(% $\Delta k/k$ )
Power share (MOEC) (core/r. bla./a. bla.)	88.5/3.5/8.0	(%)

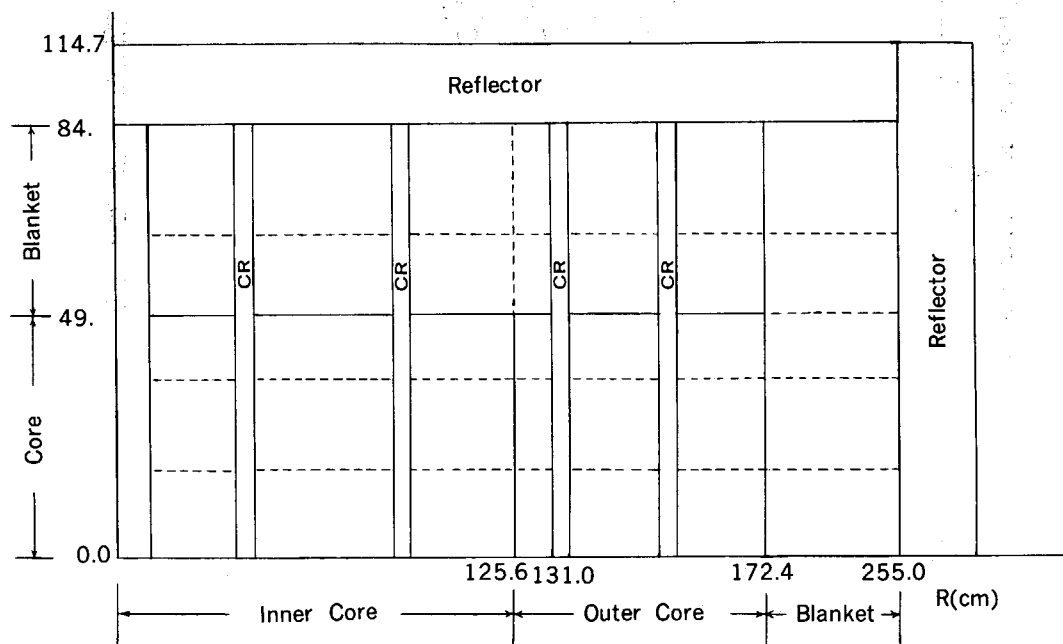


**Fig. A3.21** Two-dimensional R-Z calculational model of 1000 MWe fast breeder reactor.

has minor effects on the characteristics interested. Hence this replaced library is also called JENDL-B4 in this section.

Changes of macroscopic cross sections in the outer core region are shown in **Table A3.9**. Significant changes are

- 1) decrease of  $\Sigma_s$  above 100 keV due to the change of elastic scattering cross section,
- 2) increase of D and decrease of  $\Sigma_{rem}$  between 100 keV and 1.4 MeV as the results of decrease in  $\Sigma_s$ ,
- 3) increase of  $\Sigma_{rem}$  above 1.4 MeV due to the increase of the inelastic scattering cross section

and

- 4) increase of  $\Sigma_a$ ,  $\Sigma_s$  and  $\Sigma_{rem}$  and decrease of D below 1 keV.

Changes of  $k_{eff}$  and breeding ratio are shown in **Table A3.10**. The  $k_{eff}$ -values decrease by 1.2% as observed in the other cores. Little change appears in the breeding ratio. **Table A3.11** shows absorption probabilities of a neutron by fissile, fertile and structural material nuclei in each zone of the reactor. Absorption by structural materials increases and those by fissile and fertile nuclei decrease by the replacement.

Changes of neutron flux in the outer core and radial blanket region are given in **Table A3.12**. The flux above 1.4 MeV is lower with JENDL-B4 due to larger removal cross section as mentioned above. The flux between 10 keV and 1.4 MeV becomes higher with JENDL-B4 as the results of larger removal from the first group. The flux below 10 keV decreases because of larger leakage between 100 keV and 1.4 MeV and of larger absorption cross section below 1 keV.

Change of power distribution has the same tendency as observed in the fission rate distributions in MZB: The change is less than 1% even in the outer edge of the outer core, and the calculated power with JENDL-B4 becomes lower by 4% at the outer edge of radial blanket and by 6% at the top of axial blanket.

**Table A3.9** Change of macroscopic cross sections in outer core region of 1000 MWe LMFBR due to replacement of the structural material cross sections

$E_H$	$E_L$	(JENDL-B4 - JENDL-1)/JENDL-1 (%)					
		$\Delta\nu\Sigma_f$	$\Delta\Sigma_a$	$\Delta\Sigma_s$	$\Delta\Sigma_{rem}$	$\Delta D$	
1.05 + 7*	1.4 + 6	-0.5	0.9	-2.6	4.8	0.3	
1.4 + 6	4.0 + 5	0.1	-0.3	-5.9	-3.5	11.3	
4.0 + 5	1.0 + 5	0	0	-3.3	-1.3	3.9	
1.0 + 5	1.0 + 4	0.2	1.0	-0.8	-3.2	0.4	
1.0 + 4	1.0 + 3	-0.9	1.6	-0.2	0.1	-0.7	
1.0 + 3	1.0 + 2	0.9	3.4	3.0	3.0	-6.0	
1.0 + 2	2.15 - 1	0.5	0.9	0.7	0.7	-2.9	

\*  $1.05 + 7$  denotes  $1.05 \times 10^7$

**Table A3.10** Effective multiplication factor and breeding ratio of 1000 MWe LMFBR

	JENDL-1	JENDL-B4
$k_{eff}$	1.03881	1.02444
breeding ratio	1.2658	1.2666

**Table A3.11** Absorption probability of a neutron by fissile, fertile and structural material nuclei in each region of 1000 MWe LMFBR

Region	Fissile nuclei		Fertile nuclei		Structural material nuclei	
	JENDL-1	JENDL-B4	JENDL-1	JENDL-B4	JENDL-1	JENDL-B4
Inner core	0.2143	0.2121	0.2405	0.2371	0.0290	0.0324
Outer core	0.1514	0.1489	0.1303	0.1276	0.0161	0.0176
Radial blanket	—	—	0.0652	0.0647	0.0052	0.0066
Axial blanket	—	—	0.0968	0.0956	0.0112	0.0137
Other	—	—	—	—	0.0187	0.0214
Whole region	0.3656	0.3610	0.5328	0.5251	0.0803	0.0917

**Table A3.12** Fluxes in outer core regions and radial blanket of 1000 MWe LMFBR

E <sub>H</sub>	E <sub>L</sub>	Inner edge of outer core		Outer edge of outer core		Radial blanket	
		JENDL-1	change* (%)	JENDL-1	change* (%)	JENDL-1	change* (%)
1.05 + 7**	1.4 + 6	2.270 + 14	-2.7	9.570 + 13	-2.9	7.790 + 12	-6.7
1.4 + 6	4.0 + 5	8.047 + 14	5.3	3.293 + 14	4.8	4.596 + 13	11.2
4.0 + 5	1.0 + 5	8.448 + 14	1.8	3.419 + 14	1.6	7.094 + 13	5.7
1.0 + 5	1.0 + 4	1.081 + 15	1.3	4.391 + 14	1.2	1.507 + 14	3.7
1.0 + 4	1.0 + 3	2.206 + 14	-1.4	8.92 + 13	-1.6	4.734 + 13	-0.1
1.0 + 3	1.0 + 2	3.896 + 13	-3.4	1.687 + 13	-4.5	1.718 + 13	-4.4
1.0 + 2	2.15 - 1	1.907 + 11	6.4	2.115 + 11	-1.8	1.070 + 12	-2.4

\* (JENDL-B4 - JENDL-1)/JENDL-1

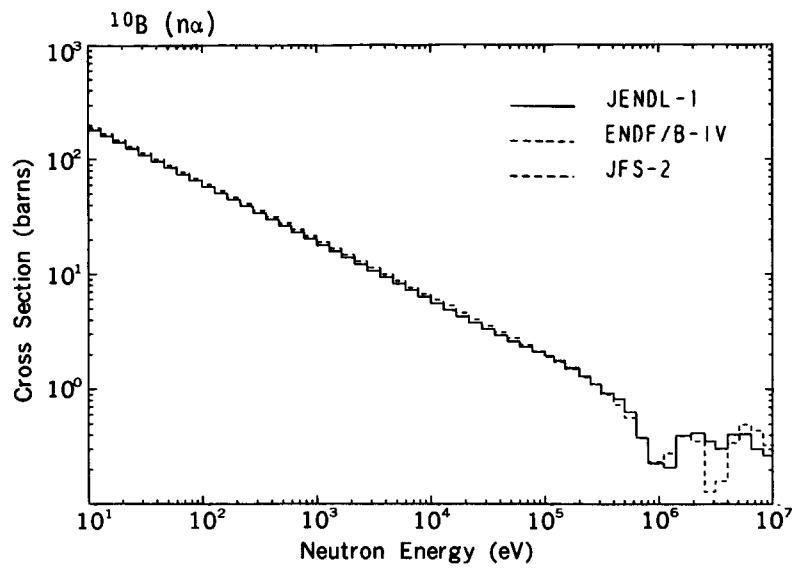
\*\* 1.05 + 7 denotes  $1.05 \times 10^7$ 

### References

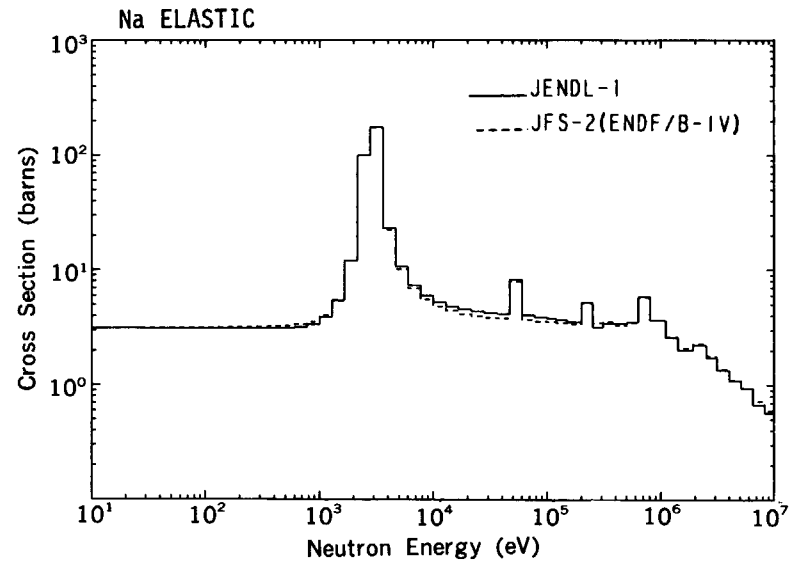
- Asami T., Kikuchi Y., Nakagawa T. and Igarasi S.: "Neutron Data of Structural Materials for Fast Reactors", Proc. Specialists' Meeting, Geel, 5-8 Dec. 1977, p. 118, Pergamon Press (1979).

### Appendix 4 Intercomparison of Group Constants among JENDL-1, JFS-2 and ENDF/B/IV

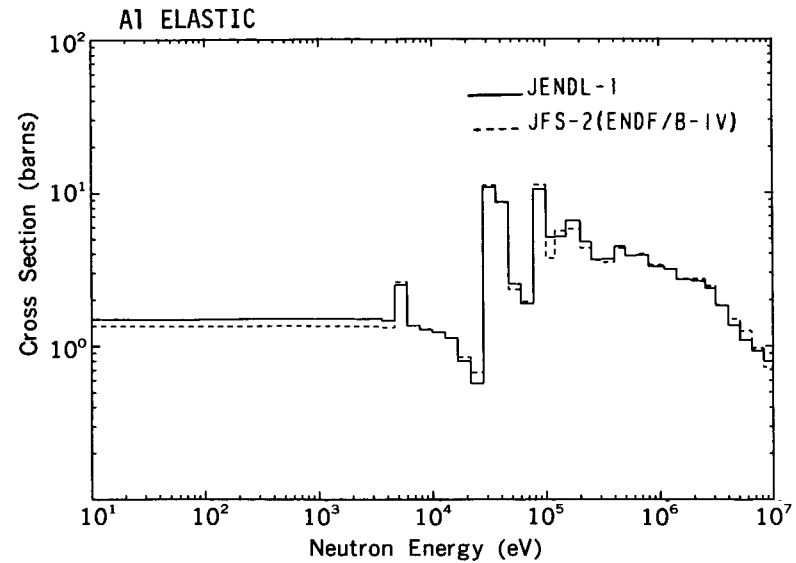
Some important group constants of JENDL-1, JFS-2 and ENDF/B-IV are graphically compared with one another in this appendix. One comment is necessary as to JFS-2. JFS-2 adopted the data of ENDF/B-IV for Al, Na, Cr, Fe and Ni. Hence the data of ENDF/B-IV are hidden by those of JFS-2 in the present graphs. As to the  $(n, \alpha)$  reaction cross section of  $^{10}\text{B}$ , the values of ENDF/B-IV are very close to those of JENDL-1.



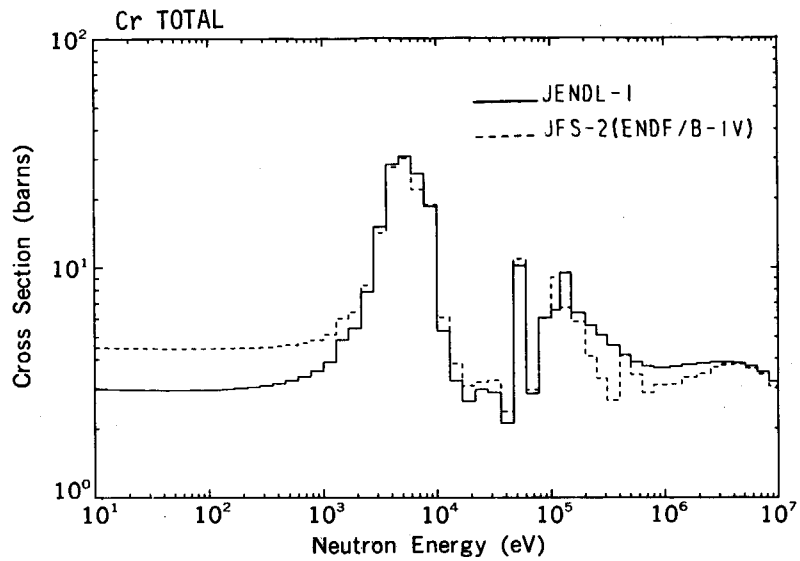
**Fig. A4.1** Neutron absorption cross sections of  $^{10}\text{B}$ .



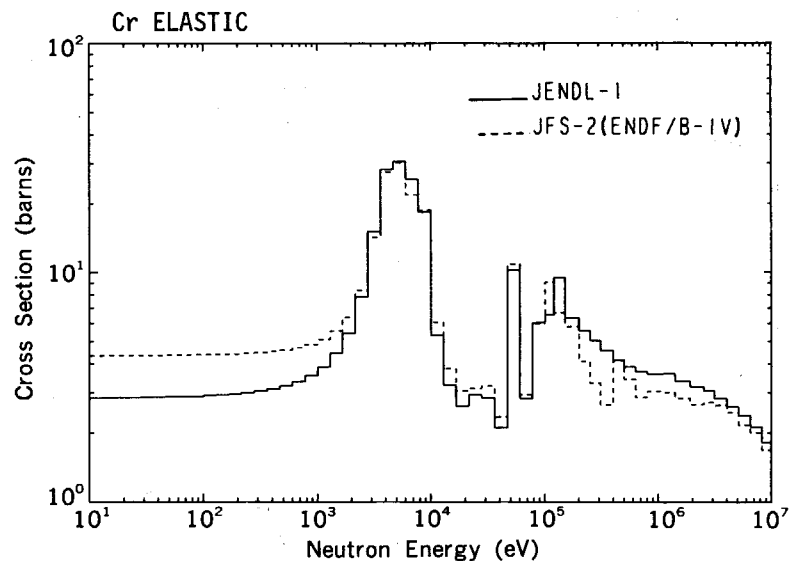
**Fig. A4.2** Elastic scattering cross sections of sodium.



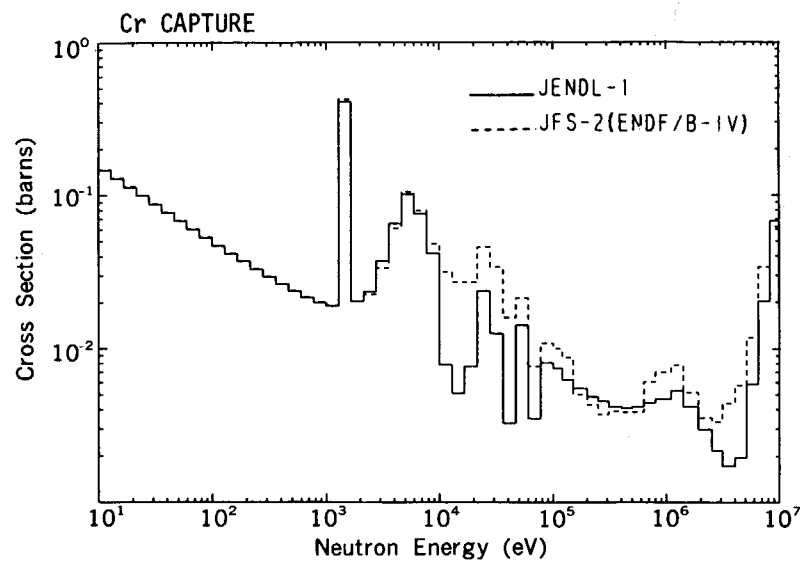
**Fig. A4.3** Elastic scattering cross sections of alminium.



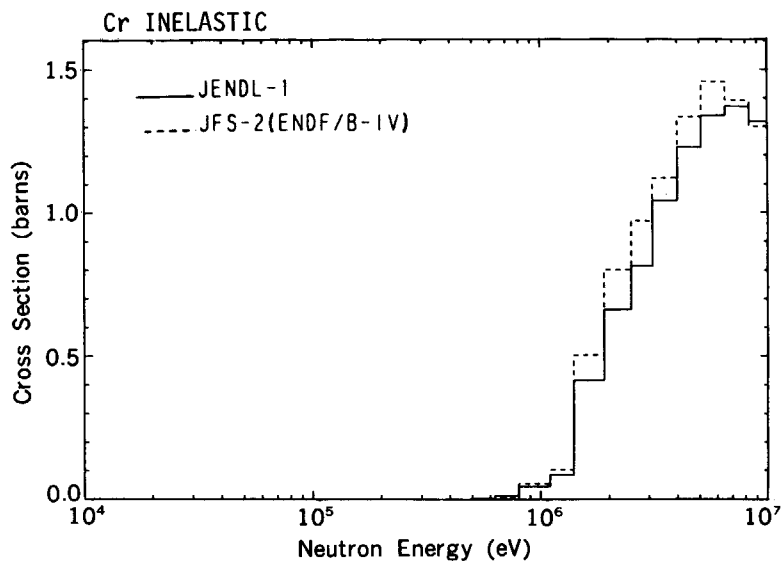
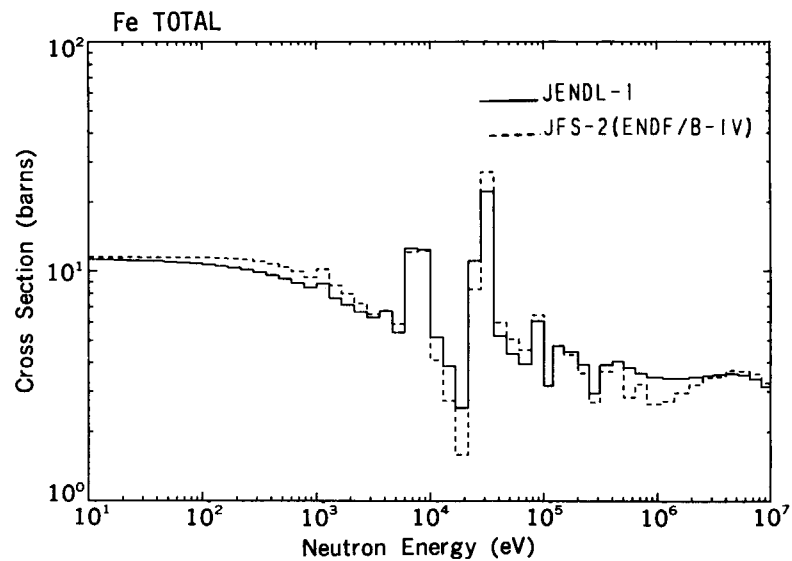
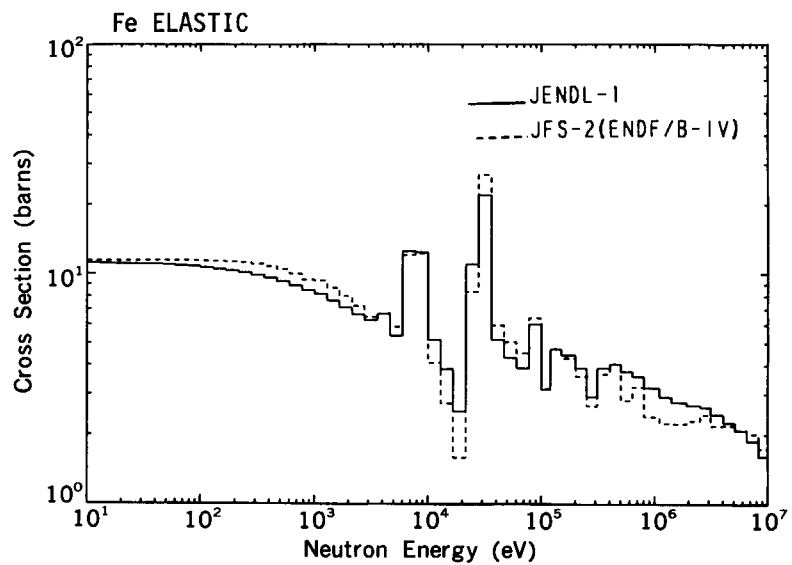
**Fig. A4.4** Total cross sections of chromium.

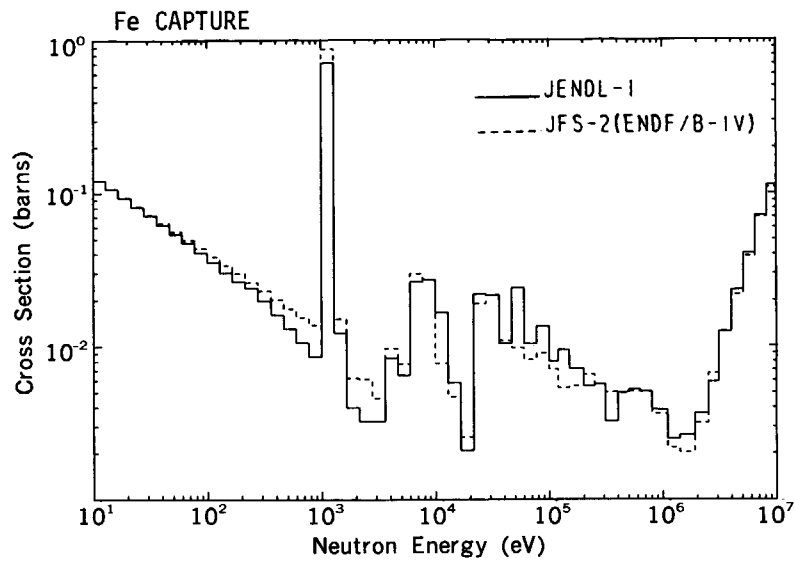


**Fig. A4.5** Elastic scattering cross sections of chromium.

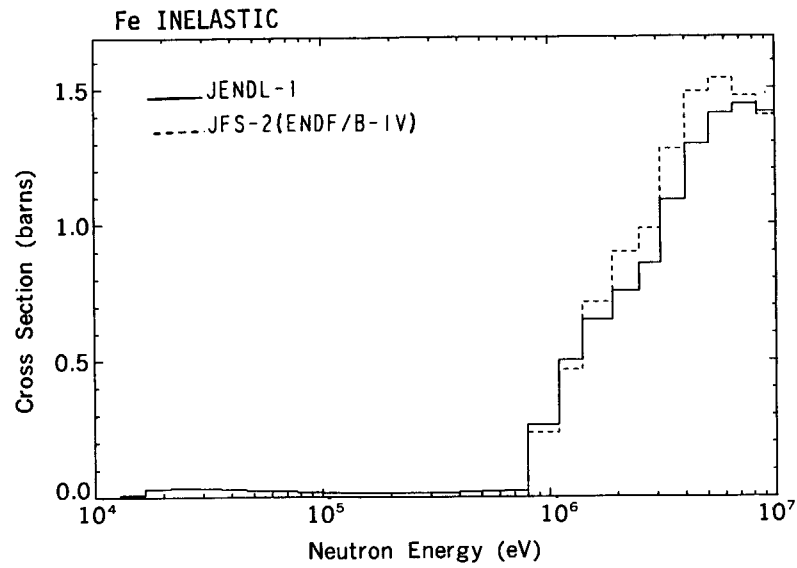


**Fig. A4.6** Capture cross sections of chromium.

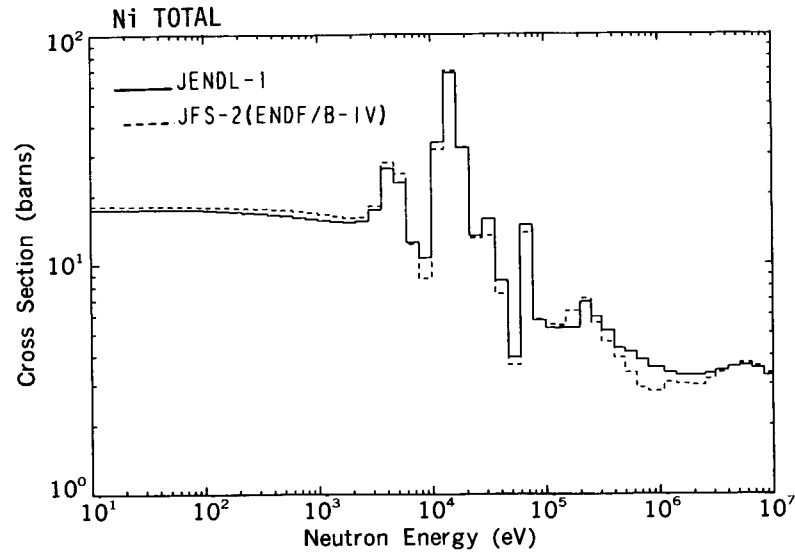
**Fig. A4.7** Inelastic scattering cross sections of chromium.**Fig. A4.8** Total cross sections of iron.**Fig. A4.9** Elastic scattering cross sections of iron.



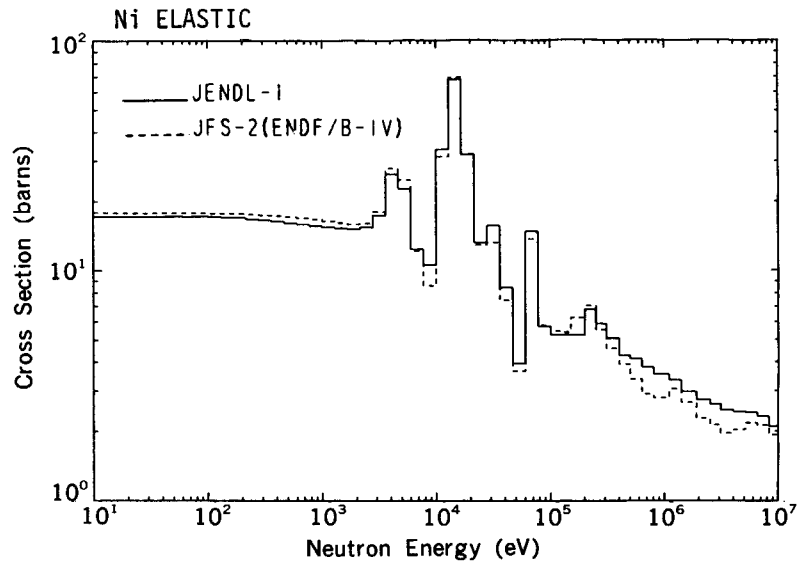
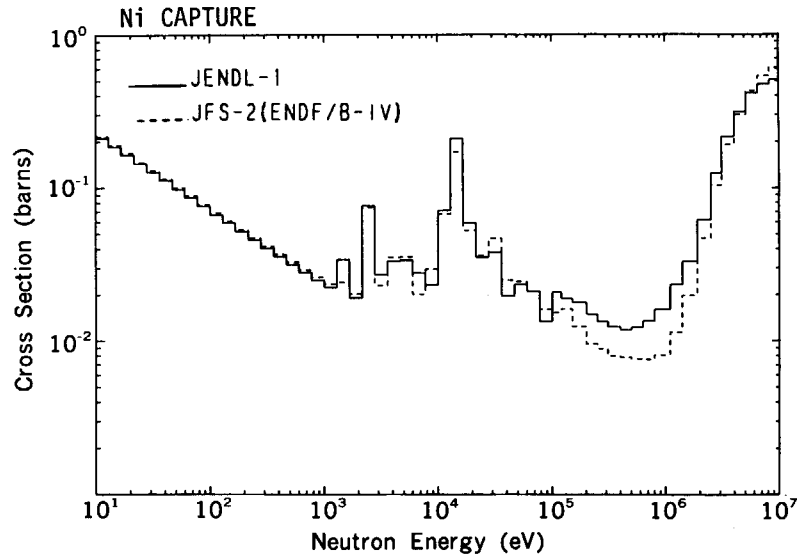
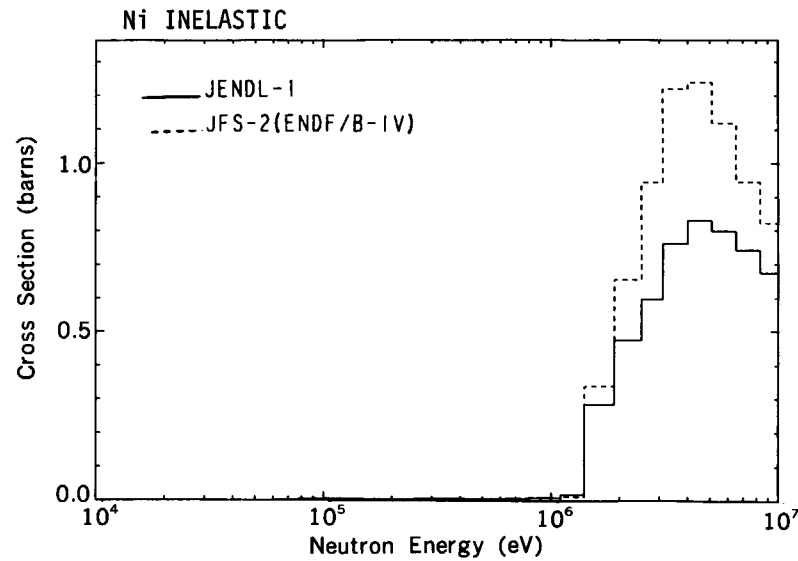
**Fig. A4.10** Capture cross sections of iron.



**Fig. A4.11** Inelastic scattering cross sections of iron.



**Fig. A4.12** Total cross sections of nickel.

**Fig. A4.13** Elastic scattering cross sections of nickel.**Fig. A4.14** Capture cross sections of nickel.**Fig. A4.15** Inelastic scattering cross sections of nickel.

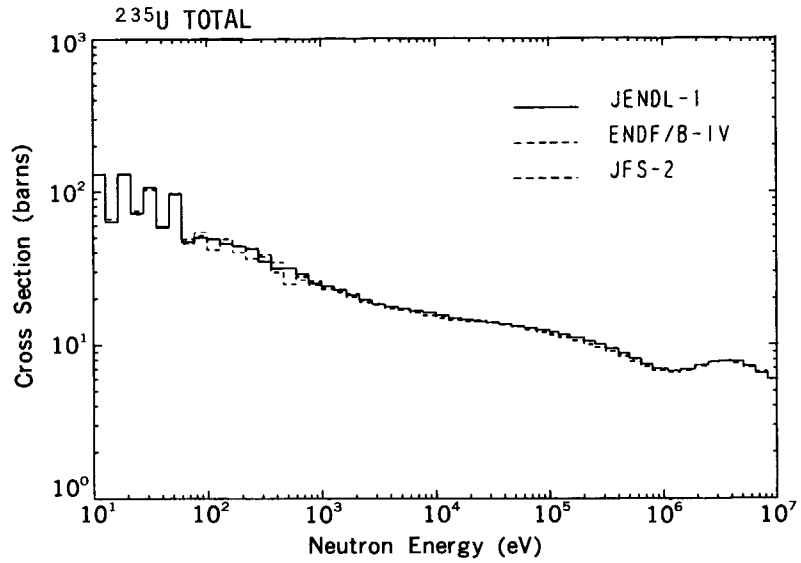


**Fig. A4.16** Total cross sections of  $^{235}\text{U}$ .

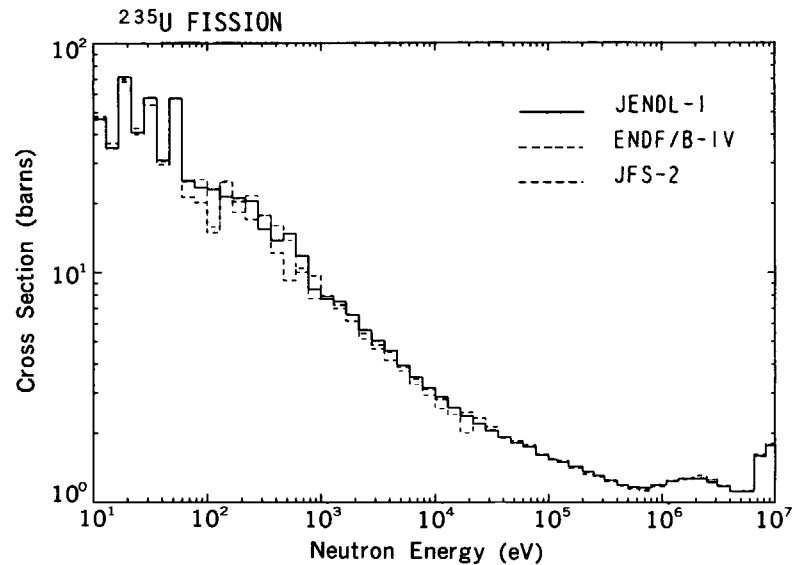


**Fig. A4.17 (a)** Fission cross sections of  $^{235}\text{U}$ .

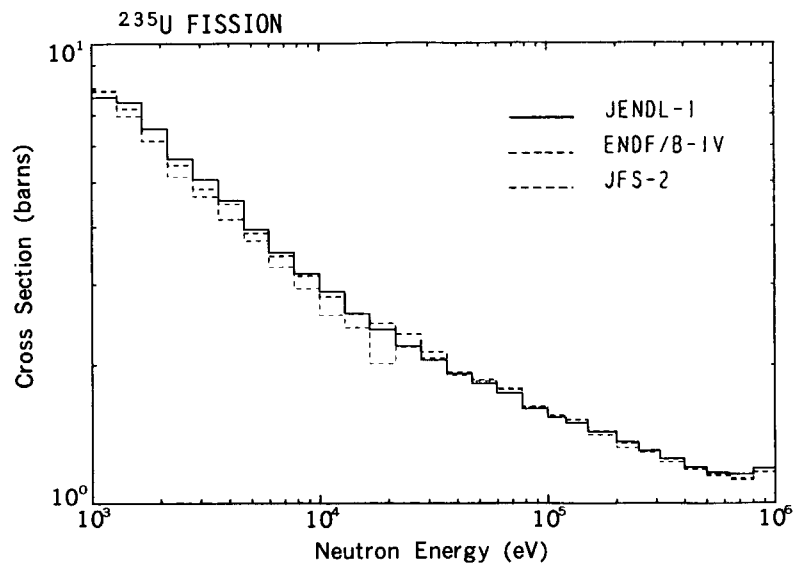


**Fig. A4.17 (b)** Fission cross sections of  $^{235}\text{U}$ .

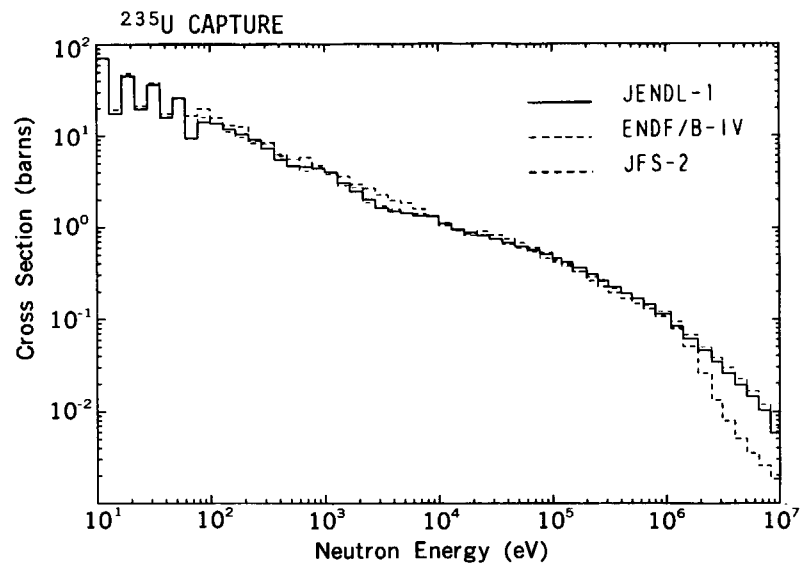


**Fig. A4.18 (a)** Capture cross sections of  $^{235}\text{U}$ .

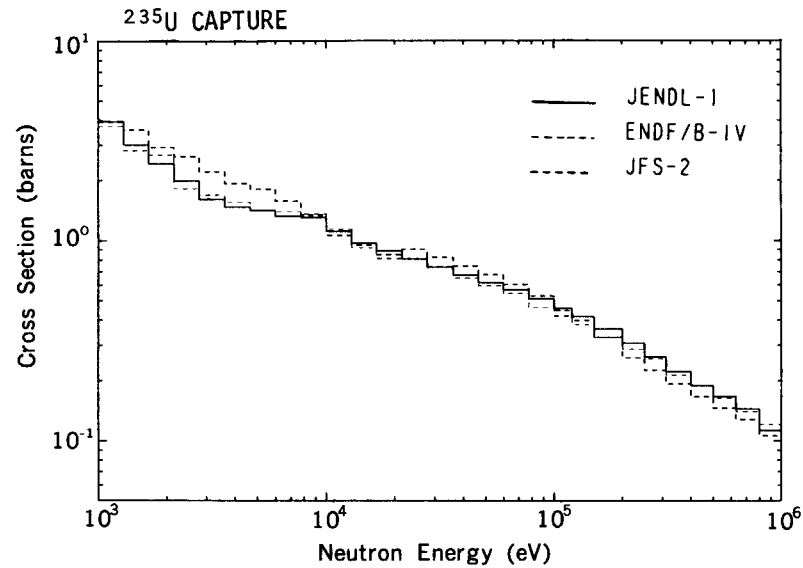


**Fig. A4.18 (b)** Capture cross sections of  $^{235}\text{U}$ .

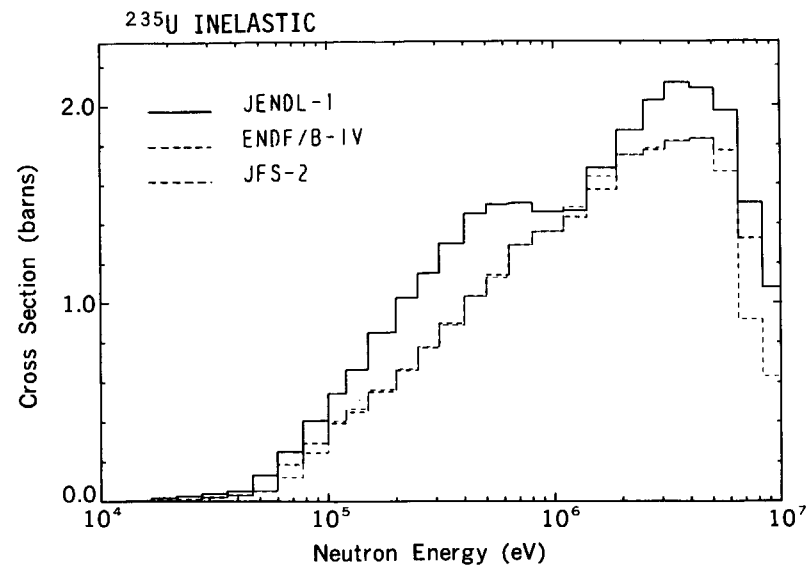


**Fig. A4.19** Inelastic scattering cross sections of  $^{235}\text{U}$ .

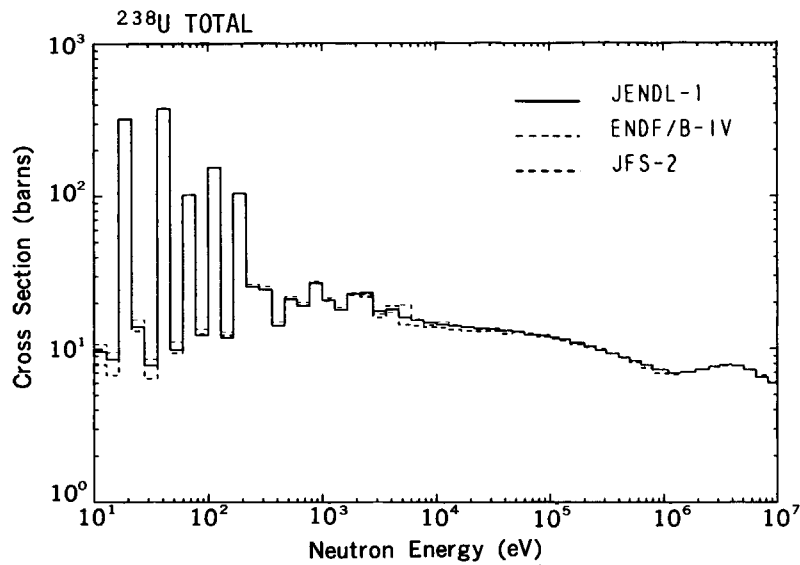


Fig. A4.20 Total cross sections of  $^{238}\text{U}$ .

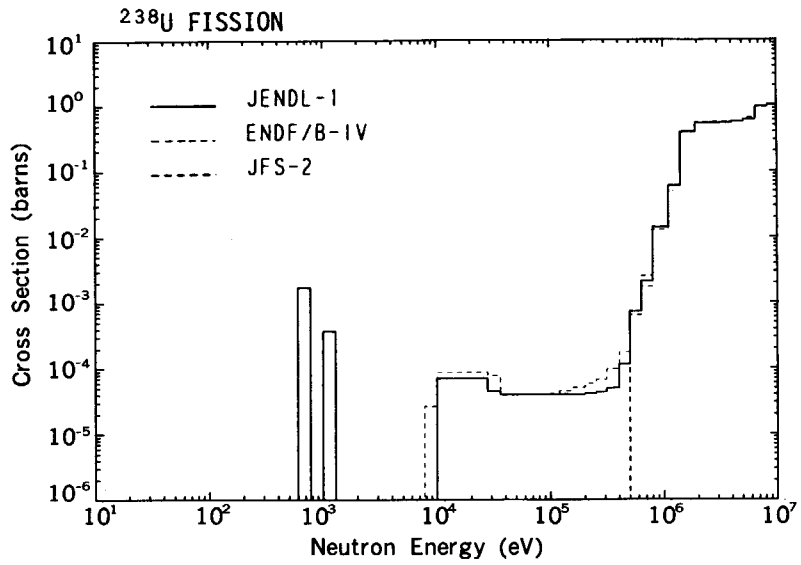


Fig. A4.21 Fission cross sections of  $^{238}\text{U}$ .

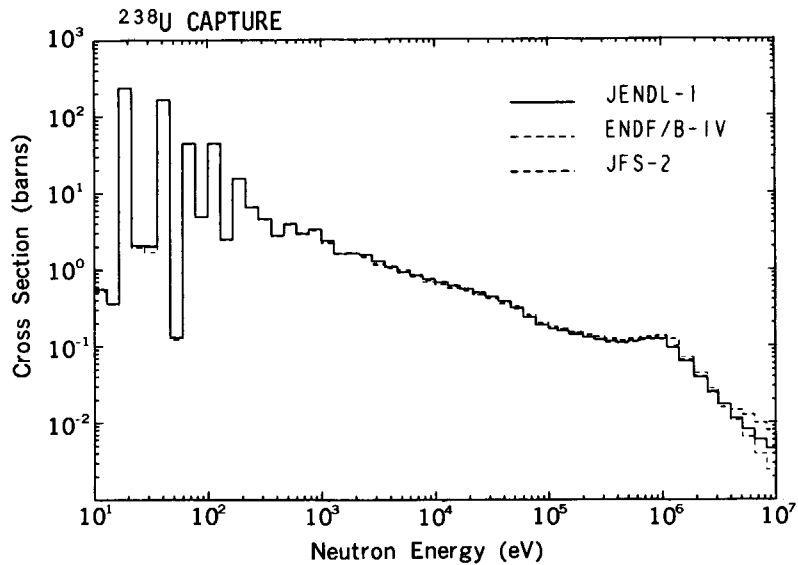
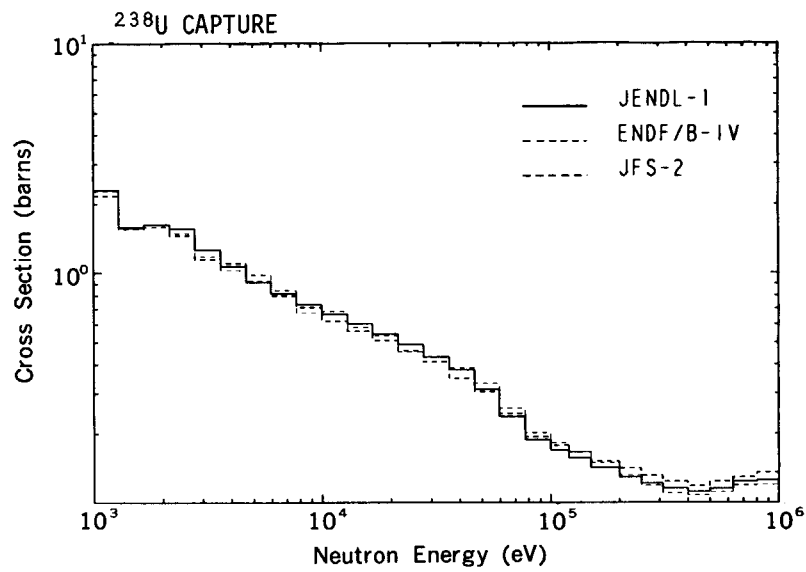
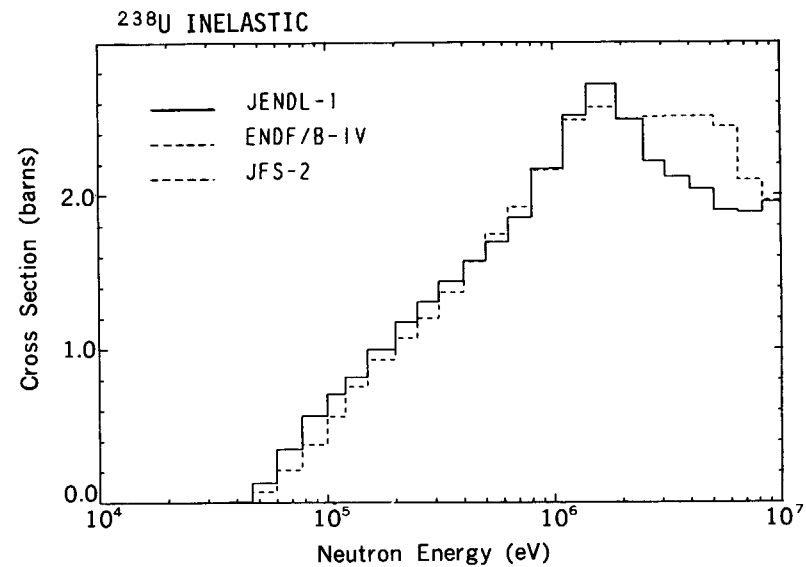


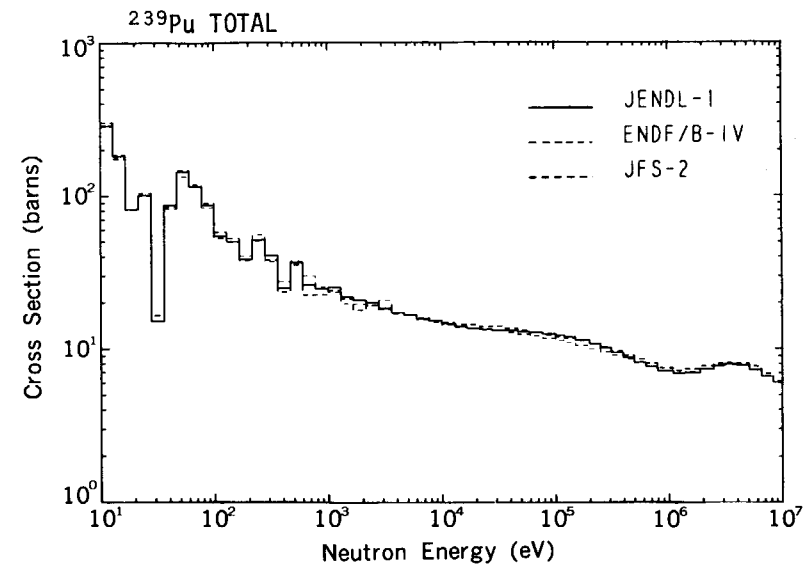
Fig. A4.22 (a) Fission cross sections of  $^{238}\text{U}$ .



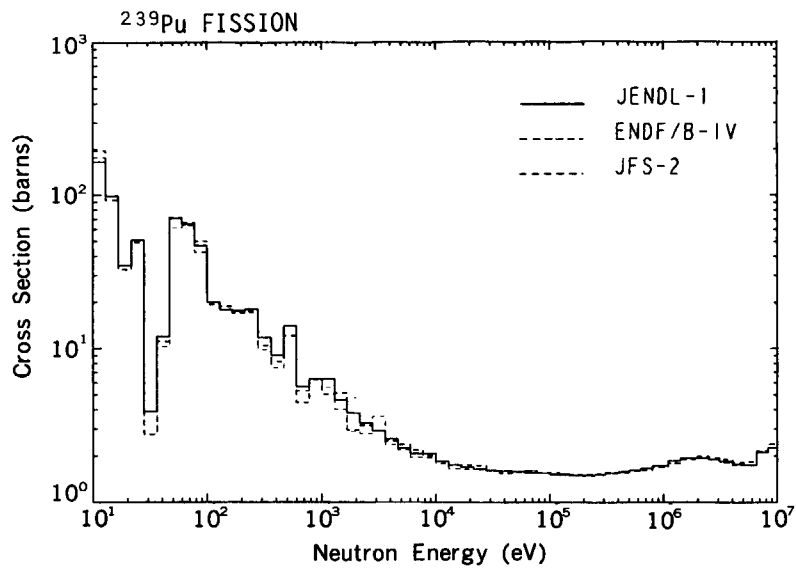
**Fig. A4.22 (b)** Fission cross sections of  $^{238}\text{U}$ .



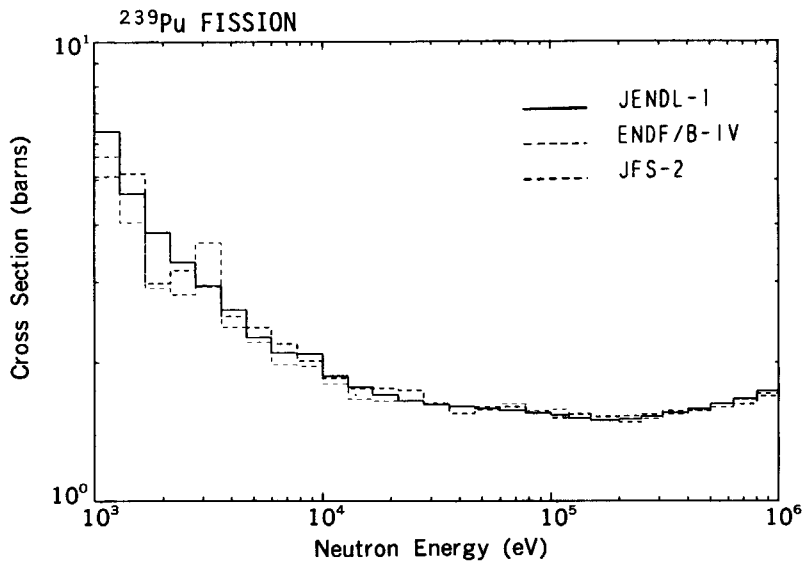
**Fig. A4.23** Inelastic scattering cross sections of  $^{238}\text{U}$ .



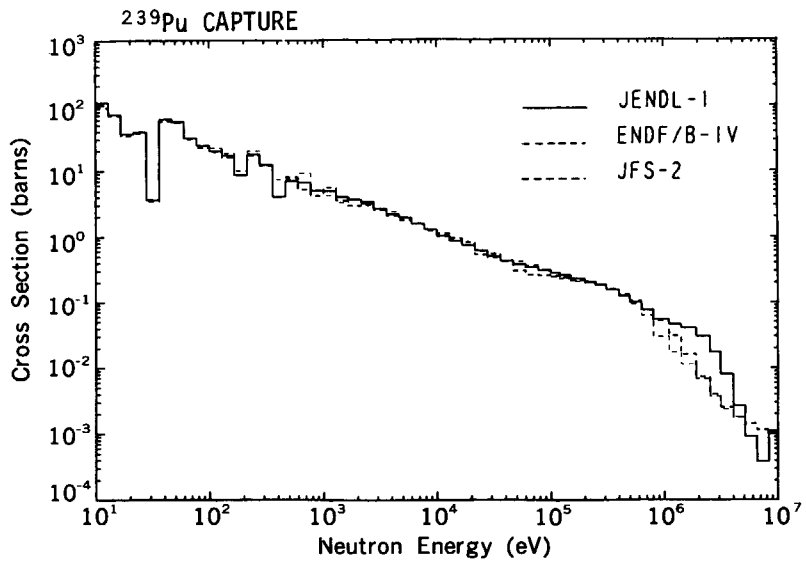
**Fig. A4.24** Total cross sections of  $^{239}\text{Pu}$ .



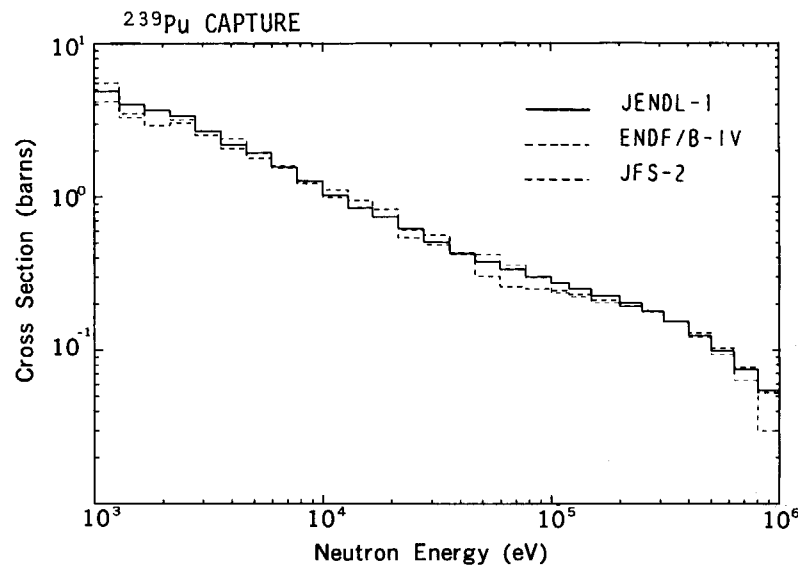
**Fig. A4.25 (a)** Fission cross sections of  $^{239}\text{Pu}$ .



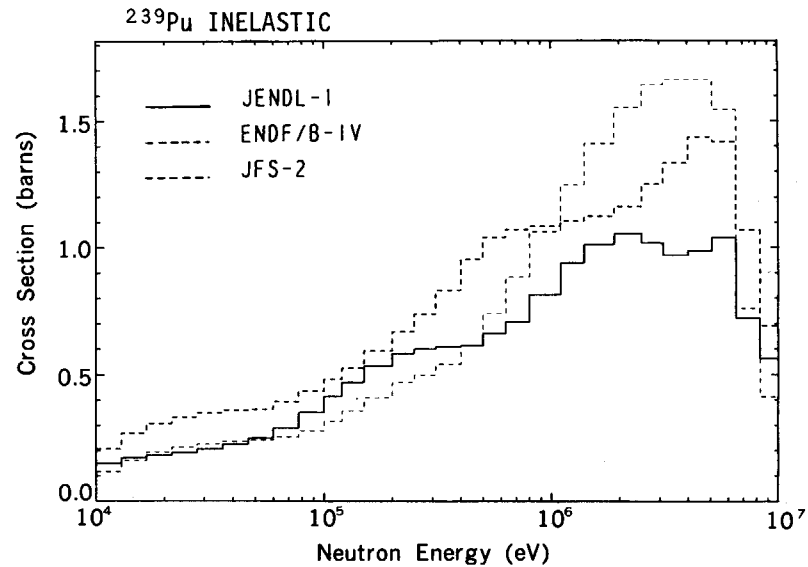
**Fig. A4.25 (b)** Fission cross sections of  $^{239}\text{Pu}$ .



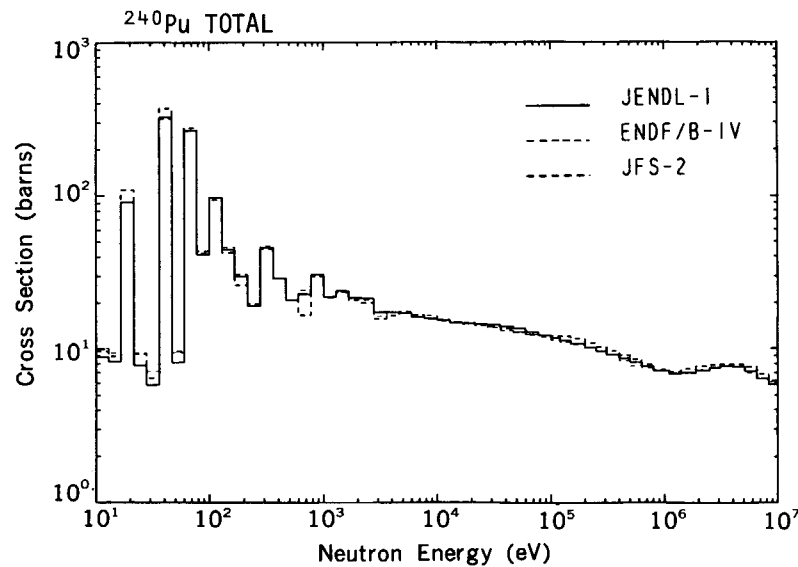
**Fig. A4.26 (a)** Capture cross sections of  $^{239}\text{Pu}$ .



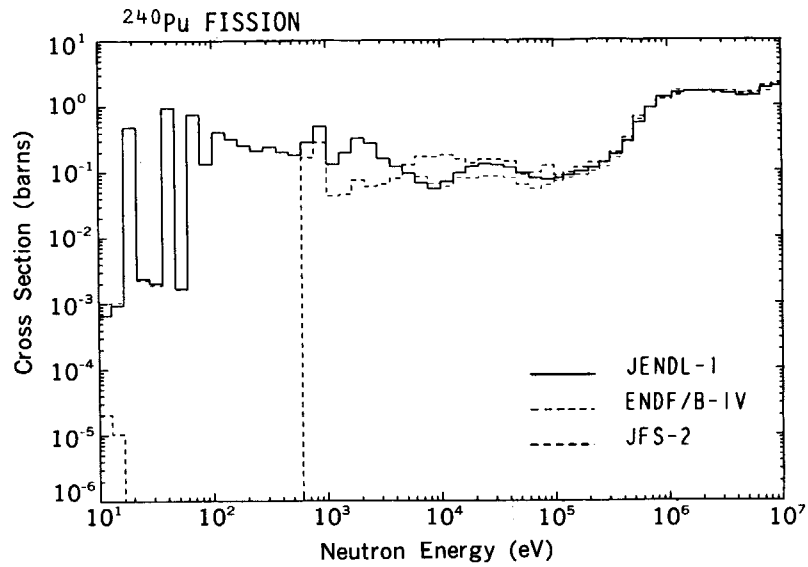
**Fig. A4.26 (b)** Capture cross sections of  $^{239}\text{Pu}$ .



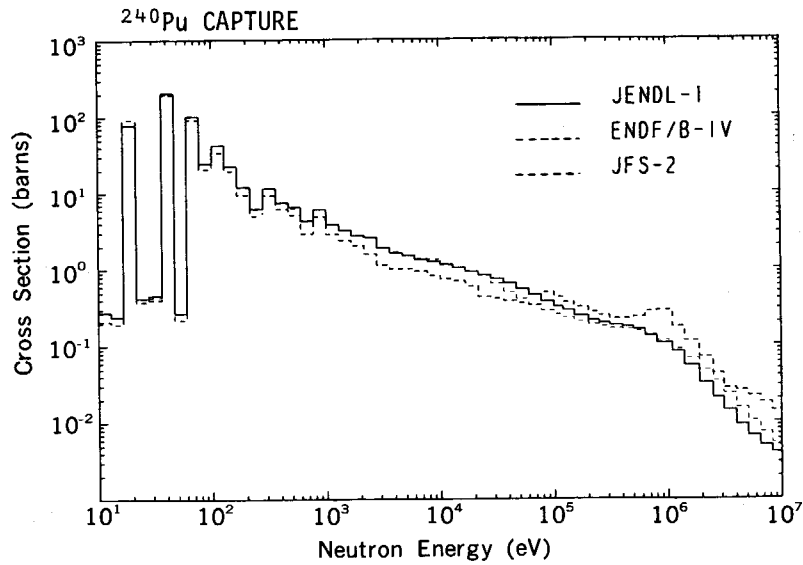
**Fig. A4.27** Inelastic scattering cross sections of  $^{239}\text{Pu}$ .



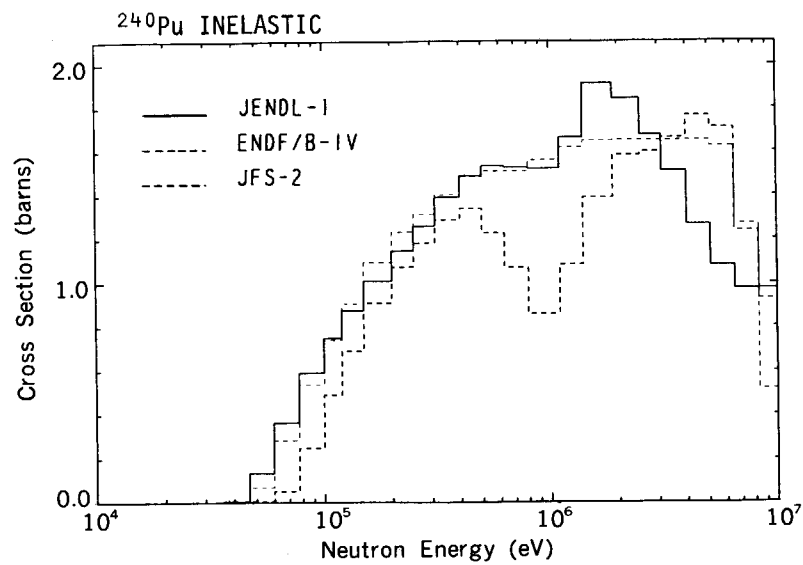
**Fig. A4.28** Total cross sections of  $^{240}\text{Pu}$ .



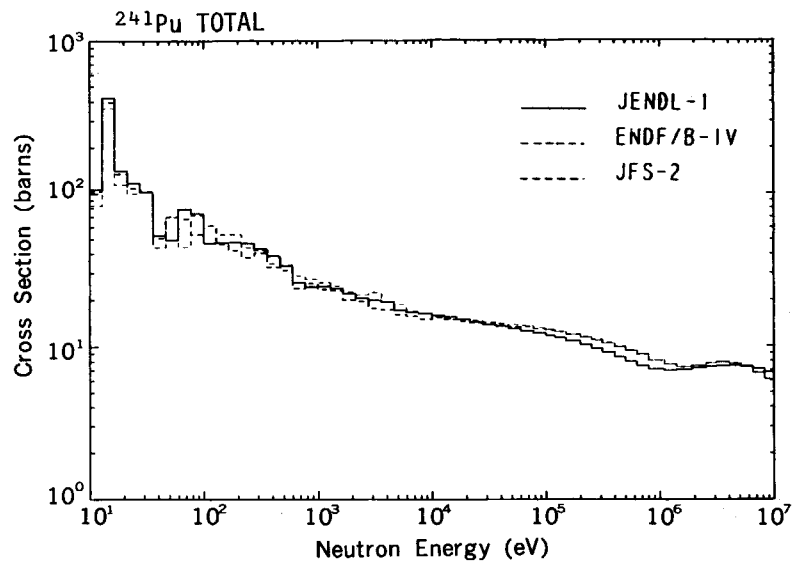
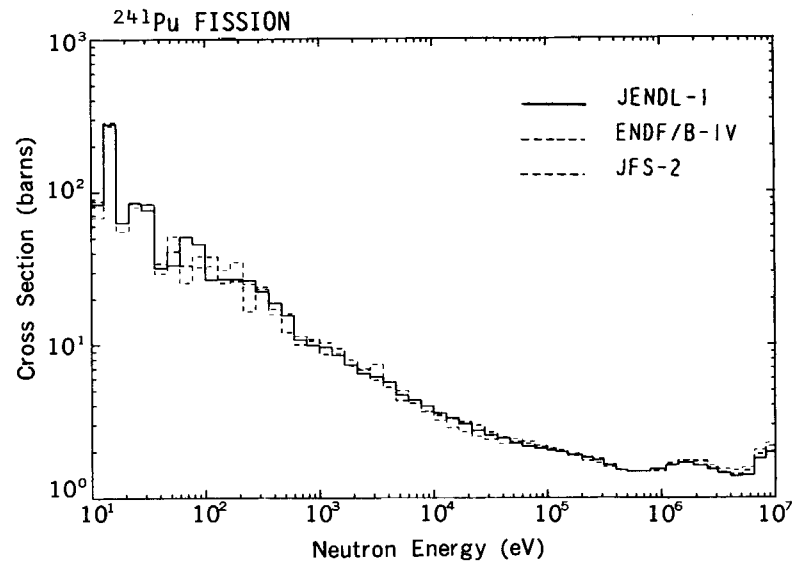
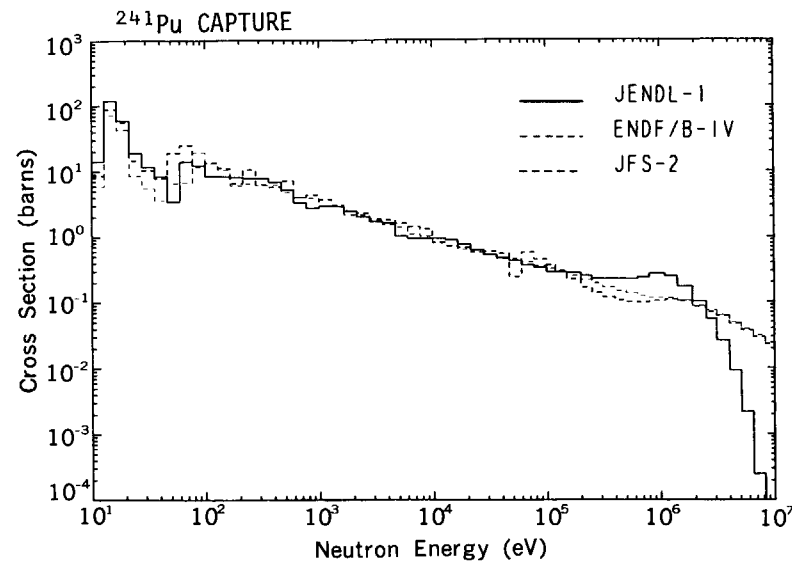
**Fig. A4.29** Fission cross sections of  $^{240}\text{Pu}$ .



**Fig. A4.30** Capture cross sections of  $^{240}\text{Pu}$ .



**Fig. A4.31** Inelastic scattering cross sections of  $^{240}\text{Pu}$ .

Fig. A4.32 Total cross sections of  $^{241}\text{Pu}$ .Fig. A4.33 Fission cross sections of  $^{241}\text{Pu}$ .Fig. A4.34 Capture cross sections of  $^{241}\text{Pu}$ .

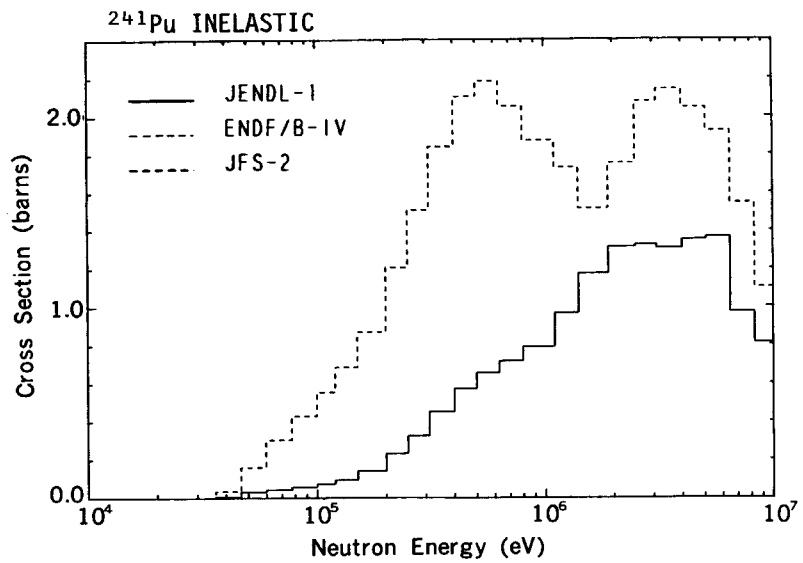


**Fig. A4.35** Inelastic scattering cross sections of  $^{241}\text{Pu}$ .